High-Temperature Interphase Properties of SiC Fiber Reinforced Titanium Metal Matrix Composites

Final Report
October 1996

By

H. Ghonem and D. Osborne

Mechanics of Materials Laboratory
Department of Mechanical Engineering
University of Rhode Island
Kingston, Rhode Island

Prepared for

Department of Air Force
Air Force Office of Scientific Research
Bolling Air Force Base, DC 20332

AFOSR-F49620-92-J-0357 (AASERT)

REPORT DOCUMENTATION PAGE

Form Approved
OMB No. 0704-0188

1. AGENCY USE ONLY (Leave blank)	2. REPORT DATE	3. REPORT TYPE AND DATES COVERED
	October 24, 1996	FINAL, June 1992 - June 1996

4. TITLE AND SUBTITLE
High-Temperature Interphase Properties of SiC Fiber Reinforced Titanium Matrix Composites

5. FUNDING NUMBERS
AFOSR-92-F49620-J-0357

6. AUTHOR(S)
H. Ghonem and D. Osborne

7. PERFORMING ORGANIZATION NAME(S) AND ADDRESS(ES)
Mechanics of Materials Laboratory
Department of Mechanical Engineering & Applied Mechanics
Wales Hall, 92 Upper College Road
University of Rhode Island
Kingston, Rhode Island 02881

8. PERFORMING ORGANIZATION REPORT NUMBER
URI-MML-96-4

9. SPONSORING/MONITORING AGENCY NAME(S) AND ADDRESS(ES)
USAF Office of Scientific Research
Bolling Air Force Base
Washington, DC 20332-6448

NA

10. SPONSORING/MONITORING AGENCY REPORT NUMBER

11. SUPPLEMENTARY NOTES
Dr. W. Jones, Program Manager

12a. DISTRIBUTION/AVAILABILITY STATEMENT
Approved for Public Release
Distribution is unlimited

12b. DISTRIBUTION CODE

13. ABSTRACT *(Maximum 200 words)*

A study has been carried out to determine the high temperature interfacial properties of two titanium metal matrix composites: SCS-6/Timetal-21S and SM1240/Timetal-21S. This report focusses on the effect of temperature on the interfacial shear strength and frictional shear stress of the fiber/matrix interphase. These properties are quantified through the use of "thin slice" fiber pushout tests, and the numerical determination of residual stresses in the composite system. Chapter 1 discusses the elevated temperature fiber pushout apparatus built for use in this study. Chapter 2 and 3 deal with two aspects of elevated temperature influence: thermal aging and test temperature. The effect of aging on the size and composition of the fiber/matrix interphase is investigated using Scanning Electron Microscopy and Auger Electron Spectroscopy. The influence of this aging on the debond shear strength as well as the influence of the actual test temperature on the mechanical properties of the interphase is identified through fiber pushout testing at different temperatures. The experimental work discussed in Chapter 2 relates to samples which were aged at high temperature in air, then cut to the appropriate size. The pushout experiments were conducted at room temperature in an air environment. Chapter 3 focusses on specimens which were aged at high temperature in a vacuum environment, as well as unaged samples. The pushout tests described in this section were conducted either at room and elevated temperatures in both air and vacuum conditions. Some numerical work was done to establish an appropriate thickness choice for the fiber pushout samples. Chapter 4 examines the influence of process-related residual stress on the shear strength of the fiber/matrix interphase in SCS-6/Timetal-21S, using a combined experimental/numerical approach. This procedure employs a concept of localized shear stress distribution along the fiber/matrix interface in the determination of the debond shear strength.

14. SUBJECT TERMS	15. NUMBER OF PAGES
Metal Matrix Composites, Fiber, Push-out, Interphase, Thermal Aging, Residual Stress, Debonding	113
	16. PRICE CODE

17. SECURITY CLASSIFICATION OF REPORT	18. SECURITY CLASSIFICATION OF THIS PAGE	19. SECURITY CLASSIFICATION OF ABSTRACT	20. LIMITATION OF ABSTRACT
Unclassified	Unclassified	Unclassified	UL

High-Temperature Interphase Properties of SiC Fiber Reinforced Titanium Metal Matrix Composites

Final Report
October 1996

By

H. Ghonem and D. Osborne

Mechanics of Materials Laboratory
Department of Mechanical Engineering
University of Rhode Island
Kingston, Rhode Island

Prepared for

Department of Air Force
Air Force Office of Scientific Research
Bolling Air Force Base, DC 20332

AFOSR-F49620-92-J-0357 (AASERT)

SUMMARY

A study has been carried out to determine the high temperature interfacial properties of two titanium metal matrix composites: SCS-6/Timetal-21S and SM1240/Timetal-21S. This report focusses on the effect of temperature on the interfacial shear strength and frictional shear stress of the fiber/matrix interphase. These properties are quantified through the use of "thin slice" fiber pushout tests, and the numerical determination of residual stresses in the composite system. Chapter 1 discusses the elevated temperature fiber pushout apparatus built for use in this study. Chapter 2 and 3 deal with two aspects of elevated temperature influence: thermal aging and test temperature. The effect of aging on the size and composition of the fiber/matrix interphase is investigated using Scanning Electron Microscopy and Auger Electron Spectroscopy. The influence of this aging on the debond shear strength as well as the influence of the actual test temperature on the mechanical properties of the interphase is identified through fiber pushout testing at different temperatures. The experimental work discussed in Chapter 2 relates to samples which were aged at high temperature in air, then cut to the appropriate size. The pushout experiments were conducted at room temperature in an air environment. Chapter 3 focusses on specimens which were aged at high temperature in a vacuum environment, as well as unaged samples. The pushout tests described in this section were conducted either at room and elevated temperatures in both air and vacuum conditions. Some numerical work was done to establish an appropriate thickness choice for the fiber pushout samples. Chapter 4 examines the influence of process-related residual stress on the shear strength of the fiber/matrix interphase in SCS-6/Timetal-21S, using a combined experimental/numerical approach. This procedure employs a concept of localized shear stress distribution along the fiber/matrix interface in the determination of the debond shear strength.

ACKNOWLEDGEMENT

The authors acknowledge the advice of Jeffrey Eldridge of NASA Lewis Research Center in the construction of the high temperature/vacuum fiber pushout apparatus. His assistance and experience were invaluable. The authors also acknowledge the discussions with and the encouragement of Dr. T. Nicholas of the Materials Directorate, WPAFB. This study is supported by the USAF Office of Scientific Research under the Augmentation Awards for Science and Engineering Research Training Program (AASERT) grant F49620-92-J-0357. Dr. W. Jones is the program manager.

LIST OF CONTENTS

LIST OF FIGURES

SECTION 1

ELEVATED TEMPERATURE FIBER PUSHOUT APPARATUS

ABSTRACT

An elevated temperature single fiber pushout apparatus was built to investigate the interfacial properties of fiber reinforced composites. Testing temperatures of up to 1000 °C in a vacuum of less than 10^{-6} torr can be obtained. Output includes applied load on the fiber and relative punch displacement. A description of the device is given.

1.1 INTRODUCTION

The complex nature of the interface in a Ti metal matrix composite has necessitated the characterization of the properties of this region. Several methods have been used in order quantify these material properties, particularly the interface shear strength and the frictional shear stress at the interface. One such technique, single fiber pushout testing, offers important features such as relative ease in setup, the ability to obtain several data points from a single sample, and reasonably simple specimen preparation. Recently, a desktop fiber pushout apparatus was introduced to replace the typical Instron-based equipment commonly employed for such testing. [1] This apparatus offered the advantages of smaller size, greater ease in setup, and lower cost.

In order to characterize the interface under conditions representative of material applications, elevated temperature testing is necessary. Due to the low oxidation resistance of Ti-based alloys at high temperature, such elevated temperature testing requires a vacuum environment. Eldridge designed such a device in the form of a desktop testing unit incorporated into a vacuum chamber. [2] This section describes the elevated temperature fiber pushout device which was built similar to that design.

1.2 DESCRIPTION OF FIBER PUSHOUT APPARATUS

Figure 1.1 is a schematic of the high temperature fiber pushout apparatus, modeled after the device designed by Jeffrey Eldridge at NASA Lewis Research Center in Cleveland, Ohio. This device has the capacity to run at less than 10^{-6} torr vacuum and sample heating temperatures of at least 1000 °C, although for the tests described in this report, temperature were limited to 650 °C.

The sample and indentor are located inside a 12 inch diameter cylindrical stainless steel vacuum chamber with Conflat ports on either end. A quartz window on either end of the chamber allow for sample observation and heating as described below. The test chamber can be evacuated with the attached turbo pump in order to prevent significant oxidation of the sample during heating.

Controlled indentor displacement is performed using a linear motion feedthrough driven by a stepper motor. The indentor is attached to a load cell, which is coupled directly to the shaft of the

linear motion feedthrough. In order to avoid lateral play, the linear motion feedthrough was modified by placing a Teflon bushing around the shaft where it entered the vacuum chamber. Another Teflon bushing was located at the point where the stainless steel tube entered the vacuum camber for the purpose of stabilizing the load train. The fiber is loaded in continuous single steps corresponding to a linear punch displacement of .0125 μm/step. The indentor used for pushing out fibers is a conical tungsten carbide punch having a 30° included angle and a flat bottom. A punch having a 100 μm diameter flat bottom was used to push out the 140 μm SCS-6 fibers, while a 75 μm diameter flat bottom was used for the 100 μm SM1240 fibers. The special conical shape of the indentor allowed the punch to hold a higher load than a straight cylindrical punch, while the flat bottom distributed the applied load over a large portion of the fiber face and minimized fiber damage by inhibiting penetration of the punch into the fiber.

The sample support was designed for high-temperature exposure and thermal isolation. The specimen is mounted with a clamping device with fibers aligned over channels in the Ta support block. The 100 μm channels were used in the support block for SM1240 fiber pushout, and channels, 280 μm wide, were used for the SCS-6 reinforced samples. These channel widths were chosen to be small enough to minimize sample bending, while large enough to allow a reasonable amount of fibers to be tested without relocating the composite sample. The Ta sample block is mounted on a low-thermal-conductivity ceramic pedestal, for thermal isolation, which was secured to a hollow stainless steel fixture. The entire support base was secured inside the vacuum chamber with two screws. This setup allowed removal of the support base to an optical microscope for alignment of the fibers in the sample with the grooves in the Ta block. This sample assembly is mounted on an x-y translation stage above a water cooled Cu plate which prevents the x-y stage from overheating.

Sample heating is achieved using a quartz halogen lamp inside an ellipsoidal reflector, with the lamp at one focal point and the sample at the other where the heating radiation is focused. The reflector is bisected by the chamber's vertical quartz window, so that the lamp itself remains outside the test chamber. The hot zone is a spot with a diameter of about 1.25 cm. Sample temperature is monitored by a thermocouple attached to the Ta sample support.

Fiber/indentor alignment is performed remotely, using motorized actuators to control the motion of the translation stages, to bring an individual fiber beneath the indentor. A quartz window tilted at an angle of 30° from vertical provides line-of-sight for a long working distance optical microscope located outside the chamber. The microscope is positioned so that the line-of-sight is perpendicular to the plane of the window in order to minimize distortion and multiple reflections.

A PC-controlled data acquisition system is used to collect data from the load cell and the encoder. Load and motor displacement data is stored on the computer hard drive, as well as being displayed, both graphically and numerically, on the monitor. In addition, the PC controls the motion of the indentor via a RS-232 communication with the stepper motor controller. Visual monitoring of the test is used to verify the occurrence of fiber sliding.

1.3 SUMMARY

An elevated temperature fiber pushout device has been successfully built for investigating the interfacial properties of fiber reinforced composite materials. Testing can be performed in vacuum

of less than 10^{-6} torr a temperatures of up to 1000 °C.

1.4 REFERENCES

[1] Eldridge, J.I., "Desktop Fiber Push-Out Apparatus," *NASA Technical Memorandum 105341*, December 1991

[2] Eldridge, J.I. and Ebihara, B.T., "Fiber Pushout Testing Apparatus for Elevated Temperatures," *Journal of Materials Research*, Vol. 9, No. 4, pp. 1035-1042, 1994

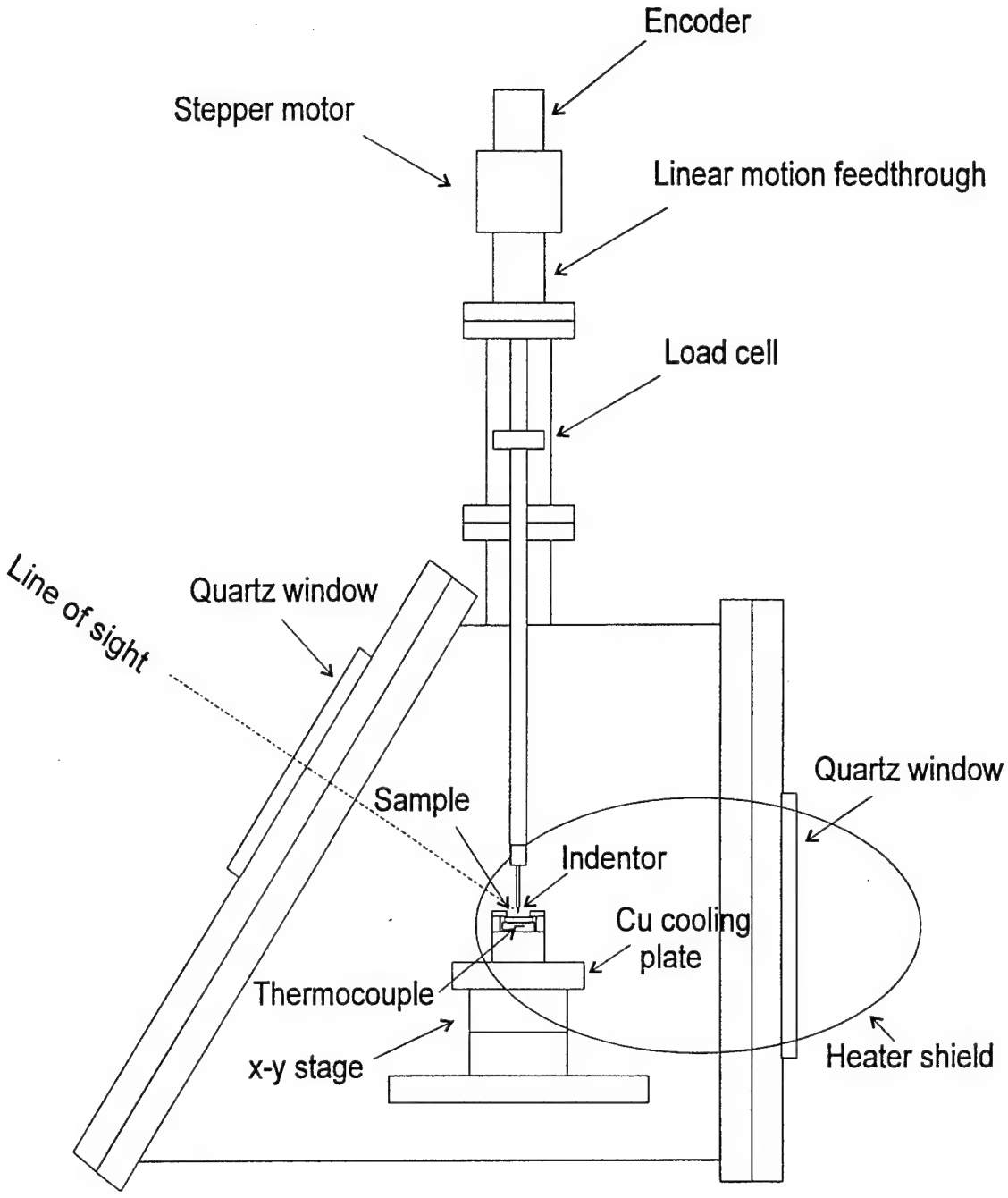

Fig. 1.1 Schematic of Elevated Temperature Fiber Pushout Apparatus

SECTION 2

HIGH TEMPERATURE INTERPHASE BEHAVIOR OF SiC FIBER REINFORCED TITANIUM MATRIX COMPOSITES

ABSTRACT

An experimental study was carried out on two continuous fiber reinforced composites; SM1240/Timetal-21S and SCS-6/Timetal-21S in order to identify the growth mechanisms of the fiber/matrix interphase and their influence on the high temperature bridging fatigue crack growth behavior. Specimens of these two composites have been aged at temperatures ranging from 500-825 °C for up to 600 hours in an air environment. The interphase thickness has been measured and calibrated using Auger Electron Spectroscopy. The interfacial growth has been found to follow the parabolic growth rate law. In order to quantify the shear stress characteristics at the fiber/matrix interface, thin slices of these specimens have been subjected to fiber push-out, employing a displacement-controlled apparatus. The SCS-6 reinforced composite has shown an initial increase, followed by a decrease, with increasing aging time, in both the debond strength, τ_d, and the frictional shear stress, τ_s, indicating the presence of two possible competing mechanisms; growth of the interphase during aging and relaxation of the composite consolidation-induced radial residual stress. SM1240/Timetal-21S has shown similar τ_s behavior, and an initial decrease, followed by an increase, in τ_d. This behavior has been attributed to interfacial growth and the matrix stress relaxation, with the initial drop in τ_s resulting from the increasingly brittle nature of the TiB_2 in the growing interfacial reaction zone. Repeated pushout/pushback testing has also been performed in order to identify the features of the steady state τ_s and the effects of wear on the sliding surfaces.

1.1 INTRODUCTION

The role of the interface in fiber reinforced composites has been established as the key factor controlling the composite behavior. Stiffening and strengthening rely on load transfer across the fiber/matrix interface, toughness is influenced by crack deflection/fiber pullout, and ductility is affected by the relaxation of peak strength near the interface. An in-depth understanding of fiber/matrix interface characteristics in metal matrix composites, particularly those influenced by high temperature thermal exposure, is necessary in order to characterize and optimize the damage tolerance behavior of these composites, including fatigue crack growth.

The fatigue crack growth behavior of fiber reinforced titanium matrix composites is controlled by several mechanisms occurring within the interface, including fiber/matrix debonding, crack bridging, fiber breakage, and fiber pullout and sliding. The introduction of stiff fibers to a ductile material was designed to increase the toughness of the material, while lowering the density. The degree of this toughening, however, is dependent on the characteristics of the interfacial bonding, both chemical and mechanical. A strong interface is desirable for high transverse strength, but an

interface that is very strong will cause the fibers to break simultaneously with the matrix, with no pullout, offering very little improvement over a monolithic material. Conversely, a weak interface is required for fatigue crack growth resistance, but an interface that is too weak will result in little work required for pullout, with little benefit.

In order for a crack to propagate through a fiber reinforced composite material, either fibers must break, or fiber bridging must occur. If fibers are much stronger than the matrix material, as in a metal matrix composite, the fiber/matrix interface tends to debond under the stress field caused by the approaching crack tip, allowing the intact fiber to bridge the matrix crack. This bridging effect shields the crack tip by the amount of load carried by the bridged fibers thereby lowering the crack tip driving force. In titanium matrix composites, the high temperatures required for consolidation of the fiber, coupled with the large difference in coefficients of thermal expansion of the fiber and matrix, result in residual stresses upon cooling. One effect of these stresses is a compressive clamping force on the fiber at the interface. After fiber/matrix debonding, this clamping force causes the two free surface to come in contact with one another, resulting in the introduction of a frictional sliding force along the debonded surfaces. Studies have shown that this sliding results in wear of asperities and deterioration of the interface. [1,2] This is followed by fracture of the fiber, and pullout.

Governing factors for crack bridging during fatigue loading are the crack opening displacement, COD, the fiber bridging stress, Δp, and the fiber/matrix frictional shear stress, τ_s. Various attempts have been made to quantify these parameters, using experimental, analytical, and numerical techniques. Analytical models represent bridging tractions by a closure pressure function c(x) acting in the direction opposite to the applied stress. The need to properly formulate the closure function has led to the development of two analytical models, the shear lag model and the fiber pressure model.

Originally developed by Marshall, Cox and Evans, the shear lag model is based on load transfer from the cracked matrix to fibers through relative sliding between fiber and matrix over a region where interfacial shear stresses exceed the strength of the interface. A force equilibrium of a concentric cylinder model is used to determine the closure pressure, c(x), which is proportional to the square root of the opening displacement and the interfacial shear stresses. The fiber/matrix interface is treated as a purely frictional interface w/ a constant frictional shear force, τ_s. McCartney modified this model by performing an energy balance calculation for bridged fibers instead of the previously used force balance. Since c(x) is a function of the COD which is unknown, an iterative scheme is used to solve for the unknown displacements. Determination of the interfacial shear stresses is generally done through experimental techniques such as fiber pushout or pullout. Studies using different methods to determining τ tend to yield different values.

The fiber pressure model considers the fiber bridged specimen as a structure whose members, the bridged fibers, can carry tensile loads created by normal stresses and/or bending stresses. Strength of materials theory is used to analyze a force balance for the calculation of stresses in a beam subject to bending and/or tensile stresses. To model the effect of bridging on the crack driving force and crack opening displacement, only the closure pressure must be predicted. This closure pressure is assumed to be equal to the stress carried by the fibers in the bridged region averaged out over the total bridged area. This formulation is applicable to systems with very stiff fibers such as metal matrix composites reinforced with ceramic fibers. The closure pressure formulation for the fiber pressure model eliminates the need to determine the shear strength coefficient, τ, and the need for an iterative

solution since c(x) is not a function of displacements.

Limitations exist for both analytical methods. The shear lag model uses a single value of the interfacial shear stress to describe the frictional load transfer over the entire crack wake, which has been proven to be inaccurate, and it ignores frictional wear. The fibers closer to the crack mouth have been exposed to more wear cycles than those near the crack tip. Studies have shown that wear decreases the τ in fatigued crack wake region [1,3] Marshall's [4] findings agree that τ decreases with an increase in interfacial wear. Kantzos [1] has shown that for individual fibers subject to cyclic loading, the amount of interfacial wear is greatest near the crack faces and progressively decreases, which means that τ increases, along the debonded interface length. Both methods described have full solutions that require extremely long, complicated formulas in order to characterize the behavior of the composite during fiber pullout. Experimental procedures are necessary to provide some of the input variables to the analytical solutions and also to obtain a full understanding of the physical process. The experimental methods include fiber pullout, fiber indention, and "thin slice" fiber pushout. Each of these procedures, and various setups within each category, have unique advantages and disadvantages.

Single fiber pullout probably most closely represents the actual conditions in a fiber and the surrounding matrix during crack bridging. In this method, interfacial debonding initiates at the surface where the fiber protrudes from the matrix and the stresses are highest. After partial debonding, the applied stress must overcome the frictional sliding stress at the interface caused by the residual clamping stress, as well as the bond strength of the bonded surface in order for the debond to propagate. Since the debond stress increases with increasing debond length, the stress required to propagate the debond is a function of the previously debonded length. When the debonding is complete, the pullout is simply a function of the frictional sliding stress at the interface. The use of a release agent coating on the fiber before fabrication is used to isolate the effects of frictional sliding on the pullout behavior.

One of the most serious complications involved in the use of single fiber pullout testing is in sample preparation. In general, sample are specially fabricated for use in such a test. A single fiber is embedded along the full length of a block of matrix material, with one end protruding. The matrix material is then clamped, and a uniaxial tensile load is applied to the free end of the fiber in order to pull it out. The size of the block and the manner of gripping is done in such a way as to allow the assumption of no deformation except in the immediate vicinity of the fiber. The special fabrication of this test sample yields very different stress states within the matrix and interface than a sample of actual composite. This fact has led to controversy over the applicability of results of this test to actual composite behavior. A recent development by Marshall [5] attempts to deal with this problem. In this new specimen preparation technique, a strong etchant solution is used to dissolve the matrix of a composite sample, exposing the fibers. A single fiber is chosen, the others cut, and the sample loaded until pullout occurs. A major drawback in the fiber pullout technique lies in the fact that only one set of data can be obtained from each sample.

Relatively simple sample preparation makes the "thin slice" fiber pushout test very appealing. Thin samples which have been cut and polished with the fibers in the 0° orientation are aligned so that the selected fiber is over a hole or groove. When the fiber is pushed, the interfacial shear stress, τ, has a maximum value at the surface where the load is applied and decreases rapidly with depth into the sample Loading was traditionally done with an Instron test frame with load vs. crosshead

displacement recorded regularly as the test progressed. Recently Eldridge [6] proposed a desktop version of this testing apparatus, using a small motor as the loading medium. "Thin slice" fiber pushout tests allow the constant monitoring of load vs. displacement as the fiber pushout progresses, thereby yielding a more complete picture. For these reasons, this is the chosen testing method for this study.

Bending stresses as the thin sample is loaded over a groove have been a major consideration in the analysis of data from thin slice pushout testing. Bending would cause tensile radial stresses at the bottom of the sample and compressive stresses at the point of loading. The tensile stresses would reduce the clamping force on the fiber near the bottom of the sample. It has been proposed that the groove size should be kept to less than two or three fiber diameters [7,8] in order to reduce the effects of these bending stresses to a negligible amount, but whether this solution eliminates the problem is debatable. Koss et al [9] have suggested an innovative method to eliminate bending, wherein a Nickel backplate is applied to a composite slice sample, leaving only the chosen fiber exposed. This is feasible for their studies on sapphire, but not SiC, fiber reinforced composites. Light transmitting characteristics of sapphire were used to develop a photoresist which protected the fiber during plating.

Another key issue in the pushout process is sample thickness. Eldridge [10] has observed no significant difference in the interfacial shear strength for room temperature sample thicknesses from 0.28 to 0.46 millimeters, a fact which he has extended in his studies to high temperature aged samples. However, finite element studies have predicted a significant redistribution of stresses in a thin slice sample, as compared to the bulk composite material. Liang and Hutchinson [8] addressed the issue of redistribution of stresses after cutting a thin slice of composite. They noted that the effect of the redistribution of stresses is to increase the force required to start the interfacial crack propagating down the interface.

The comparison of pushout results from as fabricated samples and fatigued samples cut from just below a matrix fatigue crack has been touched upon recently. Walls et al [3] have observed that pristine fibers exhibit a shear stress which decreases as the fiber is pushed out of the matrix, while fatigued fibers, although initially having a much lower shear stress, show an increase with pushout distance. This difference has been attributed to wear of asperities in the pristine fibers, and extensive fragmentation of the fiber coating in the fatigued samples.

Fiber indention methods, which were first introduced by Marshall, also allow the use of already fabricated composite samples. Sample preparation is similar to that in thin slice fiber pushout, although samples may be considerable thicker. The sample is clamped in such a way that a single fiber can be loaded. An indentor, usually either a microhardness indentor or nano indentor is used to push on the fiber. The load is gradually increased until fiber displacement is observed. The load is then slowly removed and the penetration of the tip into the matrix is measured. subtracted from the total tip movement to yield displacement of the fiber. Since the interface has completely debonded, flipping the sample and pushing on the protruding end of the fiber yields the frictional shear stress at the debonded interface. Generally, constant bending stress and frictional stress are assumed. It seems that thin slice fiber pushout methods, which yield more continuous information during the pushout process, are becoming more popular than fiber indention methods.

Results for fiber pushout and pullout of similar composite systems vary dramatically. Walls et al [3] have shown that, for the same embedded fiber length, the stress required for fiber pushout is

always greater than that for pullout. These differences have been attributed to the difference in the Poisson effect for each type of loading. During pushout, the Poisson effect causes an expansion of the fiber, which enhances the effect of the clamping stress on the frictional sliding behavior. The result of the Poisson effect during pullout is to contract the fiber, serving to reduce the effect of the clamping force and lower the shear frictional sliding stress. Many years ago, Takaku and Arridge [11] observed the variation of pullout stresses with embedded length as a result of the decrease in frictional stress due to the Poisson contraction of a steel wire. They noted that, in the absence of the Poisson effect, the interfacial frictional stress is constant along the frictional interface, and the pushout and pullout cases are similar. Many researchers have assumed a constant interfacial shear stress along the length of the fiber. The existence of the Poisson expansion or contraction make this assumption invalid to at least some degree, unless the embedded length is very short. Additionally, a significant difference occurs in the relative locations of shear and radial stresses along the embedded length of the fiber. For pullout, the shear and radial stresses are maximum near the surface where the load is applied, while in pushout configuration, the radial stress is highest at the end opposite to the maximum shear stress. Kerans & Parasarathy [7], as well as Marshall [12] have developed detailed analysis of the pullout/pushout curves obtained from experimental testing.

There has been little experimental work done to investigate the interfacial behavior at high temperatures. Recently Eldridge [10] used a high temperature pushout technique to study the temperature dependence of fiber debonding and sliding in intermetallic and metallic matrix composites. Results indicate that at low temperatures (below 300-400°C), the reduction in shear and radial stresses which occur upon heating have little effect on the load required for debonding. A drop in the average shear stress was observed at higher temperatures, leading to two possible causes. It was speculated that the location of the maximum total shear stress, the site of the mode II debond initiation, may change from the bottom of the samples at low temperature to the top of the samples at high temperatures. The other possibility was that at higher temperatures, the reduction in residual clamping stress may allow mode I debonding to occur at the bottom of the sample, although no evidence to support this theory was found during SEM observations.

When the composite system is used at high temperature, as intended, the issue of chemical interactions between the fiber/coatings and matrix have to be considered. At elevated temperatures, the fiber matrix interface is not at equilibrium. Many studies have been performed involving interfacial kinetics at various aging times and temperature in order to try to characterize this behavior.[13,14,5] It has been noted that reactions at the interphase tend to form brittle reaction products which can adversely effect the mechanical properties of the interphase, and hence, the composite as a whole. Generally the samples studied have been vacuum encapsulated, furnace heat treated to the desired time and temperature, then studied using scanning electron microscopy (SEM), Auger analysis, Electron probe microanalysis (EPMA), etc. to measure the reaction zone thickness as well as the chemical makeup of the interphase and surrounding matrix region. Such studies have shown that the titanium, and sometimes alloying elements, in the matrix reacts extensively with the SiC fiber and its coatings to increase the size of the interphase [15] Watson and Clyne [16] have observed an increase in the frictional sliding resistance during pushout testing with increased aging time. Currently, several different titanium alloys have been studied as matrix material. Each exhibits aging characteristics unique to the particular structure of the alloy. The location of the interfacial fracture has been observed to be a function of both alloy type and aging conditions.

Fatigue crack growth tests have indicated that temperature and aging conditions do indeed affect the crack growth behavior of metal matrix composites. Such tests performed by Zheng and Ghonem [17] at 24, 500, and 650 °C have shown an decrease in the crack growth rate, corresponding to an increase in crack tip shielding, with increasing test temperature during the initial crack bridging stage. (Figure 2-1) This observations confirms that the crack tip shielding force is a function of test temperature. It was also observed that crack lengths at the end of the crack bridging stage decreased and average fiber pullout lengths increased as test temperature increased.

Additional fatigue testing, at room temperature, of samples aged at 650 °C for 40 hours (approximately the time duration of a fatigue crack growth test) and as received samples can be used to support the idea of a mechanism which enhances the crack growth rate. (Figure 2-2) The very similar initial crack growth rates suggest that aging conditions have no effect on the behavior during the initial crack bridging stage. However, the transition from decelerated to accelerated crack growth occurs at a much lower applied stress intensity factor, or crack length, for the unaged sample than for the aged sample. This difference suggests that modifications which occur during the high temperature aging process, possibly phase changes, are an important factor in the total crack growth behavior of a metal matrix composite.

In systems containing multiple phases, crack growth testing should be done under conditions where phase stability is encouraged. Changes in temperature induce phase changes in the composite material, particularly in the reaction zone. For this reason, comparison of room temperature and high temperature fatigue crack growth data dictates that the room temperature samples be heat treated to stabilize the phases which occur at the corresponding high temperatures. The results of such tests would explain the influence of temperature only on the crack growth process. However, tests carried out without the pre-aging procedure include the role of phases and their response to temperature on the crack growth rate. These tests, such as those performed by Zheng and Ghonem, indicate that a combined temperature and possible phase growth during the high temperature testing could alter the crack tip driving force.

The previous studies of the fatigue crack growth and fiber pushout behavior of fiber reinforced composites have left many issues in need of clarification. Finding answers to these questions, through an in-depth investigation of the effects of temperature on the fiber debonding and sliding behavior of fiber reinforced titanium matrix composites, is the objective of this research. In order to better understand the effect of the interfacial reactions on the interfacial behavior of a composite, two composite systems were chosen. Each have the same matrix, but are reinforced with silicon carbide fibers with different coatings. One of the fibers contains an outer coating of titanium diboride, designed to control the interfacial reaction zone growth. A comparison of room temperature and high temperature pushout testing of aged samples will elucidate the effects of high temperatures on the residual stress state of a composite material. By comparing the pushout results of samples aged in a vacuum with those aged in air, the effects of the environment, including oxidation at the interphase, will be isolated.

This understanding of the interfacial behavior of the composite, particularly the shear strength and frictional shear stress, can then be applied to the fatigue crack growth behavior of titanium matrix composites. It is well known that the crack growth rate, da/dN, is governed in part, by ΔK_{eff}, the effective crack tip driving force, which is in turn dictated by the frictional sliding shear stress, τ_s at the interfacial debonding crack. The fiber pressure p, also plays a significant role in controlling da/dN.

The fiber pressure is a function of τ_d, the interfacial debond strength.

The consolidation conditions of time, temperature and pressure are also factors in the crack growth process since they directly influence the interfacial behavior. Using pushout testing, the frictional shear stress for various aging conditions can be determined, for both room temperature and high temperature conditions. Fatigue tests can be used to generate values for the crack growth rate, da/dN, for samples with similar aging histories. The comparison of data from these two types of tests will enable a direct relationship to be determined between these two important parameters. This relationship would allow the crack growth rate of a composite material to be determined by a few simple pushout tests, rather than long-term fatigue crack growth tests.

In addition to the determination of the fatigue crack growth behavior from pushout testing, the experimental data can also be used for the optimization of the composite systems. In processing a composite, many combinations of processing time, temperature, and pressure are known to produce a satisfactorily consolidated material. Since these processing conditions effect the residual stress state of the composite material, it is expected that there exists an optimum combination of parameters for any given application. A comparison of pushout test results, and the associated fatigue crack growth rates, with varying processing parameters will establish the significance of each parameter on the mechanical behavior of the composite material. This will give guidelines for controlling desired characteristics of a composite through the consolidation process.

2.2 MATERIAL AND EXPERIMENTAL PROCEDURE

Two continuous unidirectional fiber reinforced composite systems were chosen for this study, both having the same matrix, Timetal-21S, a metastable β titanium alloy. The chemical composition of Timetal-S (in wt.%) is 0.1 Fe, 16.0 Mo, 3.06 Al, 2.9 Nb, 0.2 Si, 0.22 C, 0.12 O, 0.005 N with the balance being Ti. Fiber reinforcement consisted of either SM1240 in a 6-ply composite or SCS-6 SiC fiber in a 4-ply composite. The SM1240 fiber is a 100 μm diameter tungsten cored chemical vapor deposited SiC fiber with a 1 μm inner coating of pyrocarbon and a 1 μm outer coating of titanium diboride. The 140 μm SCS-6 fiber is chemical vapor deposited on a carbon core with a 3 μm dual carbon coating.

Initial cutting of the samples was similar for the pushout study and the aging study. Samples approximately 10 mm thick were cut from a panel on a diamond wafering blade, with the crossection of the fibers perpendicular to the face of the sample. The samples were aged in an electric furnace in an air environment. Test temperatures were chosen as 500, 650, 750, and 875 °C (825 °C for the pushout testing) and aging times from 2 - 600 hours. The 500 °C corresponds to the expected use condition, 650 °C to the upper limit use of the matrix material, 750 °C to an extreme test temperature, and 875 °C to the processing condition.

2.2.1 Aging Study

Specimens for the aging study were sectioned near the midplane of the sample after thermal exposure, and mounted with the fiber crossections exposed, in an epoxy resin. One side was rough ground using progressively finer grits of silicon carbide paper from 320 grit through 600 grit. Final

polishing was done with 9 μm, 3 μm, and 1 μm diamond spray on nylon cloth. A light (10-15 sec) etching with Kroll's etchant was performed on the SM1240/Timetal-21S samples in order to better define the interphase boundaries. For each sample, four typical fibers were chosen, avoiding the fibers along the edges of the sample. The size of the interfacial reaction zone was measured with a scanning electron microscope in 65 locations around the circumference of each of the four chosen fibers. The appearance of the carbon layer was also noted for each fiber. The average interfacial reaction zone thickness was taken to be the mean of the resultant measurements for the sample under investigation.

2.2.2 Fiber Pushout Study

After thermal exposure, samples for the pushout study were sectioned, with material removed from both sides of the sample, leaving the center section approximately 500 μm thick. This center section was mounted on an aluminum block with a mounting wax and one side was ground and polished similar to the samples in the aging study. The other side was then similarly polished down to a 1 μm finish until a final thickness of approximately 250-320 μm was attained. An optical micrograph was taken of the sample, and fibers were chosen which were aligned with grooves in the sample base.

The pushout apparatus used in this study is illustrated and described in detail in Section 1.

2.3 RESULTS AND DISCUSSION

2.3.1. Aging Study

In order to isolate the effects of a phase growth in the composite during high temperature exposure, an aging study was performed. Various aging time/temperature combinations, ranging from 2-250 hours and 500 °C to 875 °C, were chosen for investigation. Scanning Electron Microscopy (SEM) was used to measure the interfacial reaction zone size for each sample. These measurements were verified using Auger Electron Spectroscopy (AES) across the fiber/matrix interface region. Figures 2-3(a)-(b) and 2-4 show examples of plots of the AES data taken across the fiber/matrix interphase of both composite systems. Fairly good agreement is seen between the two methods the SEM measurements and the AES result. It should be noted that, for the composite with the SCS-6 fibers, the interphase thickness was measured from the outer edge of the carbon layer to the outer edge of the reaction zone, both of which were easy to distinguish visually. Although the samples containing the SM1240 fibers were etched in order to locate the outer edge of the reaction zone, the boundary between the TiB_2 and the reaction zone was not clear, so the interphase thickness was measured from the outer edge of the inner carbon layer to the outer edge of the reaction zone.

Figures 2-5(a)-(d) and 2-6(a)-(d) illustrate typical interphase observations for the samples indicated. Figures 2-7 and 2-8 summarize the changes in reaction zone size for varying temperatures and time durations, as measured for the two composite systems. For both composite systems, reaction zone thickness increases linearly with the square root of time at a given temperature, as expected from previous work done on the aging of titanium matrix composites [30,15] The parabolic growth law can be used to model the reaction zone kinetics of either composite as

$$X = kt^{\frac{1}{2}} + b$$

where X is the average reaction zone thickness, t is the exposure time at the specified temperature, k is the reaction rate constant for that temperature, and b is the unaged reaction zone thickness. The temperature dependence of the reaction rate, k, can be expressed as an Arrhenius type of relationship

$$k = k_o \, e^{\frac{-Q}{2RT}}$$

where k_0 is a constant, T is absolute temperature, R is the gas constant, and Q is the activation energy for the system which can be obtained by plotting the natural logarithm of reaction rates vs. the inverse of absolute temperature. Figure 2-9 shows these plots for both composite systems. Table 1 shows the calculated values for the activation energy, Q.

Table 1.1: Activation energy of two composite systems

Activation Energy	SM1240	SCS-6
Q (kcal/mol)	39.69	30.44
Q (kJ/mol)	166.14	127.42

The activation energy for the composite reinforced with SM1240 fibers has a higher activation energy than that with the SCS-6 fibers. This higher activation energy is an indication of the ability of the titanium diboride outer coating on the SM1240 fibers to inhibit the diffusion process at the interface, particularly at very high temperatures.

It is interesting to note the effect of high temperature oxidation on a fiber/matrix interface. Figure 2-10(a) shows several fibers whose interfaces were debonded before thermal exposure. Closer examination of the interface in Figure 2-10(b) suggests that the carbon layer has oxidized completely due to the ease in which oxygen can migrate through the debonded interface. Auger Electron Spectroscopy confirms this premise. As expected, analysis of an intact interface such as that in Figure 2-5(d) yields peaks corresponding to C in the dark region and Ti and O in the lighter reaction zone. Analysis of the previously debonded interface, however, yields peaks which correspond to only Ti and O in the interface region. This indicates that the carbon layers have reacted with the oxygen to form volatile gases, while the titanium oxidized extensively to fill the gap left by the depleted carbon.

2.3.2 Fiber Pushout Study

In order to determine the effect of the aging induced interfacial changes on interfacial shear stress, room temperature "thin slice" pushout tests were performed on aged and unaged samples of the SM1240/Timetal-21S composite. (See Appendix #1 for a schematic and full description of the fiber pushout apparatus.) Approximately 6 fibers were pushed out from each sample, which represented various combinations of aging time, aging temperature, and composite type. Fiber loading was applied in continuous steps corresponding to a punch displacement of 0.0125 μm/step. Applied force from the load cell and motor displacement from the encoder were collected at every step, and averaged over the resolution of the encoder measurements. A typical pushout curve, a plot of load vs. displacement, for room temperature tests at each of several aging time/temperature conditions is shown in Figures 2-11 and 2-12. At the force required to debond the interface, a load drop occurs and visual evidence of fiber displacement was observed. The load then increases to a maximum force value. This maximum is followed by first, a rapid decrease in the load, then by a very slow decrease in load. This "steady state" portion of the curve, indicated by a slowly decreasing load, corresponds to the steady state frictional sliding shear stress. The load is decreasing because the embedded fiber length is decreasing. The peak at the maximum force is a result of debris between the two sliding surfaces at the debond crack. When the interphase is broken, pieces of the fractured layer increase the force necessary to slide the fiber out of the matrix. This debris gradually wears into smaller particles, which causes a reduction in the force as the displacement increases. Eventually, the surface will wear relatively smooth, allowing the shear stress to be purely frictional. This results in the steady state portion of the curve.

The frictional shear stress, τ_s, is calculated at any point on the load/displacement curve as

$$\tau = \frac{P}{\pi d_f l_e}$$

where P is the applied load, πd_f is the crossectional area of the fiber, and l_e is the embedded fiber length. At the debond force, F_d, the embedded length is taken to be the thickness of the composite sample. The embedded length at any point after debonding is calculated by subtracting the displacement from the sample thickness.

Due to the nature of the sample preparation, an exact measurement of sample thickness at each fiber is not exact. The thickness varies slightly along the length and width of the sample. The effect of such inaccuracies in thickness measurements on the calculated shear stress values was investigated by varying only sample thickness in the calculation of shear stress for a typical shear stress vs. fiber displacement plot. (Figure 2-13) This plot shows that an inaccuracy of up to approximately 20 μm (which is a reasonable estimate of the measurement error) has very little effect on the calculated values of the interfacial shear stress.

Plots of the interfacial shear stresses vs. aging time for SCS-6/Timetal-21S and SM1240/Timetal-21S are shown in Figures 2-14(a)-(c) and 2-15(a)-(b). (Note that the unaged condition of each composite is considered to be equivalent to a 0 hr aging time for each aging temperature.) The composite with the SM1240 fibers shows a more complex behavior, as would be expected from the

addition of the TiB_2 at the interphase.

2.3.3 The SM-1240/Timetal-21S Composite

The SM1240 reinforced composite show an initial drop in debond strength, τ_d, and an increase in the steady state shear stress, τ_s, within an aging time of approximately 50 hours or less, for all aging temperatures investigated. After this drop, the debond strength of the interphase, τ_d, is independent of the aging time for an aging temperature of 500 °C. At a slightly higher temperature, 650 °C, aging time has only a minimal effect on increasing τ_d, while τ_s decreases. Samples aged at very high temperatures, 875 °C, show a profound effect of aging time on interfacial shear stress. After the initial drop, a dramatic increase in the debond shear stress occurs in a very short amount of time (less than 50 hours.) This increase corresponds to a similarly dramatic rise and fall of the steady state shear stress. (It is hypothesized that, for the samples aged at 500 °C, the steady state shear stress, after extensive aging time, may approach the trend of the 650 °C and 825 °C samples.)

Analysis of the behavior of this composite indicates that at least two simultaneously occurring mechanisms are involved in controlling the interfacial stress state. Initially, the prominent mechanism could be the growth of the interfacial reaction zone, as seen in the aging study. The increase in size of the reaction zone with increasing aging time could cause an increase in the clamping force on the fiber, which would increase τ_s, the frictional sliding stress. The brittle nature of the reaction products, due to the TiB_2, could explain the reduction in the interfacial debond stress, particularly at higher aging temperatures. A reduction in the yield strength at the interphase would allow a brittle fracture to occur at a lower applied force than for a more ductile material, reducing the force necessary to propagate a debond crack through the interphase, resulting in the lower debond shear stress.

After a sufficient amount of time, significant relaxation of the matrix material may occur. At short aging times, this relaxation may be very slight, so as not to be noticed. As aging time increases, this relaxation becomes the prominent mechanism at the interface, overcoming the effect of the increasing interfacial reaction zone size. Matrix relaxation would reduce the force required to slide the fiber out of the matrix, thereby reducing the steady state shear stress. At higher aging temperatures, this phenomena would occur more quickly than at lower aging temperatures. An extreme case of matrix relaxation could explain why, at 825 °C for 42.5 hours aging, it was observed that the debond shear stress and the maximum shear stress occurred coincidently. During aging at such a high temperature, the matrix could relax enough so that no significant compressive residual forces exist, therefore when the crack has propagated the entire length of the sample, no significant increase in clamping forces occur. The cause of the increase, after the initial drop, in the debond stress at 825 °C is currently under investigation.

A plot of the relatively steady value of the interfacial debond stress (after the initial drop) vs. aging temperature, for the SM1240/Timetal-21S is shown in Figure 2-14(c). This curve indicates that the value of τ_s decreases as aging temperature increases.

To date, studies under the SEM of pushed out fiber surfaces have revealed no significant difference in surface morphology between samples aged at different temperatures or aging times. Figure 2-16(a) shows a typical surface of a pushed out fiber at any aging temperature and time duration. In several places on fiber surfaces for each temperature or time duration, patches of

material with a different morphology are seen, adhered to the fiber surface, as shown in Figure 2-16(b). Observation of these areas, the underlying areas, and the base of the pushed out fibers indicate that the typical interphase fracture region is between layers of the carbon coating. The patches on the fiber surface appear to be pieces of titanium diboride which have been fractured, and remain attached to the carbon layer. Currently, attempts at verifying the fracture location using Auger analysis to verify the composition of the fiber surface are underway.

2.3.4 The SCS-6/Timetal-21S Composite

The plot of interfacial shear stress vs. aging time for the SCS-6 reinforced composite are shown in Figure 2-15. This composite system shows an initial increase in both the debond strength and the steady state shear stress within 50 hours aging or less, for all aging temperatures investigated. This increase is attributed to the initial growth of the interphase during the aging process. After aging for 50 hours, the steady state shear stress is independent of aging time 500 °C. At the higher aging temperatures, a steady decrease in τ_s is seen in the 650 °C aged samples, and a similar but more dramatic decrease in the 825 °C aged samples, with increasing aging times. Additionally, debond strength decreases with increasing aging time and increasing temperature for both the 500 °C and the 650 °C aged samples. The 825 °C aged sample also seems to be following this trend. As with the SM1240 reinforced composite, relaxation of the matrix stresses can explain the decrease in the stresses after the initial increase. During the shorter aging times, this relaxation is not significant. Also, since the coatings on the SCS-6 fibers are carbon, the interface of this composite is subject to oxidation during aging in an air environment, particularly at the higher temperatures. This oxidation explains the dramatic decrease in the interfacial steady state shear stress at 825 °C after a very short time. Evidence of this oxidation has been observed during SEM investigation at longer aging time for this composite system. This oxidation would causes a reduction in the clamping force on the fiber, reducing both the debond strength and the steady state shear stress at these temperatures. Embrittlement of the carbon at the higher temperatures would also reduce the debond stress, as a brittle material would fracture at a lower shear stress than the more ductile carbon which was exposed to the lower temperature of 500 °C.

Figure 2-17 shows the typical surface of a pushed out fiber. This morphology of the fiber surface in this figure indicates that the location of the debonding and sliding is occurring between or within the layers of C coatings.

As discussed in reference to typical pushout curves for the samples studied, wear plays a significant role in the fiber sliding of these composites. Some understanding of the wear dependency of τ_s has been achieved through preliminary pushout/pushback tests. In this type of test, a fiber is pushed out, as in a normal pushout test, then the sample is inverted, and the protruding fiber is pushed back through the matrix. Figure 2-18 shows a typical pushback curve. The initial load drop which occurs in the pushback test is not nearly as dramatic as in the first pushout, because the fiber interface was fully debonded during previous pushout. The load required for the fiber to move is determined only by frictional sliding at the interface. On fibers that were pushed out a short distance (30-40 μm) a "seating drop" is observed when the fiber passes through its original position. This is because surface asperities are not uniform along the length of the fiber. The original position is the only location where the two surfaces match exactly. The fibers that were pushed out farther (~ 80 μm or

more) do not show a noticeable seating drop, probably because some of the surface roughness has been worn as the interfacial surfaces slid over each other. Preliminary pushout/pushback/pushout tests, in which the fiber is pushed through the sample 3 times have revealed that the fibers that were initially pushed the shorter distance show a decrease in the steady state frictional sliding stress with each push. Conversely, those fibers initially pushed out the longer distances do not show a significant drop in τ_s during the pushback test. These observations indicate that wear plays a significant role in fiber sliding behavior, and needs to be studied more closely.

The results of the room temperature pushout tests help to explain the fatigue crack growth data for the SM1240 reinforced composite samples shown in Figure 2-2. The pushout tests indicate that aging at 650 °C, causes an increase in the frictional shear stress and a decrease in the debond shear stress compared to unaged conditions. The decrease in the debond stress would allow the debond crack to propagate along fiber/matrix interface at a lower applied stress, thereby dissipating energy required to increase the Mode II crack. The increase in the frictional shear stress would require more energy to slide the fibers within the matrix under fiber bridging conditions, diverting that energy from the Mode II crack. These conditions, occurring in a fatigue situation, are conducive to increased crack tip shielding. This increase in the shielding would cause longer crack lengths during the initial crack bridging stage, and cause the transition from fiber bridging to accelerated crack growth to occur at a higher applied stress intensity factor, as indicated by the room temperature fatigue crack growth tests.

2.4 SUMMARY

- Aging increases the interphase thickness according to the parabolic rate law:
$$X = kt^{1/2} + b$$

- The composite reinforced with SM1240 fibers has a higher interfacial activation energy then that reinforced with SCS-6 fibers.

- Interfacial shear stress is aging time and temperature dependent

- For Timetal-21/SM1240, at least two mechanisms control the interfacial behavior: growth of the interphase dominates at shorter aging times, while relaxation of the matrix stresses dominates at longer aging times.

- Interfacial fracture occurs predominantly between the carbon and TiB_2 layers for SM1240/Timetal-21S and between layers of carbon for SCS-6/Timetal-21S.

- Wear significantly influences the interfacial sliding behavior, but this effect saturates within a few hundred μm fiber sliding distance.

2.5 REFERENCES

[1] Kantzos, P., Ghosn, L. and Telesman, J., "The Effect of Degradation of the Interface and Fiber Properties on Crack Bridging," *HITEMP Review*, Vol. 2, Cleveland, OH, pp. 32-1 - 32-14, 1992

[2] Warren, P.D., Mackin, T.J., Evans, A.G., "Design , Analysis and Application of an Improved Push-Through Test for the Measurement of Interface Properties in Composites," *Acta. metall. mater.*, Vol. 40, No. 6, pp. 1243-1249, 1992

[3] Walls, D., Bao, G., Zok, F., "Fatigue Crack Growth in a Ti/SiC Composite," *Fatigue of Advanced Materials*, pp. 343-356, January 1991

[4] Marshall, D.B., Oliver, W.C., "Measurement of Interfacial Mechanical Properties in Fiber-Reinforced Ceramic Composites," *Journal of the American Ceramic Society*, Vol. 70, No. 8, pp.542-548,1987

[5] Marshall, D.B., Shaw, M.C., Morris, W.L., Graves, J., "Interfacial Properties and Residual Stresses in Titanium and Titanium Aluminide Matrix Composites," *Workshop proceedings on Titanium Matrix Components*, P.R. Smith and W.C. Revelos, eds., Wright-Patterson AFB, OH, pp. 329-347, 1991

[6] Eldridge, J.I., "Desktop Fiber Pushout Apparatus", *NASA Technical Memorandum 105341*, December, 1991

[7] Kerans, R. J., and Parthasarathy, T.A., "Theoretical Analysis of the Fiber Pullout and Pushout Tests," *Journal of the American Ceramic Society*, Vol. 74, pp.1585-1596, 1991

[8] Liang, C., Hutchinson, J., "Mechanics of the Fiber Pushout Test," *Mechanics of Materials*, Vol. 14, pp. 207-221, 1993

[9] Koss, D. A. , Rhyne, E. P., Kallas, M. N., Hellman, J. R., "Test Techniques and the Determinations of Interfacial Shear in Metallic Matrix Composites," *Proceedings of 5th Hitemp Review*, 1993

[10] Eldridge, J.I., Ebihara, B.T., "Fiber Pushout Testing Apparatus for Elevated Temperatures," *Journal of Materials Research*, Vol. 9, No. 4, pp. 1035-1042, 1994

[11] Takaku, A. and Arridge, RGC, "The Effect of Interfacial Radial and Shear Stress in Fibre Pull-out in Composite Materials," *J. Phys. D: Appl. Phys.*, Vol. 6, pp. 2038-2047, 1973

[12] Marshall, D., "Analysis of Fiber Debonding and Sliding Experiments in Brittle Matrix Composites," *Acta metall. mater.*, Vol. 40, No. 3, pp. 427-441, 1992

[13] Caulfield, T. and Tien, J. K., "High Temperature Reaction Zone Growth in Tungsten Fiber Reinforced Superalloy Composites: Part I. Application of the Moving Boundary Equations," *Met. Trans.*, Vol. 20A, pp.255-266, 1989

[14] Bilba, K., Manaud, P., Petitcorps, Y. Le and Quenisset, J. M., "Investigation of Diffusion Barrier Coatings on SiC Monofilaments for Use in Titanium-Based Composites," *Material Science and Engineering*, Vol. 135A, pp.141-144, 1991

[15] Yang, J.-M., Jeng, S.M., "Interfacial Reactions in Titanium-Matrix Composites," *Journal of Metals*, pp. 56-59, November 1989

[16] Watson, M.C., Clyne, T.W., "The Use of Pushout Testing to Investigate the Interfacial Mechanical Properties of Ti-SiC Monofilament Composites," 7th World Titanium Conference, San Diego, June 1992

[17] Zheng, D., Ghonem, H., "High temperature/High Frequency Fatigue Crack Growth Damage Mechanisms in Titanium Metal Matrix Composites," *Life Prediction Methodology for Titanium Matrix Cmposites*, ASTM STP 1253, J.M. Larson and B.N. Cox, eds., American Society for testing and Materials, Philadelphia, PA, 1995

[18] Gundel, D.B., Wawner, F.E., "Interfacial Reaction Kinetics of coated SiC Fibers with Various Titanium Alloys", Scripta Metallurgica et Materialial Vol. 25, pp. 437-441, 1991

[19] Hancock, J. R., "Composite Materials," Vol. 5, ed. by L. J. Broutman, Academic Press, New York, 1974, pp.371-414

[20] Shetty, D. K., "Shear Lag Analysis of Fiber Push-out (Indentation) Tests for Estimating Interfacial Friction Stress in Ceramic-Matrix Composites, *Journal of the American Ceramic Society*, Vol. 71, pp.C107-109, 1988

[21] Hsueh, C. H., "Evaluation of Interfacial Shear Strength, Residual Clamping Stress and Coefficient of Friction for Fiber-Reinforced Ceramic Composites, *Acta Met. et Mat.*, Vol. 38, 1990, pp.403-409

[22] Kallas, M. N., Koss, D. A., Hahn, H. T. and J. R. Hellman, "Interfacial Stress State Present in a 'Thin Slice' Fiber Push-out Test," *J. Mat. Sci.*, Vol. 27, pp. 3821-3826

[23] Bischoff, E., Ruhle, M., Sbaizero, O., and Evans, A., "Microstructural Studies of the Interfacial Zone of a SiC-Fiber-Reinforced Lithium Aluminum Silicate Glass-Ceramic," *Journal of the American Ceramic Society*, Vol. 72, No. 5, 1989

[24] Tsai, H.C., Arocho, A.M., Gause, L.W., "Prediction of Fiber-Matrix Interphase Properties and their Influence on Interface Stress, Displacement and Fracture Toughness of Composite Material," *Materials Science and Engineering*, A126, pp. 295-304, 1990

[25] Mall, S., Ermer, P.G., "Thermal Fatigue Behavior of a Unidirectional SCS6/Ti-15-3 Metal Matrix Composite", *Journal of Composite Materials*, Vol. 25, December 1991

[26] Campbell, M.D., Cherry, B.W., "Fatigue Crack Propagation in Fibre Reinforced Composite Materials," Fracture Mechanics and Technology proceedings

[27] Chan, K.S., "Effects of Interface Degradation on Fiber Bridging of Composite Fatigue Cracks", *Acta. metall. mater.*, Vol. 41, No. 3, pp. 761-768, 1993

[28] Cox, B.N., Marshall, D.B., "Overview No. 111: Concepts for Bridged Cracks in Fracture and Fatigue," *Acta. metall. mater.*, Vol. 42, No. 2, pp. 341-363, 1994

[29] Watson, M.C., Clyne, T.W., "The Tensioned Pushout Test for Fibre-Matrix Characterization Under Mixed Mode Loading," *Materials Science and Engineering*, A160, pp.1-5, 1993

[30] Holmes, J.W., Jones, J.W., Wu, X., Hilmas, G.E., "Techniques for Testing Fiber-Reinforced Composites in Tension"

[31] Warren, P. D., Mackin, T. J., Evans, A. G., "Design, Analysis and Application of an Improved Push-Through Test for the Measurement of Interface Properties in Composites," Acta metall. mater., Vol 40, No. 6, pp. 1243-1249, 1992

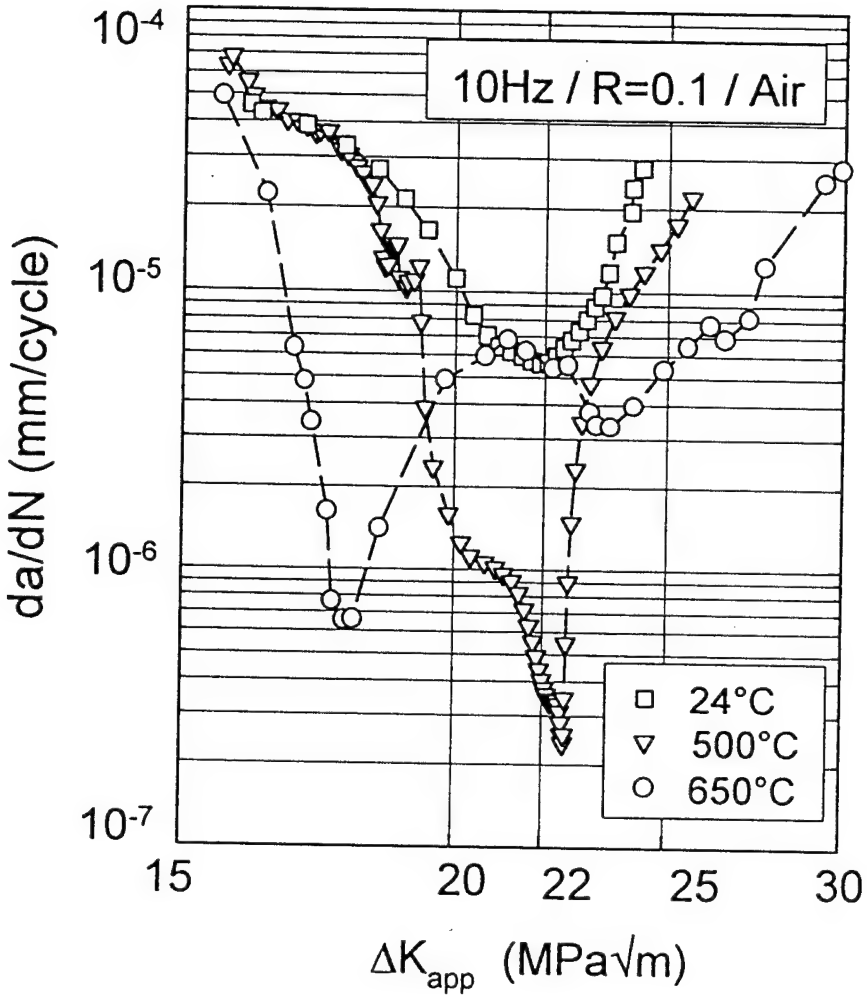

Fig. 2-1 Fatigue crack growth rates da/dN vs. applied stress intensity factor, ΔK_a, for various temperatures at 10 Hz

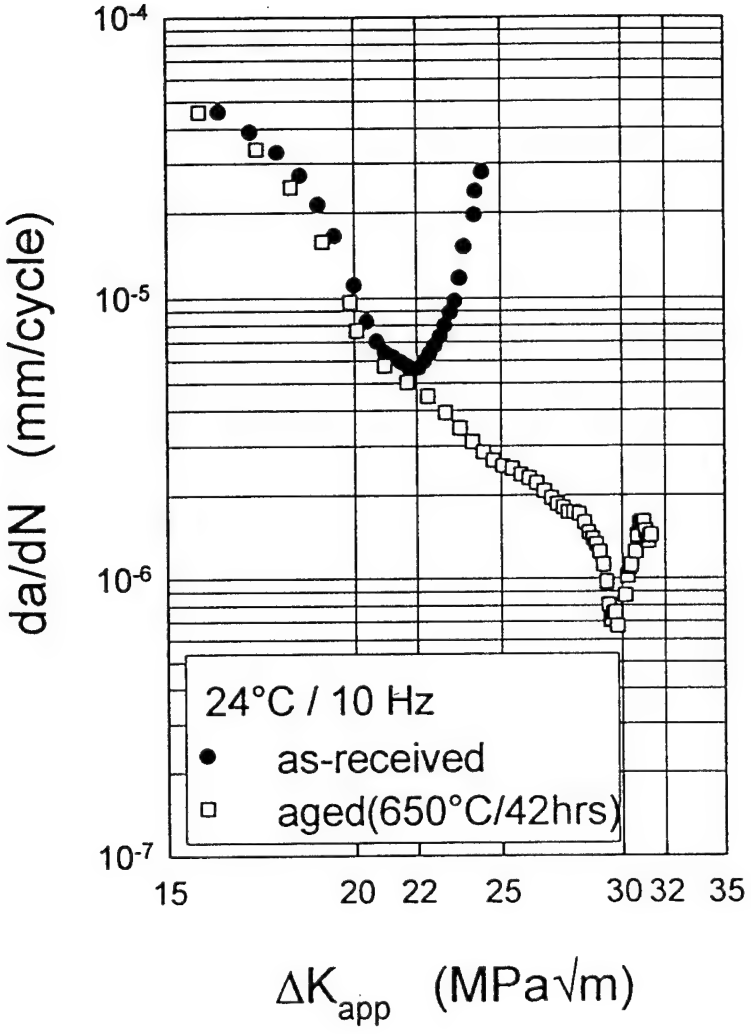

Fig. 2-2 Fatigue crack growth rates da/dN vs. applied stress intensity factor, ΔK_a, for aged and unaged samples at 24°C and 10 Hz

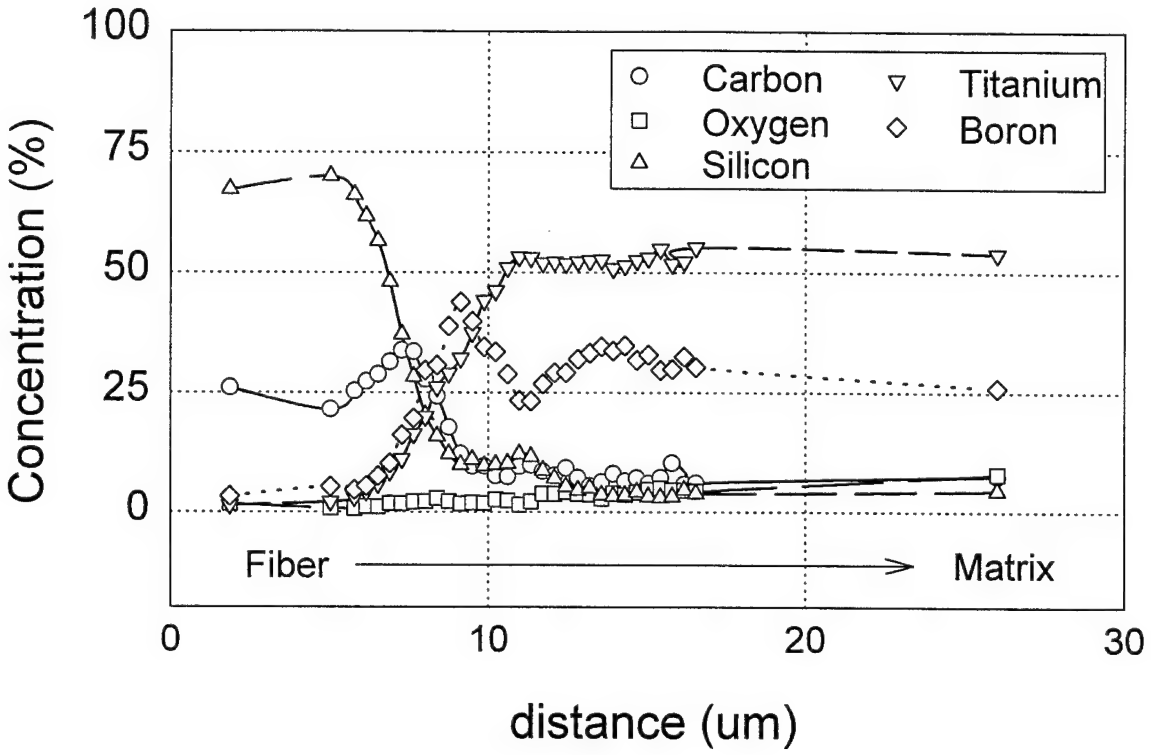

Fig. 2-3(a) Auger Electron Spectroscopy compositional data for SM1240/Timetal-21S fiber/matrix interface

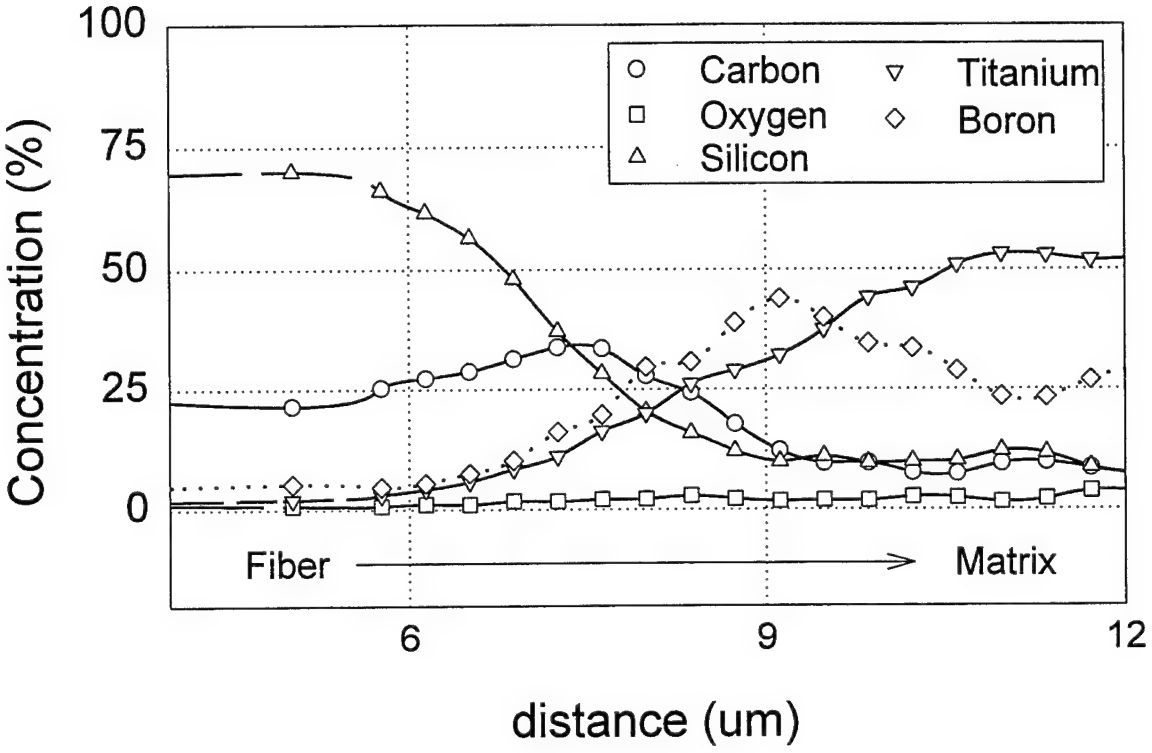

Fig. 2-3(b) Auger Electron Spectroscopy compositional data for SM1240/Timetal-21S fiber/matrix interface (closeup)

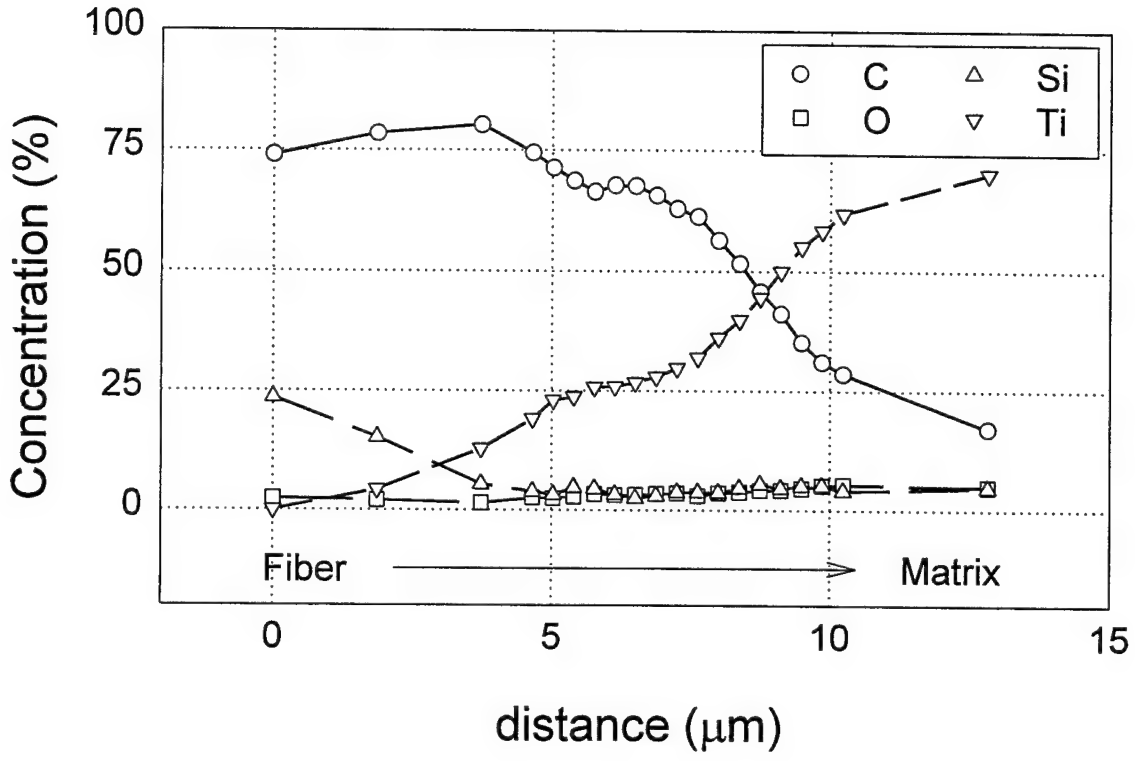

Fig. 2-4 Auger Electron Spectroscopy compositional data for SCS-6/Timetal-21S fiber/matrix interface

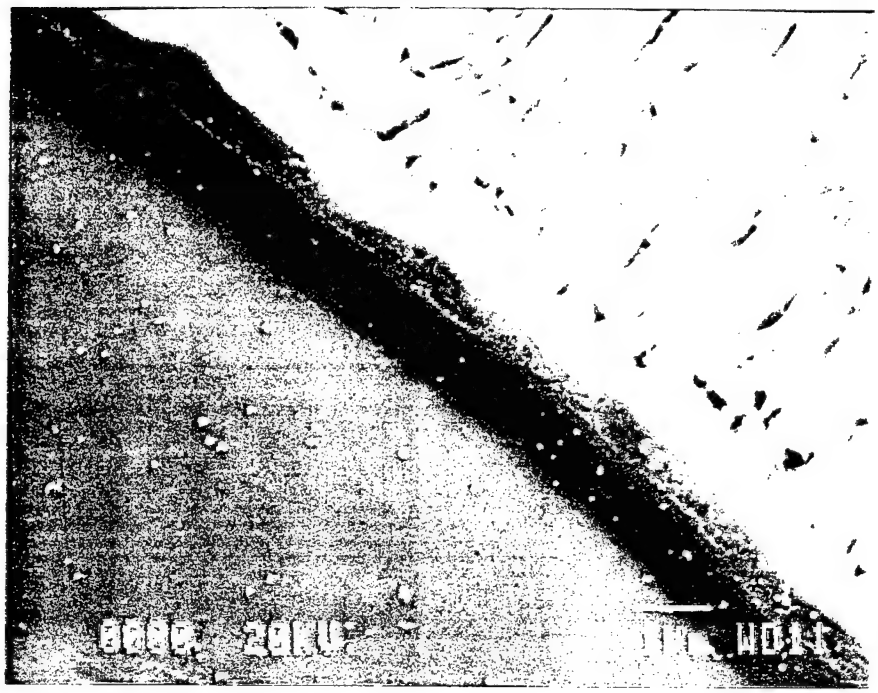

Fig. 2-5(a) SEM photo of SM1240/Timetal-21S reaction zone for unaged sample

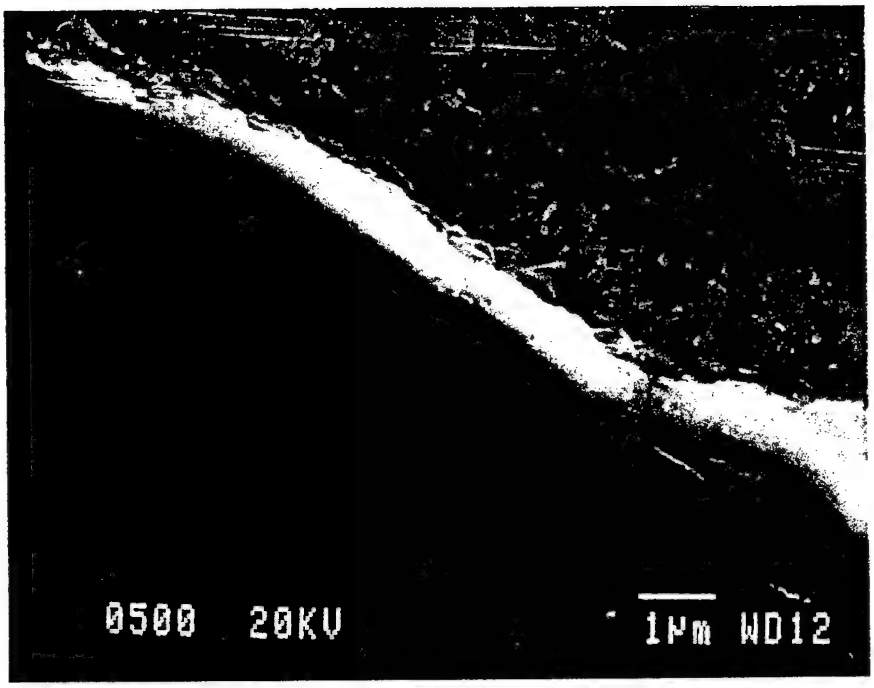

Fig. 2-5(b) SEM photo of SM1240/Timetal-21S reaction zone for 500 °C / 302 hour aged sample

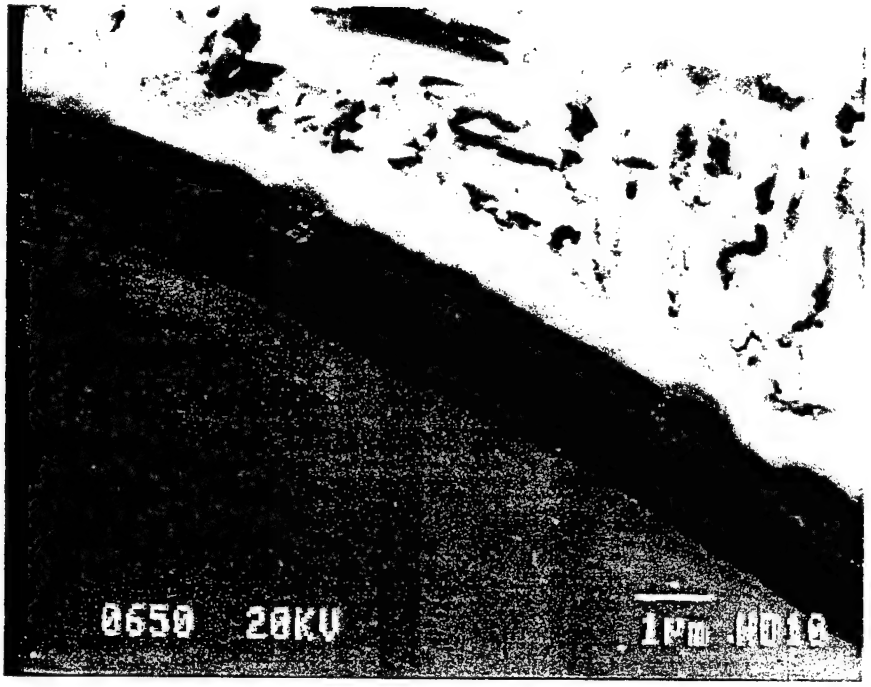

Fig. 2-5(c) SEM photo of SM1240/Timetal-21S reaction zone for 650 °C / 400 hour aged sample

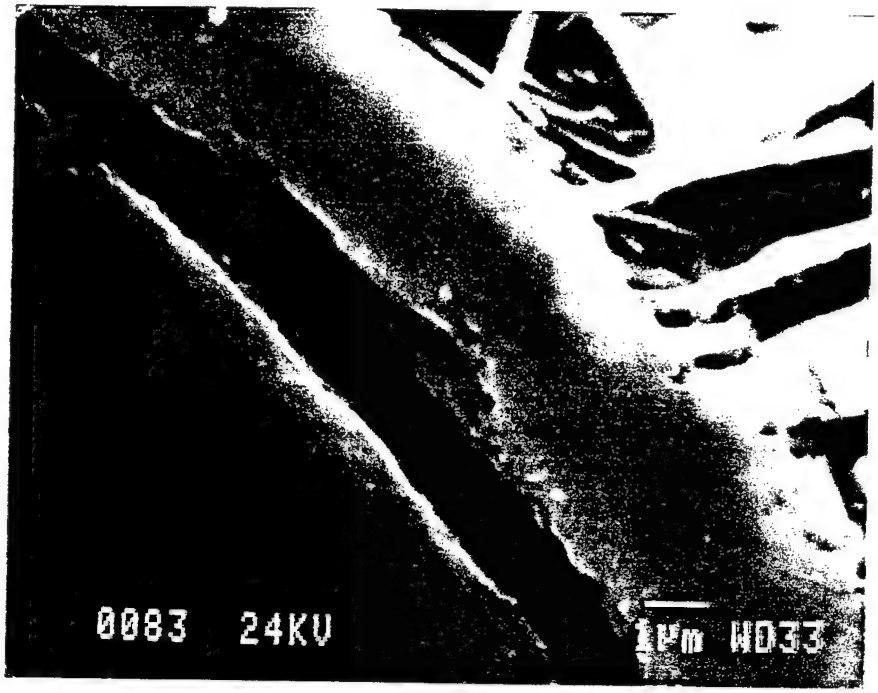

Fig. 2-5(d) SEM photo of SM1240/Timetal-21S reaction zone for 875 °C / 200 hour aged sample

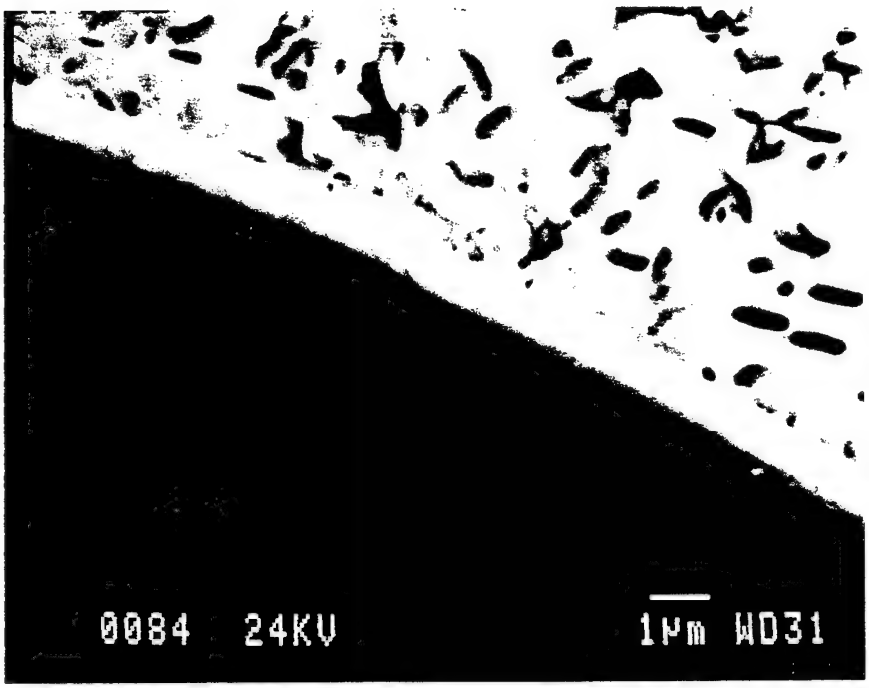

Fig. 2-6(a) SEM photo of SCS-6/Timetal-21S reaction zone for unaged sample

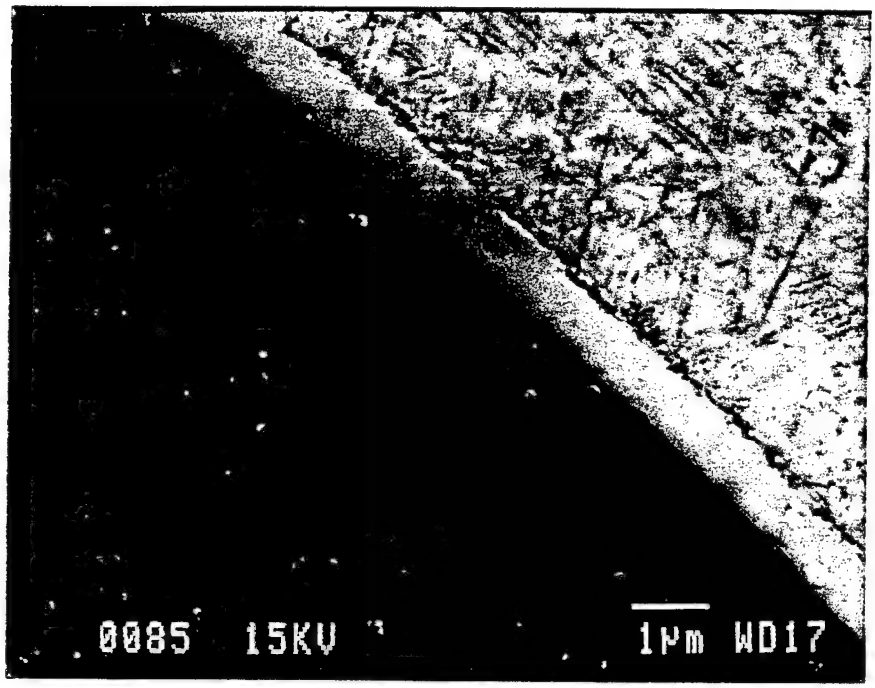

Fig. 2-6(b) SEM photo of SCS-6/Timetal-21S reaction zone for 500 °C / 600 hour aged sample

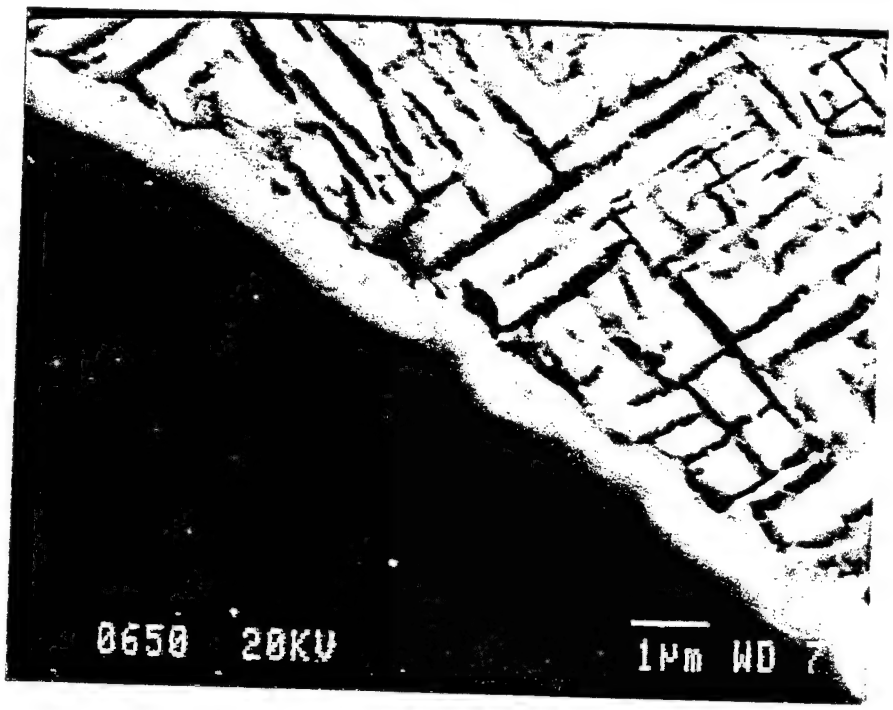

Fig. 2-6(c) SEM photo of SCS-6/Timetal-21S reaction zone for 650 °C / 401 hour aged sample

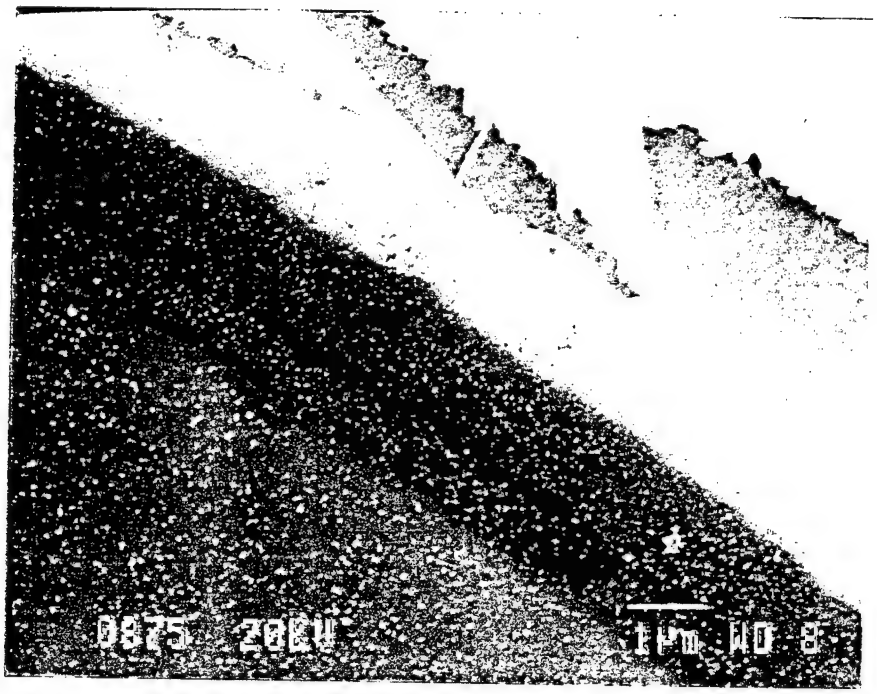

Fig. 2-6(d) SEM photo of SCS-6/Timetal-21S reaction zone for 875 °C / 27 hour aged sample

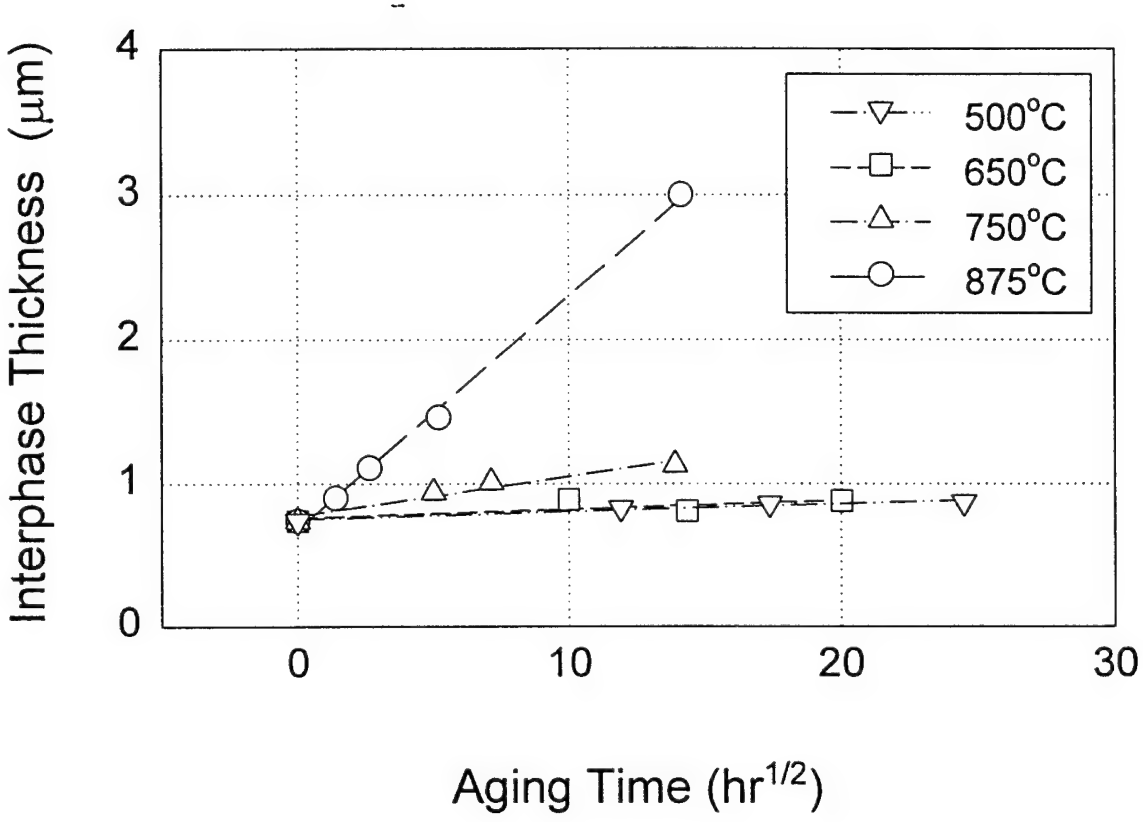

Fig. 2-7 SCS-6/Timetal-21S interphase kinetics

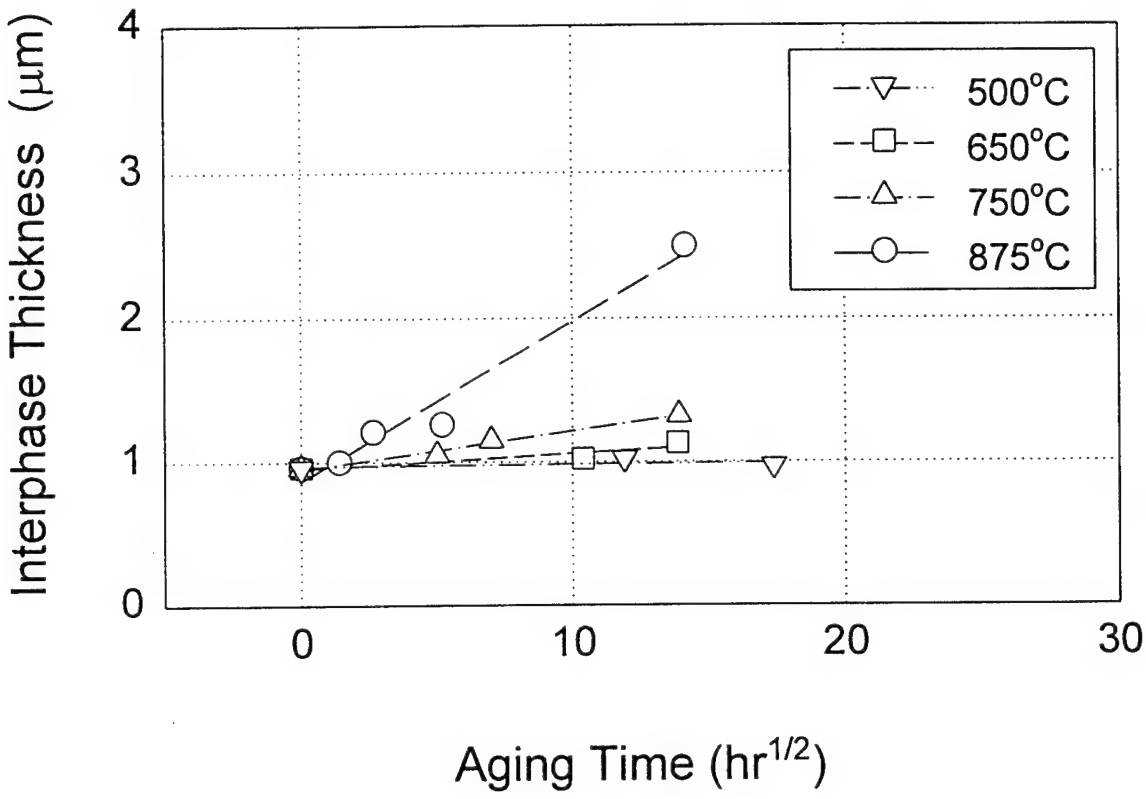

Fig. 2-7 SM1240/Timetal-21S interphase kinetics

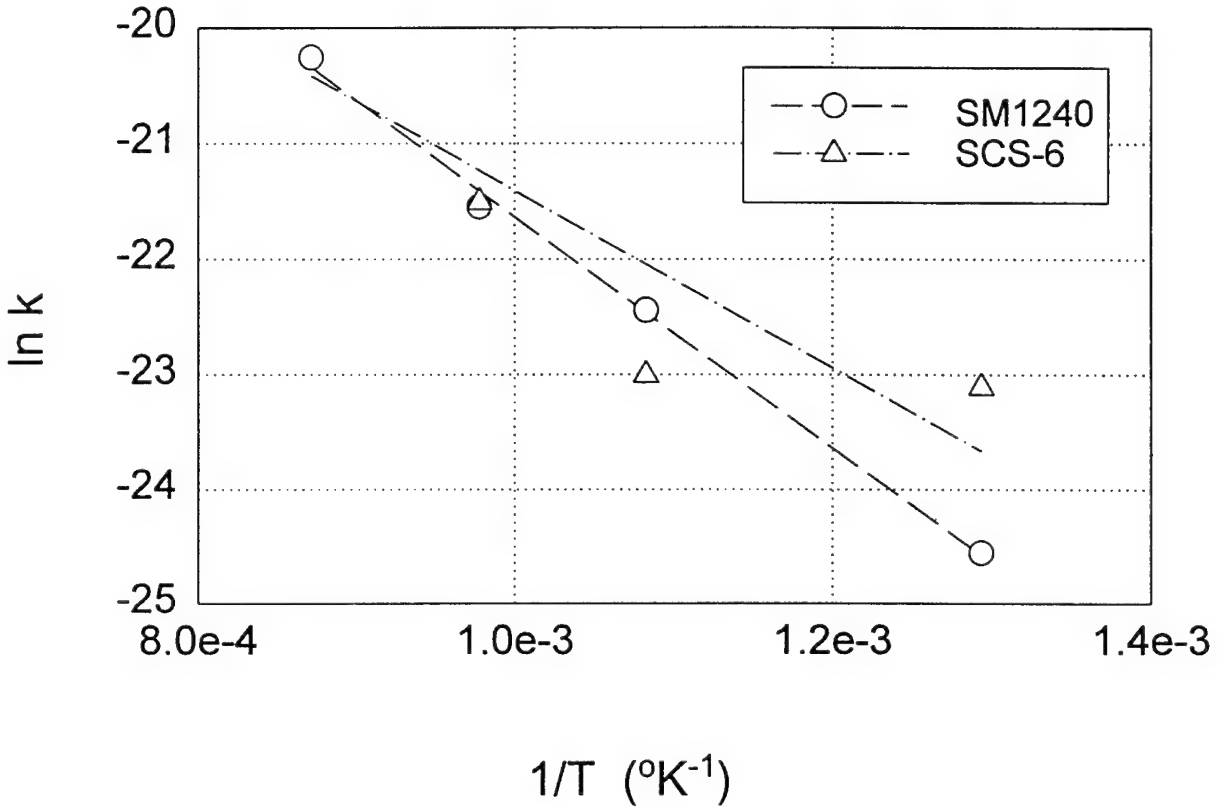

Fig. 2-9 Activation energy for Timetal-21S with SM1240 and SCS-6 fiber reinforcement

Q_{SM1240} = 39.69 kcal/mol

Q_{SCS-6} = 30.44 kcal/mol

Fig. 2-10(a) SEM photo of sample aged at 875 °C for 27 hours after the fiber/matrix interface was debonded

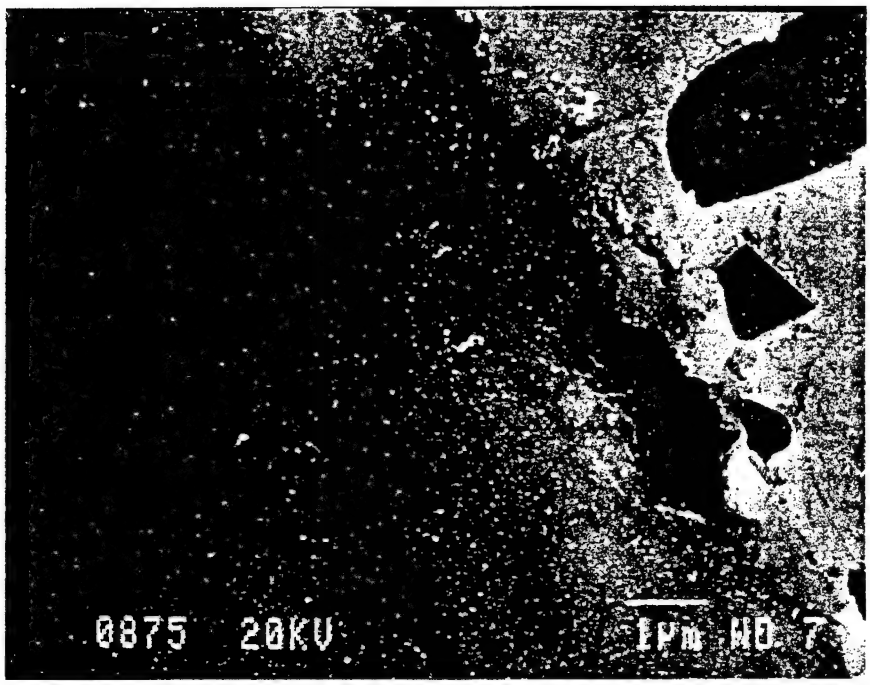

Fig. 2-10(b) SEM photo of reaction zone of sample aged at 875 °C for 27 hours after the fiber/matrix interface was debonded

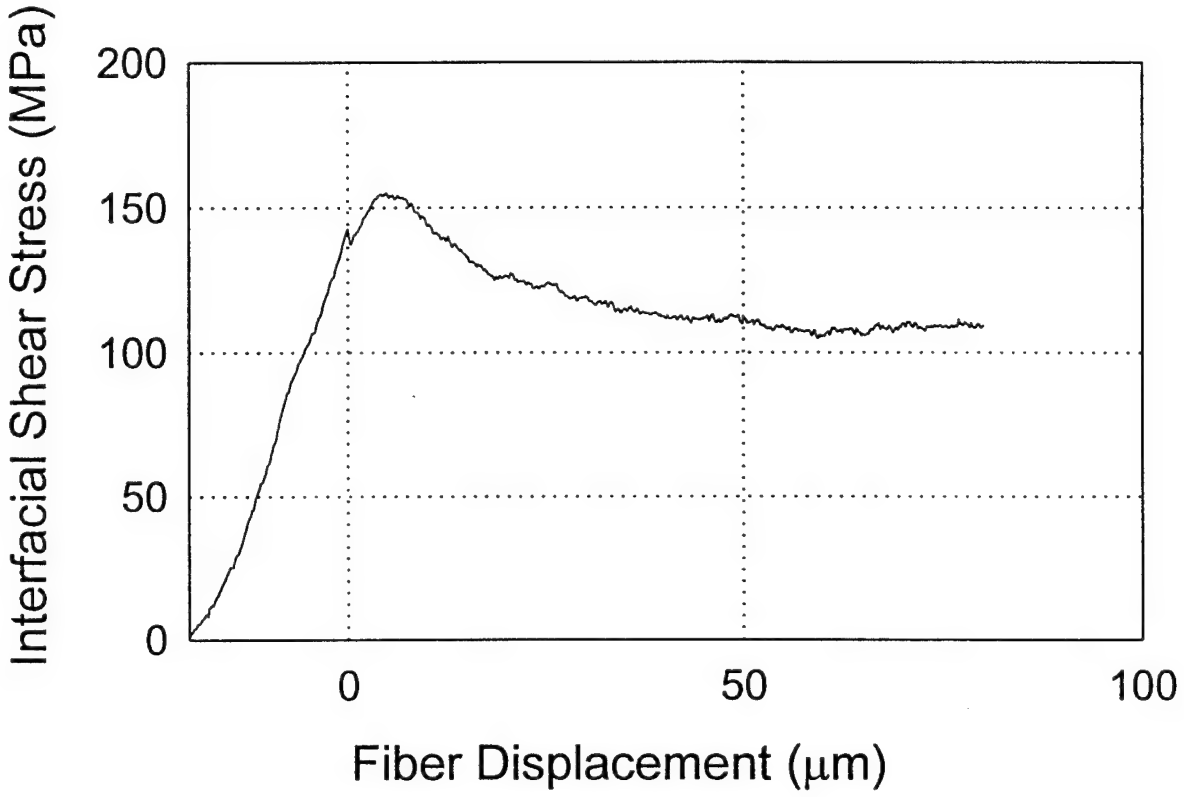

Fig. 2-11(a) Typical room temperature fiber pushout curve for SM1240/Timetal-21S at 500°C / 250 hour aging condition. Thickness, H = 0.31 mm

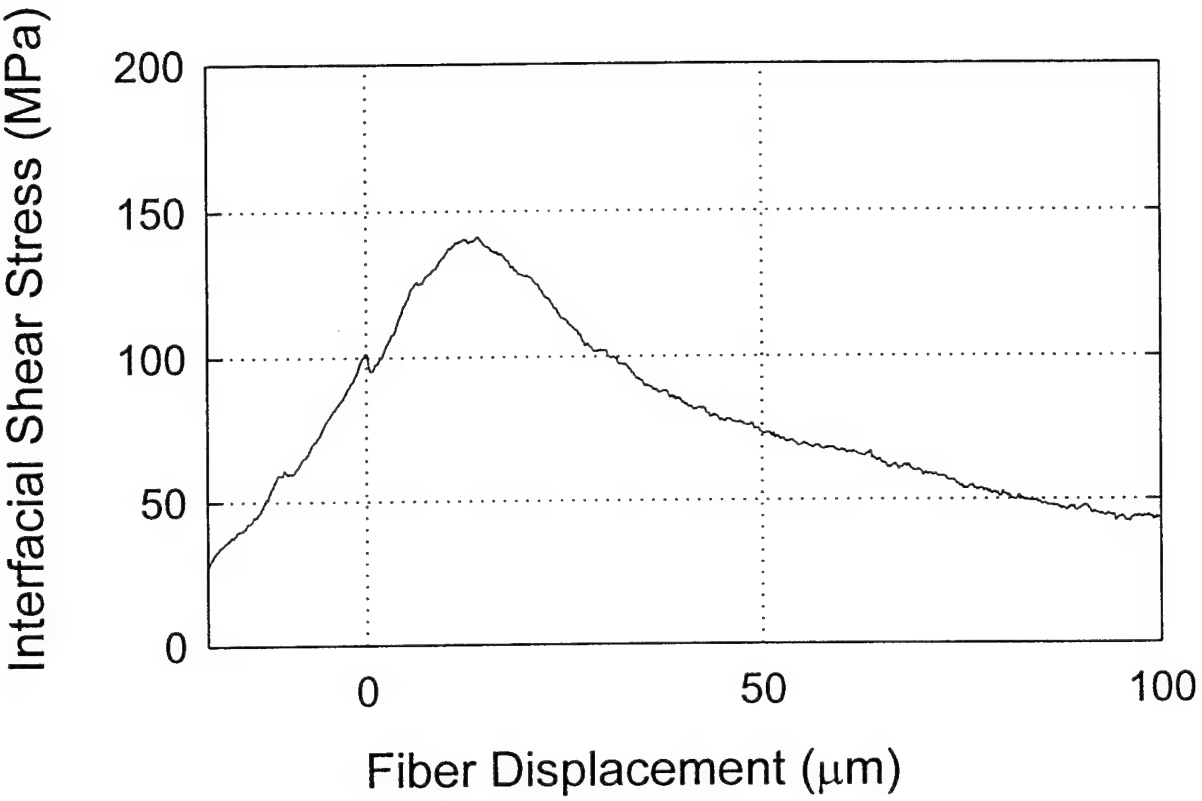

Fig. 2-11(b) Typical room temperature fiber pushout curve for SM1240/Timetal-21S at 650°C / 5 hour aging condition. Thickness, H = 0.34 mm

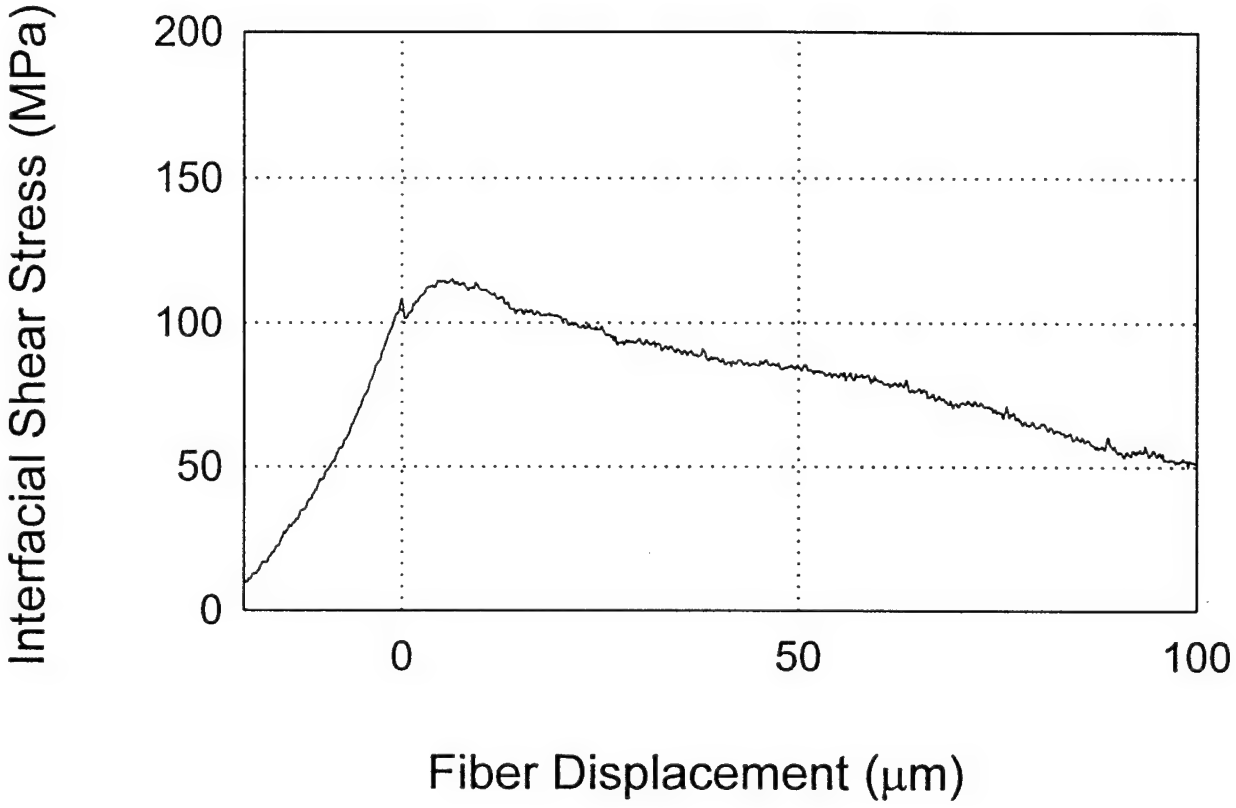

Fig. 2-11(c) Typical room temperature fiber pushout curve for SM1240/Timetal-21S at 825°C / 5 hour aging condition. Thickness, H = 0.30 mm

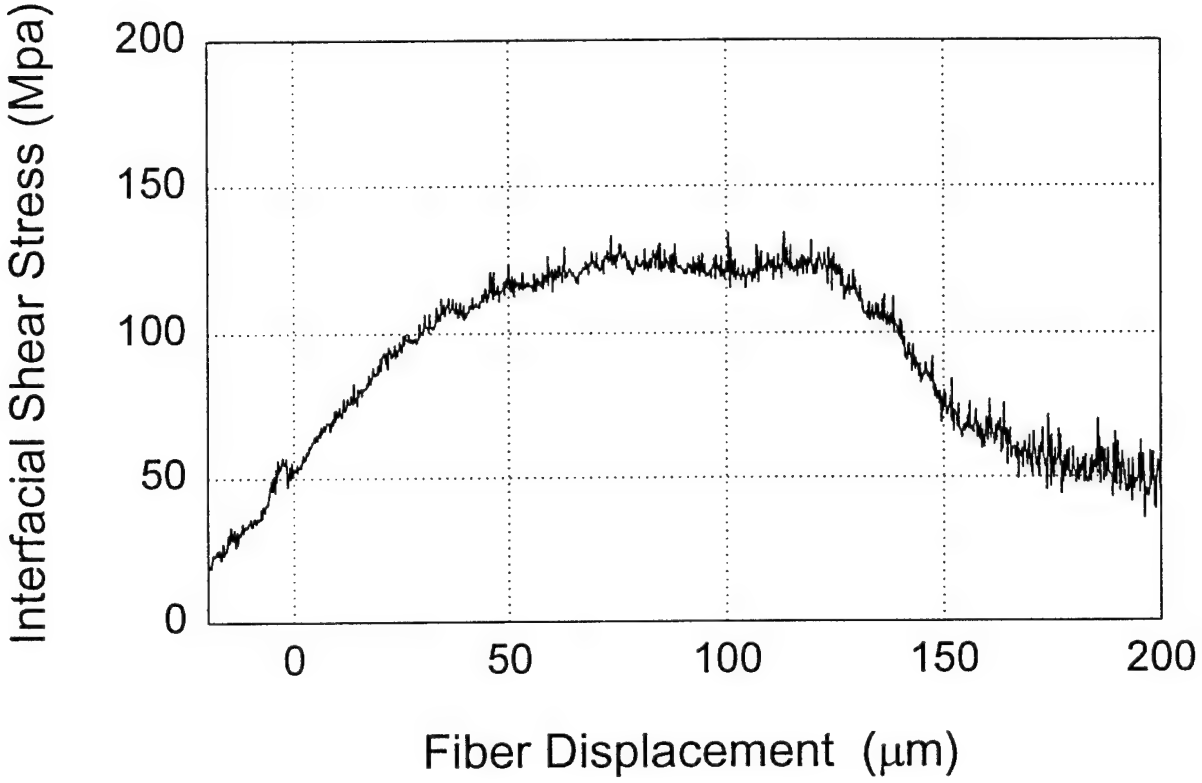

Fig. 2-12(a) Typical room temperature fiber pushout curve for Scs-6/Timetal-21S at 500°C / 5 hour aging condition. Thickness, H = 0.28 mm

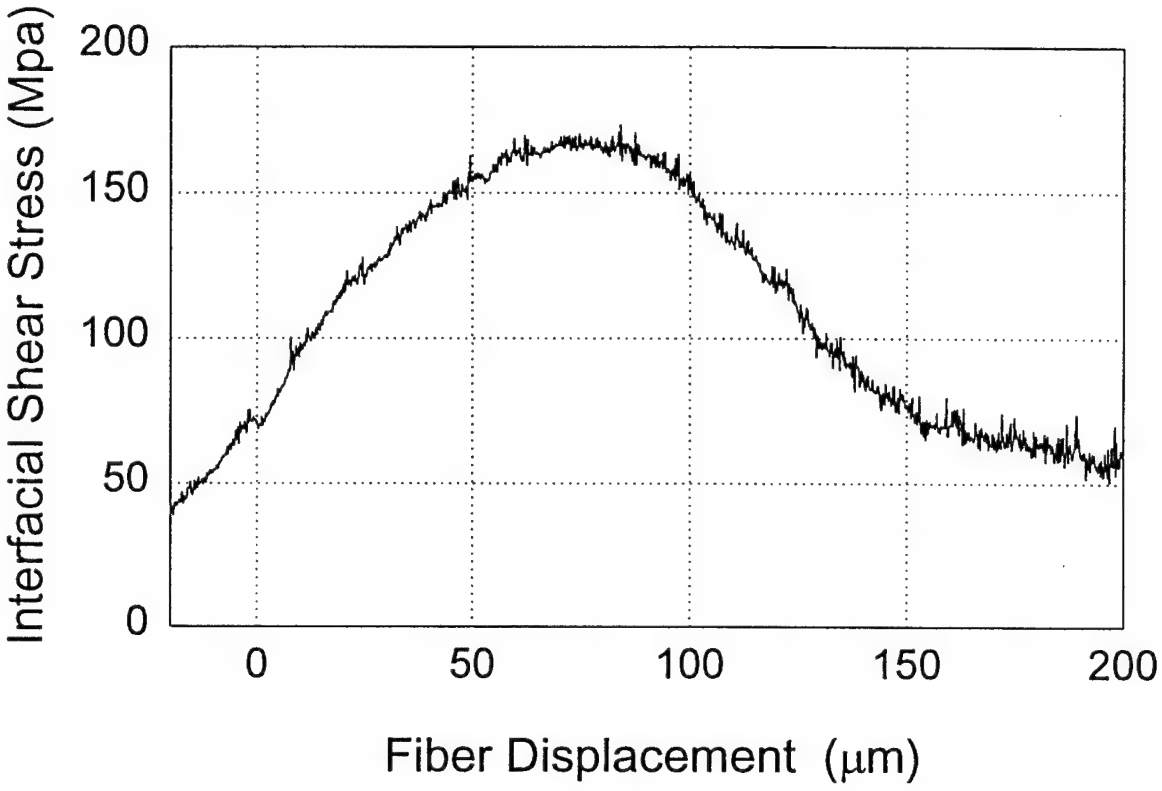

Fig. 2-12(b) Typical room temperature fiber pushout curve for Scs-6/Timetal-21S at 650°C / 5 hour aging condition. Thickness, H = 0.32 mm

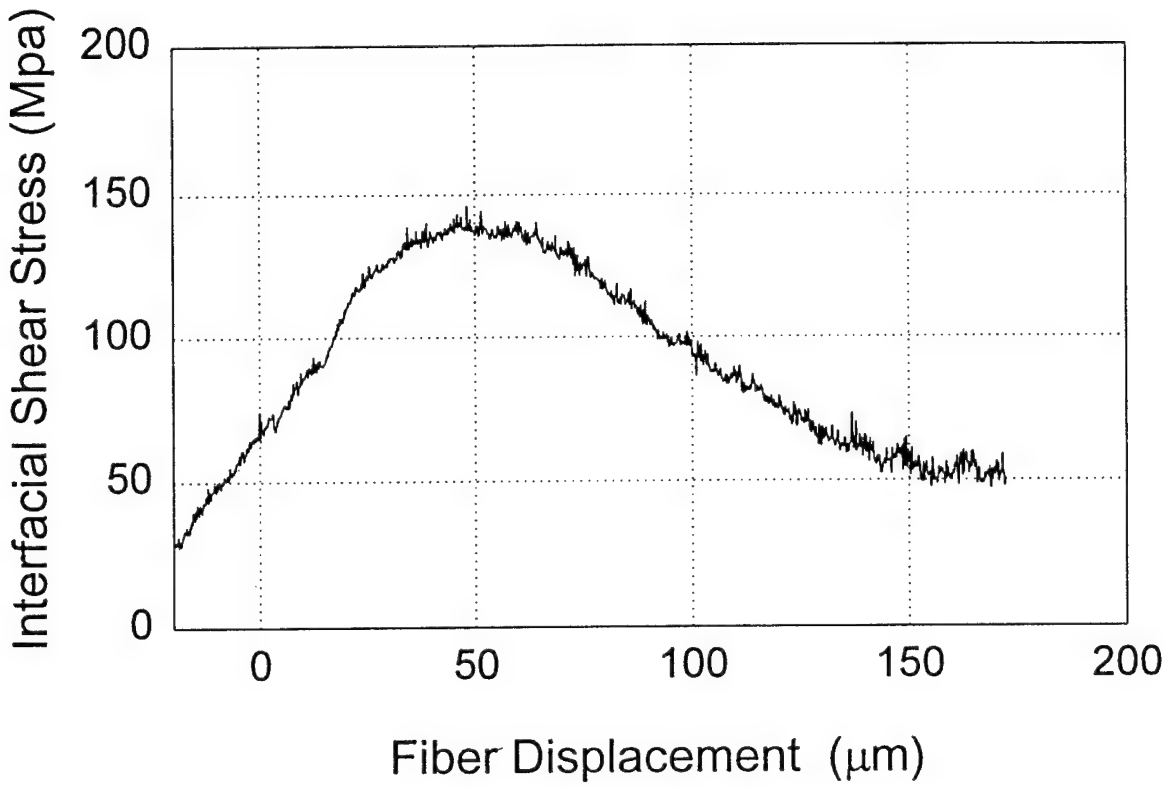

Fig. 2-12(c) Typical room temperature fiber pushout curve for Scs-6/Timetal-21S at 825°C / 5 hour aging condition. Thickness, H = 0.33 mm

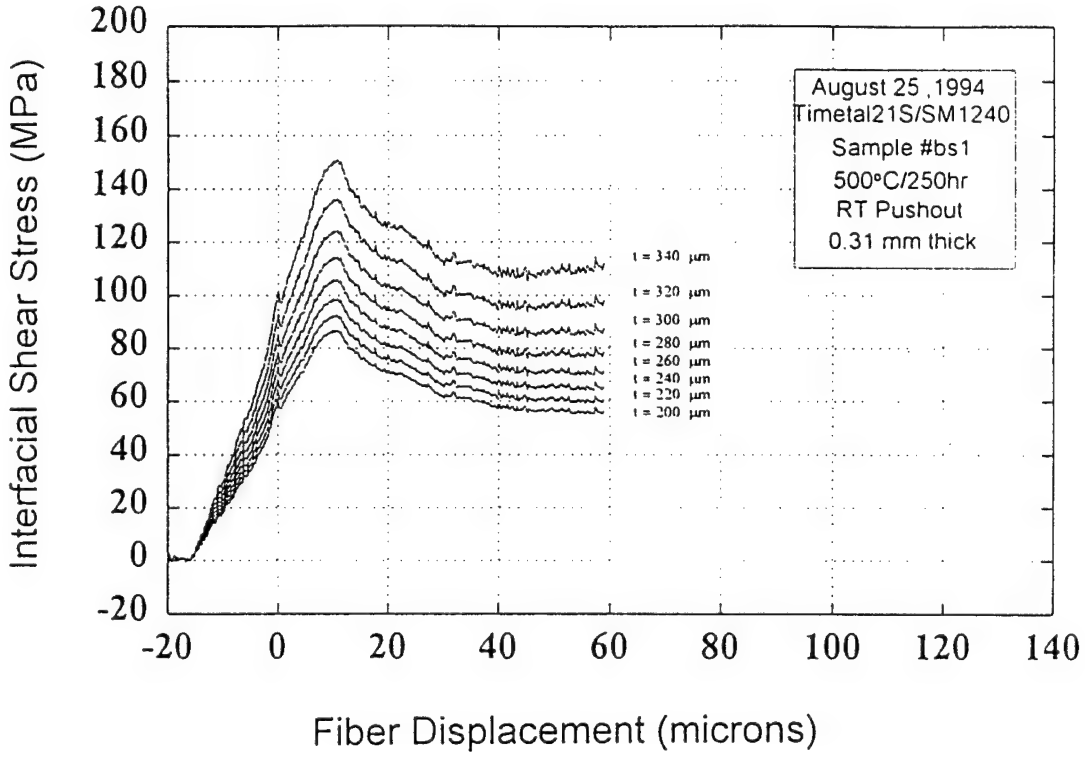

Fig. 2-13 Effect of variation of measured thickness on interfacial stress values

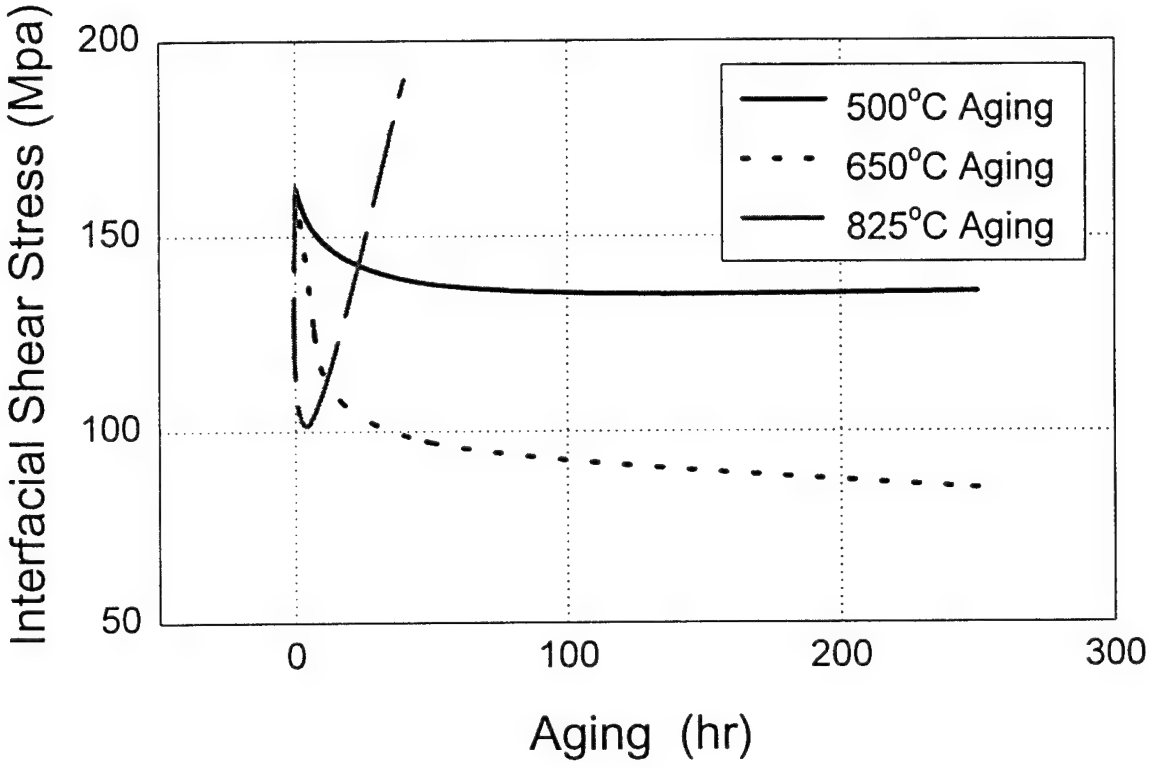

Fig. 2-14(a) Effect of aging conditions on interfacial debond shear strength of SM1240/Timetal-21S

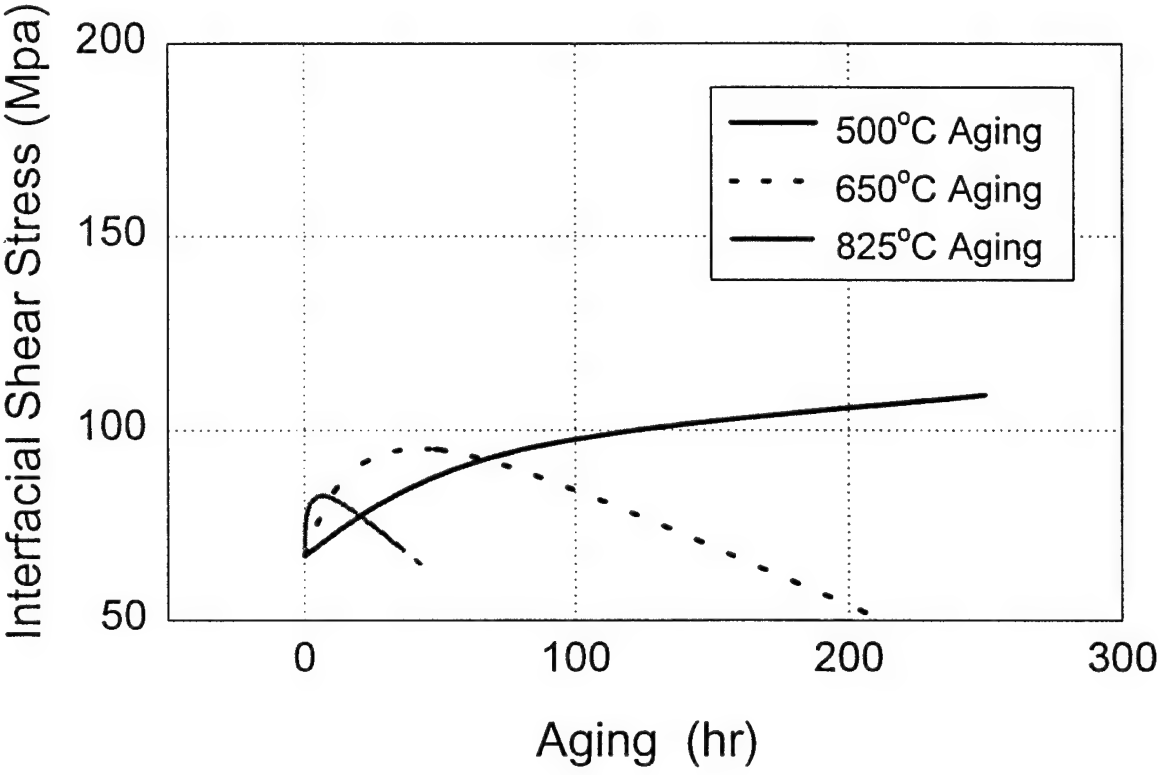

Fig. 2-14(b) Effect of aging conditions on interfacial steady state frictional shear stress of SM1240/Timetal-21S

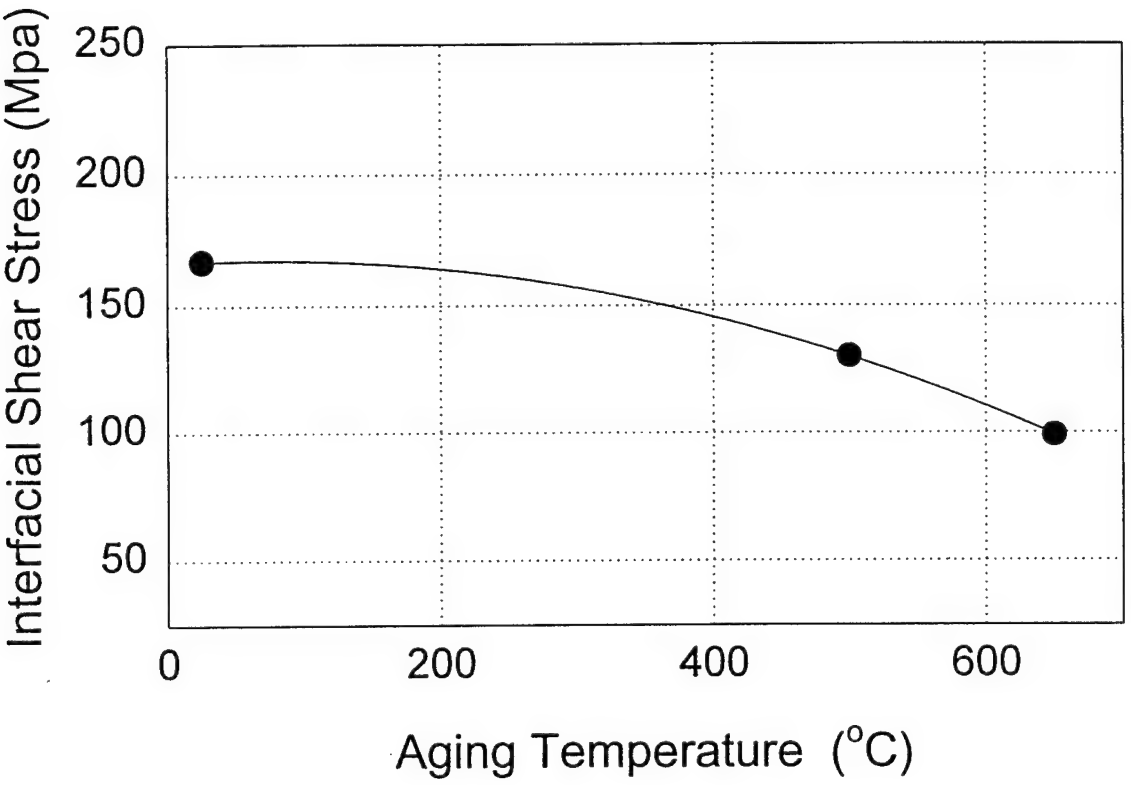

Fig. 2-14(c) Effect of aging temperature on interfacial debondshear strength of SM1240/Timetal-21S

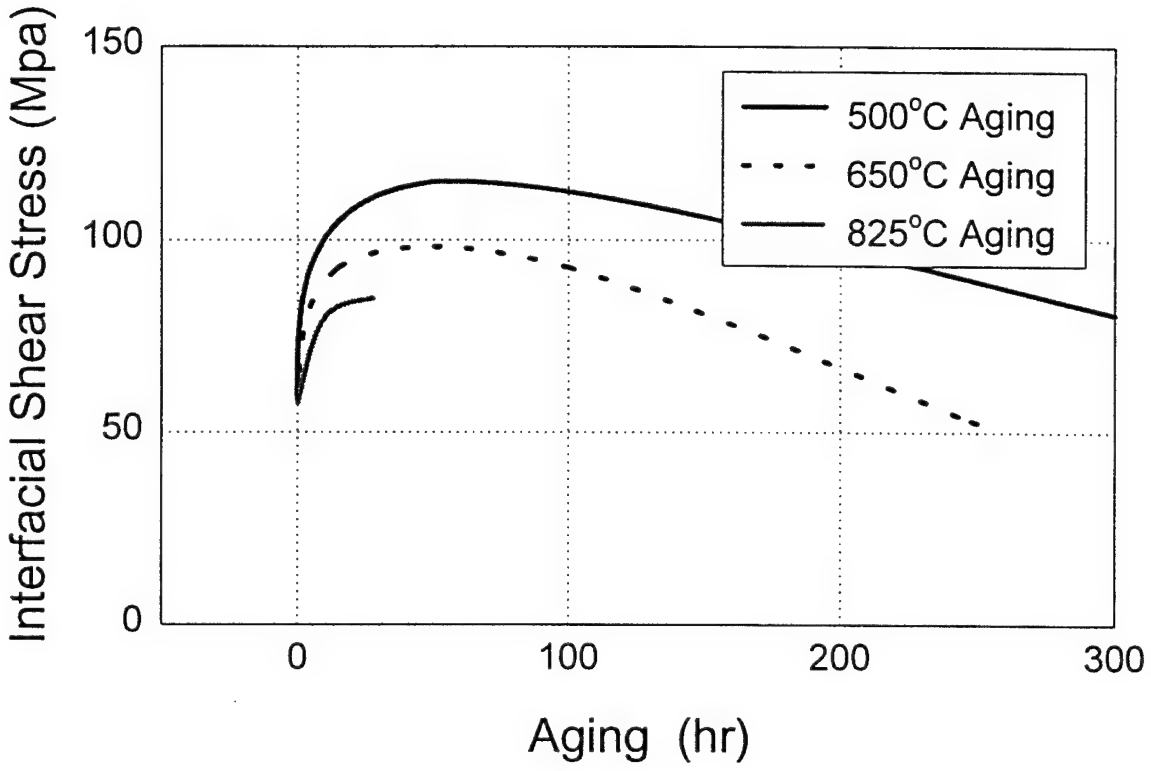

Fig. 2-15(a) Effect of aging conditions on interfacial debond shear strength of SCS-6/Timetal-21S

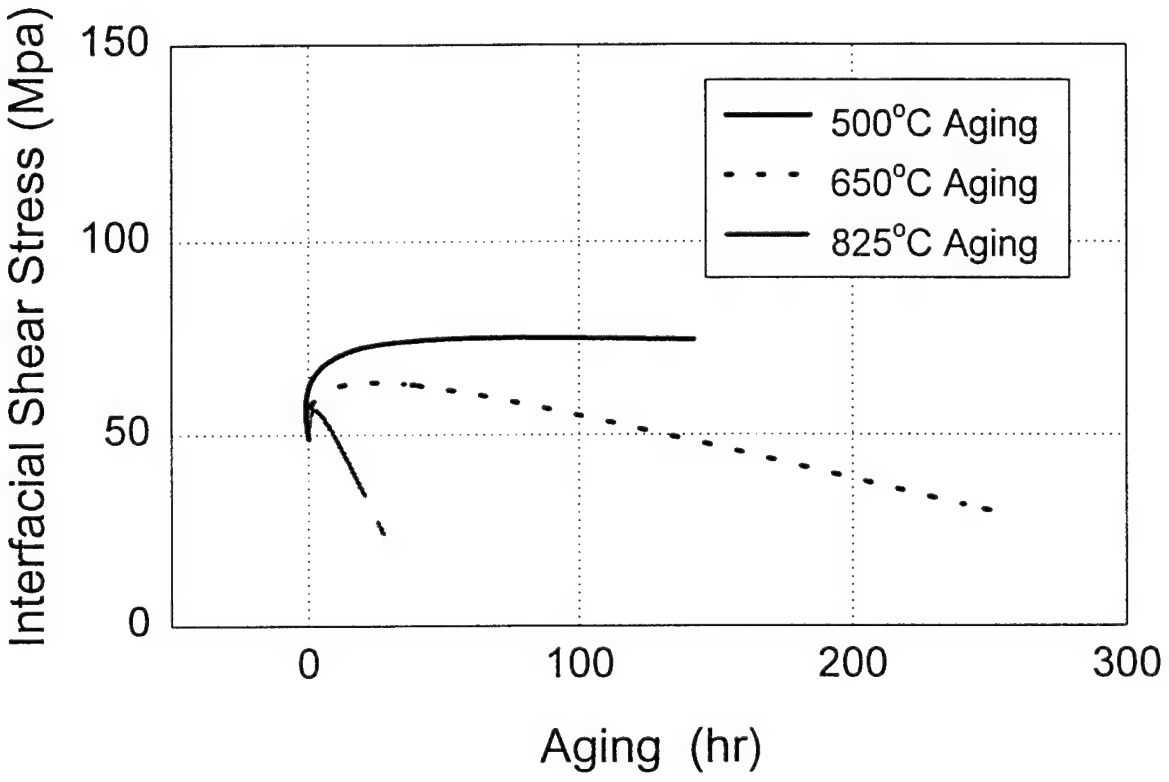

Fig. 2-15(b) Effect of aging conditions on interfacial steady state frictional shear stress of SCS-6/Timetal-21S

Fig. 2-16(a) SEM photo of typical SM1240 fiber surface morphology after pushout testing (carbon layer)

Fig. 2-16(b) SEM photo of typical SM1240 fiber surface morphology after pushout testing (TiB2 adhered to carbon)

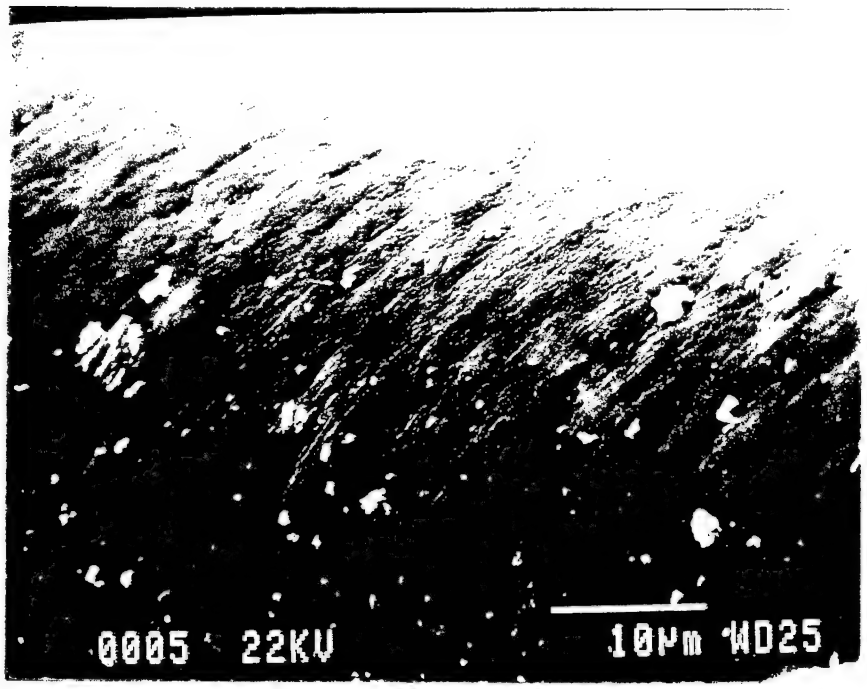

Fig. 2-17 SEM photo of typical SCS-6 fiber surface morphology after pushout testing (carbon layer)

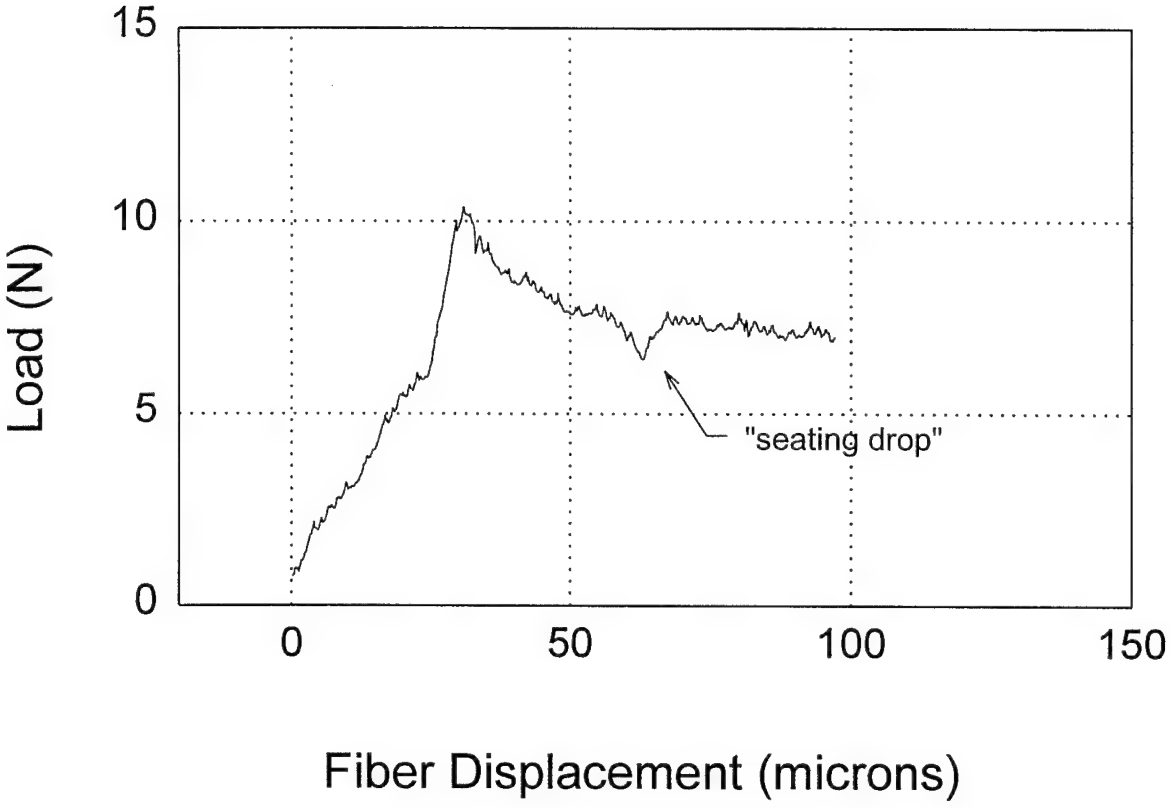

Fig. 2-18 Typical fiber pushback curve (SM1240/Timetal-21S) with "seating drop". Thickness, H = 0.29 mm.

SECTION 3

HIGH TEMPERATURE INTERFACIAL PROPERTIES OF Ti-MMCs AND THEIR INFLUENCE ON DAMAGE MECHANISMS

ABSTRACT

The interphase behavior of the Ti metal matrix composites, SCS-6/Timetal-21S and SM1240/Timetal-21S are investigated in this study at both ambient temperature and elevated temperatures. Vacuum aging studies are utilized to examine the interfacial growth kinetics for these composite systems. The debond shear strength and interfacial shear stress are identified through the use of elevated temperature thin-slice fiber pushout tests at temperatures ranging from 24 to 650 °C. The results of this study show no significant growth of the interfacial region for the temperatures under consideration, as well as no change in the interfacial shear strength due to aging for time durations of up to 200 hours. The debond shear strength of the interface for both composites was found to decrease with increasing test temperature. The effect of these temperature variable properties on the failure modes of the SCS-6/Timetal-21S composite has been used to establish a temperature dependent damage map, which describes the failure modes as a function of the stress intensity factor and temperature.

3.1 INTRODUCTION

Increased usage of continuous fiber reinforced composites has focused much attention on understanding the properties and behavior, particularly those of the fiber-matrix interface. The key properties of fiber reinforced composites rely on the characteristics at the fiber/matrix interphase, including brittleness, bond strength and chemical reactions between matrix and fiber constituents. In composites consisting of strong fibers embedded in a relatively weak matrix, the longitudinal strength relies extensively on strong fiber-matrix bonding to promote efficient transfer of stress from the matrix to the fibers. Such bonding will result in the longitudinal strength of the composite being on the order of the fiber strength. The interface region, or interphase, in addition to enabling this load transfer from matrix to fiber, can accommodate the strain mismatch between the fiber and matrix and act as a crack blunting layer to minimize crack propagation [1]. However, due to the high stresses induced during fabrication, and the brittle nature of the interphase constituents, this region can also act a s a site of crack initiation. Additionally, due to the directional nature of the reinforcement, good bond strength is necessary for the transverse strength of the composite, which will only be on the order of the matrix strength. Conversely, in some composite systems, a weak fiber matrix interface is desired. Toughness is achieved in brittle matrix composites through energy absorption during frictional sliding and pullout of broken fibers. Stress is transferred to the fiber by frictional forces until the fully loaded fibers fail

according to the weakest link statistics [2]. The greater the frictional stresses, the more efficiently the fibers become loaded and the shorter the pullout lengths. In metal matrix composites (MMCs), which have strong fibers and a ductile matrix, strong interfacial bonding is generally desired, although in some cases, such as in fatigue crack growth, frictional sliding and fiber pullout are important. The fatigue crack growth rate at elevated temperature for these types of materials under fiber bridging conditions has been found to decrease with increasing crack length, contrary to the materials' monolithic counterparts [3,4,5]. This phenomena is a result of the behavior of the crack when it encounters the fiber reinforcement. The interface tends to debond under the stress field caused by the approaching crack tip, allowing the intact fiber to bridge the crack. Matrix crack propagation is retarded when the bridging fibers carry some of the applied load, thus reducing the crack tip driving force.

Fiber bridging in MMCs is a direct result of fiber/matrix debonding behavior under the applied stress conditions. This debonding consists of two stages: debond crack initiation and propagation of the debond crack after initiation. When the matrix crack approaches a fiber, a large interfacial shear stress is induced by the crack opening displacement. This stress results in the initiation of a debond crack along the interface. The initial debond length will be a function of the fiber stress and the properties of the interphase at that temperature. In SiC/Ti MMCs, compressive residual forces are present at the interface, induced by the effect of cooling from the composite consolidation temperature on the matrix and fiber, which have a large difference in coefficients of thermal expansion. These compressive forces cause the now free surfaces of the debond crack to come into contact with one another, introducing a frictional sliding force along the debonded surfaces. Propagation of the debond crack is then a function of both the debond strength of the interface and the frictional sliding stress along the debond crack surfaces. Studies have shown that this sliding results in wear of surface asperities and deterioration of the interface [6,7]. This interfacial degradation is followed by fiber breakage and pullout.

In order to optimize properties of MMCs for particular applications, it is essential that the properties of the fiber/matrix interface are understood , as well as the many factors that influence these properties. The factors of most concern relate to the processing conditions, including consolidation temperature, pressure and cooling rate, and the in use or testing conditions such as temperature and environment. These variables result in alterations of the interphase properties, and therefore influence the subsequent behavior of the composite during loading.

Processing procedures, which vary for different composite types, subject the material to a variety of time/temperature/pressure conditions. The foil-fiber-foil technique is one of the most common methods for fabricating metal matrix composites with continuous fiber reinforcements. This method involves alternating layers of matrix material, in the form of a thin rolled foil, with layers of fibers. Two methods are used in maintaining the alignment and spacing of the fibers prior to consolidation. These fibers can be rolled on a drum and held in place by an organic binder which will be burned off during consolidation, then cut into sheet form. Alternately, sheets of fibers are woven with a thin metal wire, typically molybdenum for Ti matrix composites, which will be chemically integrated into the matrix phase upon composite consolidation. A vacuum hot pressing technique is used to consolidate the layers of fiber and foil into the composite material. During this hot pressing procedure, the temperature and pressure are such that the matrix material experiences a plastic deformation, and flows around the fibers, resulting in a fully consolidated material upon cooling.

At the consolidation temperature, above 900 °C for Ti-MMCs [8,9], a stress free condition exists within the composite. Upon cooldown, residual stresses arise due to the large difference in coefficients of thermal expansion between the SiC fiber ($5x10^{-6}$ /°C) and Ti alloy matrix material ($11x10^{-6}$ /°C) [5]. This difference causes an inherent residual compressive stress at the interface, in both the radial and axial direction. The extent of this compressive stress is dependent on the actual consolidation temperature and the cooling rate. A slower cooling rate allows a time dependent relaxation of the material which reduces the level of residual stress significantly. Bahei-El-Din, et al. [10] observed, in their work with SCS-6/Ti-15-3, that the cooling rate has a very significant effect on the radial stress at the fiber/matrix interface, while the effect of the consolidation pressure is only significant at cooling rates higher that about 1 °C/s. The high temperature necessary for consolidation also results in the formation of a brittle reaction zone between the fiber and/or fiber coatings and the matrix, and a corresponding increase in the compressive residual stress in this area. Due to the brittle nature of the interfacial reaction zone, and the strain mismatch between the reaction zone, fiber and matrix constituents, it is probable that micro cracks will form in this region during composite processing. Also, the porous nature of the carbon coatings make it likely that small defects will exist in this area. These defects, which can be thought of as notches, can act as stress concentrations in the composite, leading to fiber and/or matrix crack initiation [11].

In use, or test conditions, such as temperature, loading frequency and environment, also effect the properties of the interphase, and therefore the composite as a whole. As temperature increase in the composite system, approaching the stress free consolidation temperature, the residual stresses at the fiber/matrix interface decrease. High frequency fatigue crack growth studies performed by Zheng and Ghonem [12] have shown a decrease in the crack growth rate of unaged SM1240/Timetal21S samples during the initial crack bridging stage, corresponding to an increase in crack tip shielding, with increasing test temperature (from 24 - 650 °C). Eldridge and Ebihara [13] have noted a marked drop in the experimental values of interfacial shear strength and frictional shear stress with increasing test temperatures (from 300 to 825 °C) in unaged SCS-6/Ti-24-11 intermetallic composite for thin slice push out samples (0.28 - 0.48 mm thick). Conversely, from 25 - 300 °C, a possible slight increase was seen in the debond stress with increasing temperature. Ananth and Chandra [15] also calculated an increase in the values of peak push out load, and therefore debond strength, with increasing temperature (25 °C to 200 °C) for 0.5 mm samples using finite element modeling of the fiber push out test. These results show that the properties of the interface are indeed temperature dependent.

Long-term low frequency, high temperature use or testing of MMCs induce a thermal aging effect which can result in interphase growth, which is detrimental to the strength of the composite. Several authors have observed significant interphase growth under vacuum conditions, particularly at higher temperatures (600 -1000 °C) [16,17,18]. Due to the brittle nature of the interphase, defects and micro cracks can form in this region, which act as stress concentration, leading to fiber and/or matrix crack initiation. Additionally, it is likely that large interfacial growth will change the residual stress characteristics of the fiber/matrix interface due to volume changes associated with the growth and/or consumption of various constituents of the interphase. This can be seen in the increase in the frictional shear stress, generated by room temperature fiber push out testing, that has been observed with increasing aging time at 700 and 815 °C by Watson & Clyne [19]. Osborne and Ghonem [20] observed an aging temperature dependence for both the debond strength and the frictional shear stresses in Timetal-21S/SCS-6 and Timetal-21S/SM1240 samples aged in air and pushed out at room

temperature.

In order to characterize the interphase and its response to the various factors which influence it, specific interphase parameters must be identified. The properties of the interface can be defined according to various combinations of parameters such as physical, chemical, microstructural, etc. It is convenient to choose the parameters with which to describe these properties according to the material characteristics under consideration. When investigating the macrostructural properties of the composite, such as strength, toughness or fatigue crack growth rate, it is useful to express the properties of the fiber-matrix interface in terms of the experimentally obtained values of interfacial debond strength, frictional shear stress, coefficient of friction of the materials comprising the interface, and energy release rate for an interface crack. The first two parameters, the debond shear strength, τ_d, and the frictional sliding stress, τ_s, are used to describe a crtical stress value for interface debonding and frictional sliding. The coefficient of friction of the sliding interfacial crack faces can be calculated once the residual stress state at the interface is determined. The energy release rate, G, characterizes the propagation of an existing interphase crack.

A criterion for the initiation of the debond crack and its corresponding initial crack length has been proposed by Tamin, et al [21], based on the notion that the interface will debond where the shear stress induced by the crack opening displacement exceeds the debond shear strength, τ_d, of the interphase. From observations that the fiber pullout length from fatigue crack growth specimens is an increasing function of temperature, and the assumption of propertionality between fiber pullout length and fiber/matrix debond length, they proposed that the debonding length is also temperature dependent. It is assumed for this debonding criterion that when the octahedral shear stress exceeds the interfacial shear strength of the interface, a debond crack initiates, and continues to the point where this stress condition is no longer met. According to this criterion, the controlling parameters for crack initiation, which may vary with temperature, are the aging characteristics of the fiber/matrix interface and the debond shear strength, τ_d, of the interphase region, while the interfacial shear stress, τ_f defines the characteristics of the debonded interface.

Several experimental methods have been used in an attempt to establish these interfacial parameters, including fiber pullout, fiber indention , and "thin slice" individual fiber pushout. Each method unique advantages and disadvantages. Single fiber pushout, while most closely representing the actual conditions in a fiber and the surrounding matrix during loading, involves complicated specimen preparation which may keep the composite from being truly representative of the composite stress state. Pushout methods allow relatively easy sample preparation, the ability to obtain several data points from one sample, and the ability, with the proper choice of sample thickness, to preserve the true composite stress state in the sample.

The key issues in the fiber pushout process related to sample thickness are the redistribution of residual stresses during cutting, and bending of the sample during application of load. Such bending would cause tensile radial stresses on the fiber at the bottom of the sample and compressive radial stresses at the top. The tensile stresses would reduce the clamping force on the fiber near the bottom of the sample, aiding the initiation of a debond crack in that location. Eldridge and Ebihara [13] has observed no significant difference in the interfacial shear strength at room temperature for sample thicknesses from 0.28 to 0.46 mm, a fact which they extended to high temperature applications. In his high temperature studies, however, variations in debond shear stresses were attributed to a possible change in location of the initiation of the debond crack, from the bottom to the top of the sample.

This could be attributed to a combination of bending and the changes in residual stress levels due to sample thickness at elevated temperatures. Finite element studies have predicted a significant redistribution of stresses in thin slice samples, as compared to bulk composite material. Liang and Hutchinson [22] addressed this issue and noted that the effect of the redistribution of stresses is to increase the force required to start the interfacial crack propagating through the interface. Ideally, the sample thickness will satisfy two requirements; it will be thick enough to preserve the stress state of the composite so that the interphase properties obtained are representative of the composite system, and to ensure that the interfacial debonding process during pushout is shear-controlled, i.e. that it does not occur due to Mode I failure at the bottom of the sample due to bending, especially at high temperature.

During the pushout process, as in actual composite debonding, propagation of the Mode II debond crack can be modeled as a crack running along an interface between two dissimilar materials (the fiber and the matrix). Analysis of cracks in bi-material interfaces show that the different elastic constants possessed by the fiber, matrix and interface results in a mixed mode stress state, even when loading is uniaxial. [23] Consequently, the fracture mechanics description of this type of crack is more complicated than that required to describe crack propagation in a homogeneous material, where only one parameter, the critical stress intensity factor, K_{ic}, is needed. The additional complexities arise from the shearing of the crack surfaces due to the modulus mismatch. In such a case, the parameter K is scale sensitive. However, the critical strain energy release rate, G_{ic}, is not, and is therefore a convenient parameter by which to describe the debonding process. He and Hutchinson [24] have devised a delamination diagram based on calculated values of the energy release rate for deflection, G_d, compared with the energy release rate for penetration, G_p . A recent paper by Chan [25] has refined this work to include fiber fracture, interface fracture, and fiber bridging, using as the controlling parameters the interfacial properties, τ_d, and τ_s . The effect of temperature on these properties and subsequent influence on these damage modes, however, was not addressed.

During cyclic loading at elevated temperatures, three possible failure processes can occur: fracture of the fibers ahead of the crack tip and linkage of the resulting micro-cracks with the main crack, crack deflection and branching at the fiber/matrix interfaces, followed by extensive interface crack propagation and ultimately fiber fracture, and fiber bridging of the fracture surfaces in the crack wake with frictional sliding of fiber/matrix interfaces located within the bridging zone [25]. A combination of the properties of the fiber, matrix and fiber-matrix interface zone will determine the presence and/or dominance of each of these fracture processes. Failure of composite systems having strong interfaces and relatively weak fibers are generally dominated by fiber fracture, while high temperature failure of systems with weak interfaces is dominated by interface cracking. Composite systems such as SiC/Ti, having relatively low interface strength but high fiber strength can exhibit fiber bridging at room and elevated temperatures under certain combinations of stress ratio and applied stress range. The damage mechanisms of a MMC composite can be divided into three unique groups, described by the failure modes occurring immediately prior to fiber fracture: fiber bridging, interfacial debonding, and matrix yielding. The criterion for establishing boundaries between these failure modes is based on work done by Chan [25]. Expanding upon the work of He and Hutchinson [24], he has shown that the critical ratio τ_d / σ_f , where σ_f is the fiber strength, can be used to predict the failure modes of fiber composites. In the current research, the work of Chan will be expanded to include elevated temperature effects and will be applied to two Ti matrix composite systems.

The purpose of this study is to characterize the elevated temperature properties of MMCs, particularly those of the fiber/matrix interface, considering both the effect of aging and elevated temperature debonding, and to identify the effect of these properties on the failure modes of the composite under fatigue loading conditions. Using an optimized sample thickness, the parameters necessary to describe the debonding behavior of the composite system will be investigated with respect to typical in-use temperatures. The effect of thermal exposure on the interphase zone will be identified under vacuum aging conditions. Temperature dependency of the fiber/matrix interface debond shear strength, τ_d, and the frictional shear stress, τ, will be investigated through a series of room temperature and elevated temperature fiber pushout tests for both aged and unaged conditions. These parameters will be used to predict the controlling failure mode in the MMC systems under consideration.

MATERIAL AND EXPERIMENTAL PROCEDURE

Two materials are considered in this study, an 8 ply Timetal-21S/SM1240 and a 6 ply Timetal-21S/SCS-6 composite. The matrix of both composites consists of Timetal-21S, a metastable β titanium alloyed with 0.1 Fe, 16.0 Mo, 3.06 Al, 2.9 Nb, 0.2 Si. 0.22 C, 0.12 O, 0.005 N (wt %.) SCS-6 fibers have a 140 μm carbon cored SiC body with a 3 μm dual carbon coating. SM1240 fibers have a 100 μm tungsten cored SiC body with a 1 μm inner coating of pyrocarbon and a 1 μm outer coating of TiB_2. Additionally, Ti-15-3/SCS-6 (Ti -15V-3Al-3Cr-3Sn), another metastable beta alloy composite, was included in the aging study only for comparison of results to existing literature. Most samples received a stabilization heat treatment in vacuum; however, as received samples were also tested for comparison. Samples were wrapped in Ta foil (to absorb any stray oxygen) and aged under a continuous vacuum (10^{-6} torr) at 500 and 650 °C for time durations of up to 200 hours for the push out and aging tests, with some at 900 and 1200 °C for aging tests only. Upon cooling, specimens were sectioned to the desired thickness with a diamond wafering blade at a high speed/low load, ground on SiC paper, then diamond polished through 1 μm grit.

Specimens used in the aging study were lightly etched with Kroll's etchant (15 sec x 2) in order to clearly define the interphase boundaries. For each sample, several centrally located fibers were chosen for examination. Scanning Electron Microscopy (SEM), calibrated with Auger Electron Spectroscopy (AES), was used to identify the thickness of the reaction zone around the circumference of the fiber for each of the aged samples. The average interphase thickness was taken to be the mean of the measurements from all fibers examined.

Push out specimens were polished on both sides until an appropriate thickness was attained. (See Appendix A for analysis of optimum sample thickness.) The sample was mounted in the specimen holder of the fiber push out apparatus and a low magnification optical micrograph was taken of each sample. Fibers aligned with grooves in the pushout base were chosen and marked on the micrograph for ease of identification during testing.

The fiber pushout apparatus consists of a load train and a specimen holder assembly incorporated into a 12" cylindrical vacuum chamber (Fig. 1-1). Loading is applied by a stepper motor with an attached encoder which reads motor displacement. The motor shaft is coupled with a linear motion feedthrough at the vacuum chamber. A load cell is mounted between the feedthrough shaft and a

hollow stainless steel tube to which the punch assembly is attached. The carbide punches used in this study are tapered at 30° included angle with a flat tip of 100 μm diameter for the SCS-6 fibers and 75 μm diameter for the SM1240 fibers. The specimen holder is mounted on an removable assembly including an x-y stage with motorized actuators for remote alignment of the chosen fiber with the punch.

After the chosen fiber was aligned with the punch, the fiber was monotonically loaded at the sample's corresponding aging temperatures under vacuum conditions until fiber pushout occurred. A typical elevated temperature pushout curve is shown in Fig. 3-1. At elevated temperatures, a change in linearity such as that occurring at point A, which has been described as the onset of fiber debonding [26], is fairly evident. The interface debond strength, τ_d, was taken to be the stress corresponding to this change in linearity, while the initial drop in the pushout curve (B), occurring when the debond crack propagates completely through the thickness of the sample and slip occurs, was also noted. This drop is evident at all temperatures. The frictional shear stress, τ_s, was considered to be the value of stress at the bottom of the load drop (C), where the fiber will stop sliding due to frictional resistance. Fiber pushout was verified through SEM observations of the reverse side of the sample. In addition, the surface morphology of the pushed out fibers were compared for the various aging and test temperature combinations.

RESULTS AND DISCUSSION

Vacuum aging studies on both Timetal-21S composites at temperatures of 500, 650, and 900 °C showed no significant growth of the interphase region for exposure times of up to 200 hours. The interphase thickness was approximately 1 μm for all aging conditions from 23 °C to 900 °C, similar to that of the unaged specimens shown in Fig 2-5(a) for the SM1240/Timetal-21S and Fig. 2-6(a) for SCS-6/Timetal-21S. This is contrary to the results of several authors in their studies of aging in the composite system, SCS-6/Ti-15-3. (Ti -15V-3Al-3Cr-3Sn, commonly known as Ti-15-3, is a metastable beta Ti alloy with properties similar to Timetal-21S, although inferior oxidation resistance.) Morel [16] observed growth of approximately 5 μm at 600 °C and 12 μm at 875 °C for 100 hours of aging. Yang & Jeng [17] also saw much larger growth of approximately 4.5 μm after 44 hours at 850 °C and 8 μm after 11 hours at 950° C in Ti 15-3. However, the vacuum range of 10^{3} torr used in both of these studies may not be sufficient at the elevated temperatures to completely avoid oxidation effects at the interface in this composite. One effect of high temperature oxidation of SCS-6/Timetal-21S has been observed by Osborne and Ghonem [20] through an air aging study, as a large growth of the reaction zone, particularly at the higher temperature investigated (875 °C). Gunnel and Wawner [18], on the other hand, observed an interface of only 1.5 μm after 1000 hours of thermal exposure at 700 ° C in vacuum for Ti-15-3. They also observed that below 925 C, the reaction rates for Timetal-21S were slightly lower than those of Ti-15-3, although no long term experimental results were quoted for the SCS-6/Timetal-21S composite system. The vacuum level of 10^{-6} torr used for aging in the current study is assumed to be sufficient to avoid any oxidation effects. In order to verify these results, samples of Ti-15-3/SCS-6 were vacuum aged at very high temperatures (900 and 1200 °C). As with the Timetal-21S composites, no significant growth was observed at 900 °C. After 200

hours at 1200 °C, an interphase thickness of 3 μm (growth of approximately 200%) was observed, accompanied by a marked deterioration of the carbon coating.

The lack of growth in these composite systems at the lower temperatures was verified using Auger Electron Spectroscopy (AES). By analyzing points in a line across the fiber, coating, interphase and matrix, plots were constructed of the chemical composition in these regions. Fig. 2-4 shows an example of such a plot for SCS-6/Timetal-21S in the as received condition. Very similar plots were obtained for all the aging conditions analyzed. The AES analysis shows the boundaries between the various regions as a gradual increase or decrease in the constituents inherent to that region. Due to the gradual change in constituents, this data provides qualitative verification of the interphase sizes measured using the Scanning Electron Microscope.

The results of a series of pushout tests to determine the aging effect on the debond strength of SCS-6/Timetal-21S is shown in Fig. 3-2 as a plot of the interphase shear strength at various aging times. Samples were aged at two elevated temperatures in vacuum, then pushed out at their respective aging temperatures. As indicated by the fitted line in the figure, no time dependent aging effect was found for temperatures of up to 650 °C and aging time durations of up to 200 hours. The effect of increasing test temperature was to lower the debond strength. These results, coupled with the observation of no significant increase in interface thickness with aging time indicate that the decrease in the shear strength with increasing temperature is primarily due to a relaxation of the mechanical clamping force on the fiber. This result is supported by recent work done by Tamin and Ghonem [27]. They established, through finite element simulation of composite cool-down from the consolidation temperature, the decrease in residual stress level with decreasing temperature temperatures. Figure 3-3 shows the results of this work in the form of a plot of the residual radial, axial, and hoop stress evolution upon cooldown from 815 °C to room temperature. A nearly linear increase in the residual stresses occur as the material cools. Based on the assumption that this stress evolution is a reversible process, this is equivalent to a decrease in residual stresses with increasing temperature. At 23 °C, the compressive radial stress is approximately 120 MPa, while at 650 °C, the radial stress is significantly reduced by approximately 75%.

The effect of this relaxation of the residual stresses as the key factor in reducing the interfacial shear strength at elevated temperatures was clearly shown by a phenomena observed during testing at 650 °C. For either composite system tested, an constant load of less than 25% of τ_d applied to a fiber for approximately 3-5 minutes resulted in fiber pushout with no increase in load. This indicates that the residual stresses, in the form of a clamping force, are relaxing enough under load at that temperature to allow the fiber to slide. This is a reinforcement of the fact that the decrease in debond strength is primarily due to relaxation of the clamping force.

Typical high temperature push out curves for unaged samples of Timetal-21S/SCS-6 are shown in Figure 3-4(a) for room temperatures, 500, and 650 °C. The slope of the loading portion of the curve increases with increasing temperature as a result of the increasing material compliance. Figure 3-4(b) shows the same curves with the compliance removed. The change from linearity seen in the two elevated temperature plots corresponds to the initiation of the interfacial debond crack [26]. As noted on the diagram, these samples (at 500 and 650 °C) are approximately the same thickness and can be compared directly, while, due to maximum force limitations, the room temperature sample is thinner. Comparison of the elevated temperature curves shows increasing compliance with temperature, in the form of a decreasing slope, as the debond crack propagates along the length of the interphase. This

slope change is terminated with a load drop, with the maximum (point B), corresponding to the load at which the remaining bonded region has reached the minimum critical length, this portion debonds catastrophically, and the entire length of the fiber begins to slide. The value of shear strength corresponding to the bottom of the drop, where the interphase is completely debonded, is taken to be the frictional shear stress of the interphase, while the magnitude of the drop is an indication of the interfacial fracture toughness [25,26].

The samples tested in ambient temperature do not show the region of increasing sample compliance indicative of incremental debonding. The nature of the pushout curve and the corresponding SEM observations of samples indicate that at this temperature, the debonding is catastrophic along the entire length of the specimen. Similar shaped curves were obtained for the testing at 160, 250 and 350 °C, even in thicker samples (greater than 0.90 mm). This observation is consistent with the effect of temperature on the elastic properties of the matrix material. At the lower temperatures, the matrix material behaves elastically. Higher temperatures, above about 400 °C, enhances the ability of the matrix phase to flow under the applied stress, thereby blunting the crack tip and inhibiting a catastrophic failure of the interface.

For this study, the debonding load is taken to be point A, where the debond crack initiates, for high temperature tested samples, and at the maximum point (B) for those tested at lower temperatures. Typically, interphase shear strength has been determined using the assumption of an average shear stress distribution along the interphase at this load level. The average values of the debond shear strength, τ_d, determined using this average shear stress assumption are plotted in Fig 3-5 for SCS-6/Timetal-21S for the above mentioned temperatures. This plot shows a decrease in τ_d and τ_s with increasing temperature, due to the relaxation of the compressive residual stress at the interface with elevated temperature. This relaxation will reduce the force necessary to push the fiber out, and also reduce the effect of friction on the sliding surfaces once the fiber has completely debonded and begins to slide.

The interface toughness is plotted in Fig. 3-6 for this composite, calculated from the discussed values of τ_d and $_s$ and the other material properties listed in Tables 1 and 2. The interface toughness is relatively low and doesn't change significantly from room temperature to about 400 °C. Beyond this temperature, the toughness rapidly increases with increasing temperature.

Table 3-1 Properties of SCS-6 fibers (no temperature dependence)

E_f (GPa)	ν_f	σ_f (MPa)
400	0.25	3600

Table 3-2 Properties of Timetal-21S matrix at various temperatures

T (^{O}C)	E_m (GPa)	ν_m	σ_m (MPa)
24	98.2	0.32	1043
204	90.3		779
316	84.8		696
482	76		589
649	47.6		245

Fig. 3-7 shows a plot of τ_d and τ_s for the system SM1240/Timetal-21S. The values for τ_d and τ_s values for the two composite systems were similar, particularly at elevated temperatures, despite the dissimilar coatings on the two fibers. (The SCS-6 fiber has a 2 μm coating of C while the SM1240 has 1 μm of C and 1 μm of TiB_2.) At room temperature, the debond strength was slightly lower for the SM1240/Timetal-21S composite. An investigation into the location of the debond crack in each of the composite systems explains these similarities Typical fiber surface morphology for each of the composite systems are shown Figs. 2-16(a)-(b) and 2-17. SEM observation of the fibers after pushout reveals that the location of interfacial debonding for the SCS-6 reinforced matrix is between layers of the C coating. For the SM1240 composite, the debond location is predominantly between the C and TiB_2 layers. This indicates that the bonding is slightly better between the similar materials, i.e., C-C layers, than for dissimilar materials, C-TiB_2 interface, at room temperature, while at elevated temperatures, the effect of the matrix relaxation is more prevalent. SEM observations reveal a smooth surface on the pushed out fiber, with similar surface morphology for the SCS-6 and SM1240 fibers. These similar sliding surfaces result in the similar frictional shear values for the two components.

Application of these experimentally obtained interfacial properties allow the establishment of a temperature dependent map of the damage mechanism occurring in the composite system. Calculation of the boundaries between these damage modes requires the knowledge of the temperature dependence of the interfacial shear strength and frictional shear stress, which have been established in this work, and also the fiber strength and various properties of the matrix such as yield strength and Young's modules. The yield strength of Timetal-21S has been established by several authors as a decreasing function of temperature [28,29]. For this analysis, the Poisson ratio of the fiber and matrix materials are considered to be equivalent, and the fiber strength, σ_f, is considered constant for the temperature range investigated. The values for these have been obtained from existing literature. (Table 1) The boundaries are calculated from experimentally obtained shear strength and interfacial shear stress data up to 650 °C and extrapolated to higher temperatures based on the assumption that above the stress free consolidation temperature, no distinction will occur between any of the failure modes.

The complete derivations for the equations which define the boundaries between the damage

modes can be found in Appendix B. Briefly, the boundary which describes the fiber bridging at any temperature can be written as

$$K < \left(1.416\,\sigma_f^2\sqrt{D}\right)\frac{1}{C^2\tau_s}$$

where the temperature dependent components are $_s$ and C (which is a function of the Young's modules of the matrix), and K is the stress intensity factor, σ_f is the fiber strength, and D is the fiber diameter. Similarly, the equation which describes the boundary of the matrix yielding region can be written as

$$K > \left(\sqrt{\frac{\pi D}{3}}\,\sigma_f\right)\frac{\sigma_y}{\tau_d}$$

where the proportionality factor between the stress intensity factor and the temperature dependent material parameters, τ_d , debond strength, and σ , yield strength of the matrix, is the constant function of temperature independent material parameters in the parenthesis. Between these two regions, interfacial debonding is expected to occur prior to fiber failure.

Fig 3-8 shows such a map for the system SCS-6/Timetal-21S. As indicated by the equation of this line, along the boundary between fiber bridging and interfacial debonding K_{max} is inversely proportional to the square of C, which is an inverse function of the matrix Young's modules, and of τ_d, the interfacial debond strength, illustrated in Fig. 3-5. As temperature increases the Young's modules of the matrix decreases, causing C to increase, slowly at lower temperatures, and more rapidly at higher temperatures. In the same temperature range, the frictional shear stress along the interface is decreasing. The net effect of the temperature variation of these parameters is to decrease the size of fiber bridging region with increasing temperature. It should be noted that the effect of temperature on the matrix is more significant to the determination of the failure mode than that of the interfacial shear stress.

The boundary between interfacial debonding and matrix yielding is governed by the ratio of τ_d/σ_y. The stress intensity factor, K_{max}, is directly proportional to τ_d, and inversely proportional to σ_y, both of which decrease with temperature. The net effect of these parameters is causes a small change with temperature until after 400 °C, after which a large increase is observed in this parameter sum. This causes the region of interfacial debonding on the damage map (Fig. 3-8) to decrease rapidly at temperatures above 400 °C.

Since K values exceeding 100 MPa √m, and temperatures above the melting point of the matrix material, Timetal-21S, are unrealistic, the map will be redrawn with these limits, as in Fig. 3-9. It is clear from this composite diagram that for temperatures for which this system has been developed (<650 °C), matrix yielding will never be the dominant failure mode. This observation is as expected, since the interface is relatively weak compared to the strength of the fiber.

Such a map can be used to predict the failure mode of a composite system under particular loading

conditions. Fiber bridging is generally desirable for reduction in fatigue crack growth in these types of composites in order to retard crack growth. This diagram indicates that in order to stay within the desired fiber bridging zone, as temperature is increased, the stress intensity factor must be lowered in order to avoid crossing into the region of interfacial debonding followed by fiber fracture. Also, optimization of a composite system is possible for a required application through the modification of the key interphase properties, according to this failure diagram. Comparison of such damage maps for materials with different reinforcing fibers, or similar fibers with different processing conditions, and therefore different values of τ_d and $_s$ can be used to distinguish the effect of theses variables on the loading conditions required to obtain failure through a particular damage mechanism.

CONCLUSIONS

The high temperature interfacial properties have been established for two MMC composite systems: SCS-6/Timetal-21S and SM1240/Timetal-21S.

1. The interfacial reaction zone size did not change with variation of aging temperatures up to 650°C for time durations of up to 200 hours.

2. For SCS-6/Timetal-21S, the interfacial shear strength were found to be independent of high temperature aging effects for temperature up to 650 °C.

3. The debond strength and frictional shear stress, τ_d and τ_f, for both systems were found to decrease with increasing temperature, due to the relaxation of the clamping force at elevated temperatures.

4. These properties can be used to derive equations for the boundaries of a high temperature composite damage map which describes the dominant failure mode as a function of the stress intensity factor and the temperature. From the damage map established for SCS-6/Timetal-21S, it was shown that matrix yielding can not be the dominant failure mode, and that the boundary between fiber bridging and interface debonding occurs at decreasing K_{max} with increasing temperature.

3.5 REFERENCES

[1] Agarwal, B.D., Broutman, L.J., Analysis and Performance of Fiber Composites, John Wiley & Sons, Inc., New York, NY, 1990

[2] Thouless, M.D., Evans, A.G., "Effects of Pull-out on Toughness of Reinforced Ceramics," *Acta metall mater.*, Vol. 36, No. 3, pp. 517-522, 1988

[3] Zhang, T. and Ghonem, H., "Time-Dependent Fatigue Crack Growth in Titanium Metal Matrix Composites," *Fatigue and Fracture of Engineering Materials and Structures*, Vol. 18, No. 11, pp. 1249-1262, 1995

[4] Cotterill, P.J. and Bowen, P., "Fatigue Crack Growth in a Fiber-Reiforced Titanium MMC at Ambient and Elevated Temperatures," *Composites*, Vol. 24, No. 3, pp. 214-221, 1993

[5] Davidson, D.L., "The Micromechanics of fatigue Crack Growth at 25 °C in Ti-6Al-4V Reinforced with SCS-6 Fibers," *Metallurgical Transactions*, Vol. 23A, pp. 865-879, 1992

[6] Kantzos, P., Ghosn, L., Telesman, J., "The Effect of Degradation of the Interface and Fiber Properties on Crack Bridging," HITEMP Review,Vol. 2, Cleveland,OH, pp. 32.1-32.14, 1992

[7] Warren, P.D., Mackin, T.J., Evans, A.G., "Design , Analysis and Application of an Improved Push-Through Test for the Measurement of Interface Properties in Composites", *Acta. metall. mater.*, Vol. 40, No. 6, pp. 1243-1249, 1992

[8] Yang, J.M., Jeng, S.M., Yang, C.J., "Failure Mechanisms of Fiber Reinforced Titanium Alloy Matrix Composites, Part I: Interfacial Behavior," *Materials Science and Engineering*, Vol. A138, pp. 155-167, 1991

[9] Sohi, M., Adams, J., Mahapatra, R., "Transverse Constitutive Response of Titanium-Aluminum Metal Matrix Composites," Constitutive Laws for Engineering Materials, C.D. Desai, ed., ASME Press, New York, NY, pp. 617-626, 1991

[10] Mirdamadi, M., Johnson, W.S., Bahei-El-Din, Y.A., and Castelli, M.G., "Analysis of the Thermomechanical Fatigue of Unidirectional Titanium Metal Matrix Composites," *Fatigue and Fracture, ASTM Spec Publ*, No. 1156, pp. 591-607, 1993

[11] Metcalfe, A.G. and Klein, M.J., "Composite Materials," A.G. Metcalfe, ed., Academic Press, New York and London, Vol. 1, 1974

[12] Zheng, D., Ghonem, H., "High temperature/High Frequency Fatigue Crack Growth Damage Mechanisms in Titanium Metal Matrix Composites," in *Life Prediction Methodology forTitanium Matrix Composites, ASTM STP 1253*, W.S. Johnson, J.M. Larson and B.N. Cox, eds. American Society for Testing and Materials, Philadelphia, PA, 1995

[13] Eldridge, J.I., Ebihara, B.T., "Fiber Pushout Testing Apparatus for Elevated Temperatures", *Journal of Materials Research*, Vol. 9, No. 4, pp. 1035-1042, 1994

[14] Terry, Brian, and Jones, Glyn, Metal Matrix Composites: Current Developments and Future Trends in Industrial Research and Applications, Elsevier Advanced Technology, Oxford, UK

[15] Ananth, C.R. and Chandra, N., "Numerical Modeling of Fiber Push-out Test in Metallic and

Intermetallic Matrix Composites - Mechanics of the Failure Process," *Journal of Composite Materials*, Vol. 29, No. 11, pp. 1488-1514, 1995

[16] Morel, D.E., "Reaction Kinetics in Continuous Silicon Carbide Reinfirced Titanium 15V-3Cr-3Al-3Sn", *Journal of Materials Engineering*, Vol.13, No.4, pp.251-255, 1991

[17] Yang, J.-M., Jeng, S.M., "Interfacial Reactions in Titanium-Matrix Composites", Journal of Metals, pp. 56-59, November 1989

[18] Gundel, D.B., Wawner, F.E., "Interfacial Reaction Kinetics of Coated SiC Fibers with Various Titanium Alloys", *Scripta Metallurgica et Material*, Vol. 25, pp. 437-441, 1991

[19] Watson, M.C., Clyne, T.W., "The Use of Pushout Testing to Investigate the Interfacial Mechanical Properties of Ti-SiC Monofilament Composites," 7th World Titanium Conference, San Diego, June 1992

[20] Osborne, D.J., Ghonem, H., "High Temperature Interphase Behavior of SiC Fiber Reinforced Titanium Matrix Composites", *USAF Ofice of Scientific Research Annual Report*, March 1995

[21] Tamin, M.N., Osborne, D.J., Ghonem, H., "Influence of Interfacial Properties on Fiber Debonding in Titanium Metal Matrix Composites," Fatigue and Fracture at Elevated Temperature, A. Nagar and S. Mall, eds., The American Society of Mechanical Engineers, New York, NY, AD- Vol. 50, pp. 121-134, 1995

[22] Liang, C., Hutchinson, J., "Mechanicscs of the Fiber Pushout Test", *Mechanics of Materials*, Vol. 14, pp. 207-221, 1993

[23] Rice, J.R., Sih, G.C., "Plane Problems of Cracks in Dissimilar Media", *Journal of Applied Mechanics*, pp.418-423, June 1965

[24] He, M.Y., and Hutchinson, J.W., "Crack Deflection at an Interface Between Dissimilar Elastic Materials," *Int. J. Solids Structures*, Vol. 25, No. 9, pp. 1053-1067

[25] Chan, K.S., "Effects of Interface Degradation on Fiber Bridging of Composite Fatigue", *Acta. metall. mater.*, Vol. 41, No. 3, pp. 761-768, 1993

[26] Kerans, R. J., and Parthasarathy, T.A., "Theoretical Analysis of the Fiber Pullout and Pushout Tests," *Journal of the American Ceramic Society*, Vol. 74, pp.1585-1596, 1991

[27] Tamin, M.N., and Ghonem, H., "Evolution of Bridging Fiber Stress in Titanium Metal Composites at Elevated Temperature," *Advances in Fatigue Lifetime Predictive Technique, 3rd Volume, ASTM STP 1292*, M.R. Mitchell and R.W. Landgraf, eds., American Society for Testing and Materials, pp. 24-38, 1996

[28] Neu, R.W., and Bodner, S.R., "Determination of Material Costants of Timetal-21S for a Constitutive Model," *Contributive Research and Development*, Vol. 6, Prepared for Wright-Patterson AFB, Ohio

[29] Ghonem, H., Wen, Y., Zheng, D., Thompson, M. and Lindsey, G., "Effect of Temperature and Frequency on Fatigue Crack Growth in Ti-β21S Monolithic Laminate," *Material Science and Engineering*, Vol. 161, pp. 45-53, 1993

[30] Chan, K.S., He, M.Y., Hutchinson, J.W., "Cracking and Stress Redistribution in Ceramic Layered Composites," *Mater. Sci Eng.*, A167, pp. 57-64, 1993

[31] Irwin, G.R., *Trans. ASME, J. Appl. Mech.*, Vol. 24, pp, 361-364, 1956

[32] Budiansky, B. and Amiziago, J.C., "Toughness by Aligned Frictionally Constrained Fibers," *J. Mech. Phys. Solids*, Vol. 37, pp. 93-109, 1989

[33] Hutchinson, J.W., and Jensen, H.M., "Models for Fiber Debonding and Pullout in Brittle Matrix Composites with Friction," *Mechanics of Materials*, Vol. 9, pp. 139-163, 1990

[34] Shetty, D. K., "Shear Lag Analysis of Fiber Push-out (Indentation) Tests for Estimating Interfacial Friction Stress in Ceramic-Matrix Composites," *Journal of the American Ceramic Society*, Vol. 71, pp.C107-109, 1988

[35] Hsueh, C. H., "Evaluation of Interfacial Shear Strength, Residual Clamping Stress and Coefficient of Friction for Fiber-Reinforced Ceramic Composites," *Acta Met. et Mat.*, Vol. 38, 1990, pp.403-409

[36] Kallas, M. N., Koss, D. A., Hahn, H. T. and J. R. Hellman, "Interfacial Stress State Present in a 'Thin Slice' Fiber Push-out Test," *J. Mat. Sci.*, Vol. 27, pp. 3821-3826

[37] Tsai, H.C., Arocho, A.M., Gause, L.W., "Prediction of Fiber-Matrix Interphase Properties and their Influence on Interface Stress, Displacement and Fracture Toughness of Composite Material," *Materials Science and Engineering*, A126, pp. 295-304, 1990

[38] Mall, S., Ermer, P.G., "Thermal Fatigue Behavior of a Unidirectional SCS6/Ti-15-3 Metal Matrix Composite," *Journal of Composite Materials*, Vol. 25, December 1991

[39] Campbell, M.D., Cherry, B.W., "Fatigue Crack Propagation in Fibre Reinforced Composite Materials," Fracture Mechanics and Technology proceedings

[40] Cox, B.N., Marshall, D.B., "Overview No. 111: Concepts for Bridged Cracks in Fracture and Fatigue," *Acta. metall. mater.*, Vol. 42, No. 2, pp. 341-363, 1994

[41] Watson, M.C., Clyne, T.W., "The Tensioned Pushout Test for Fibre-Matrix Characterization

Under Mixed Mode Loading," *Materials Science and Engineering*, A160, pp.1-5, 1993

[42] Chan, K.S., Davidson, D.L., "Driving Forces for Composite Interface Fatigue Cracks," Engineering Fracture Mechanics, Vol 33, No. 3, pp.451-466, 1989

[43] England, A.H., "A Crack Between Dissimilar Media," *Journal of Applied Mechanics*, pp.400-402, June 1965

[44] Hutchinson, J.W., Mear, M.E., Rice, J.R., "Crack Paralleling an Interface Between Dissimilar Materials," *Journal of Applied Mechanics*, Vol.54, pp.828-832, Dec. 1987

[45] Walls, D., Bao, G., Zok, F., "Fatigue Crack Growth in a Ti/SiC Composite," *Fatigue of Advanced Materials*, pp. 343-356, January 1991

[46] Marshall, D.B., Oliver, W.C., "Measurement of Interfacial Mechanical Properties in Fiber-Reinforced Ceramic Composites," *Journal of the American Ceramic Society*, Vol. 70, No. 8, pp.542-548,1987

[47] Eldridge, J.I., "Desktop Fiber Pushout Apparatus," *NASA Technical Memorandum 105341*, December 1991

[48] Koss, D. A. , Rhyne, E. P., Kallas, M. N., Hellman, J. R., "Test Techniques and the Determinations of Interfacial Shear in Metallic Matrix Composites," *Proceedings of 5th Review*, 1993

[49] Takaku, A. and Arridge, RGC, "The Effect of Interfacial Radial and Shear Stress in Fibre Pull-out in Composite Materials," *J. Phys. D: Appl. Phys.*, Vol. 6, pp. 2038-2047, 1973

[50] Marshall, D., "Analysis of Fiber Debonding and Sliding Experiments in Brittle Matrix Composites," *Acta metall. mater.*, Vol. 40, No. 3, pp. 427-441, 1992

[51] Caulfield, T. and Tien, J. K., "High Temperature Reaction Zone Growth in Tungsten Fiber Reinforced Superalloy Composites: Part I. Application of the Moving Boundary Equations," *Met. Trans.*, Vol. 20A, pp.255-266, 1989

[52] Bilba, K., Manaud, P., Petitcorps, Y. Le and Quenisset, J. M., "Investigation of Diffusion Barrier Coatings on SiC Monofilaments for Use in Titanium-Based Composites," *Material Science and Engineering*, Vol. 135A, pp.141-144, 1991

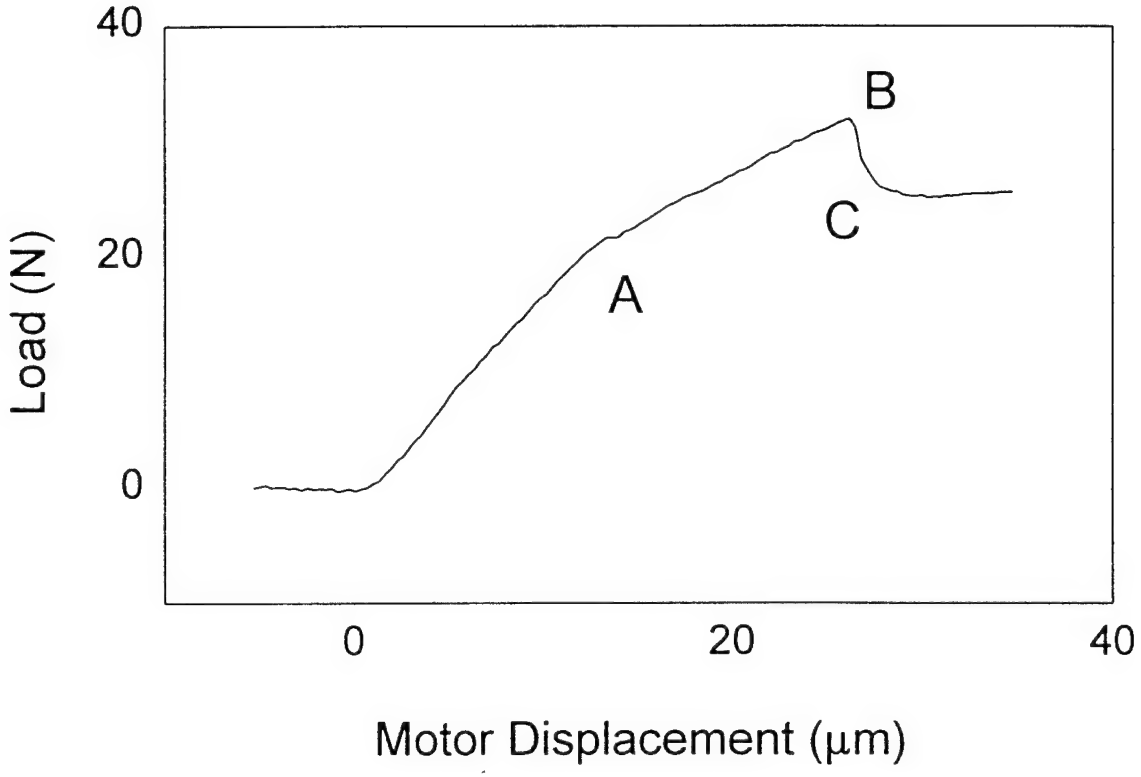

Fig. 3-1 Description of a typical elevated temperature fiber pushout curve

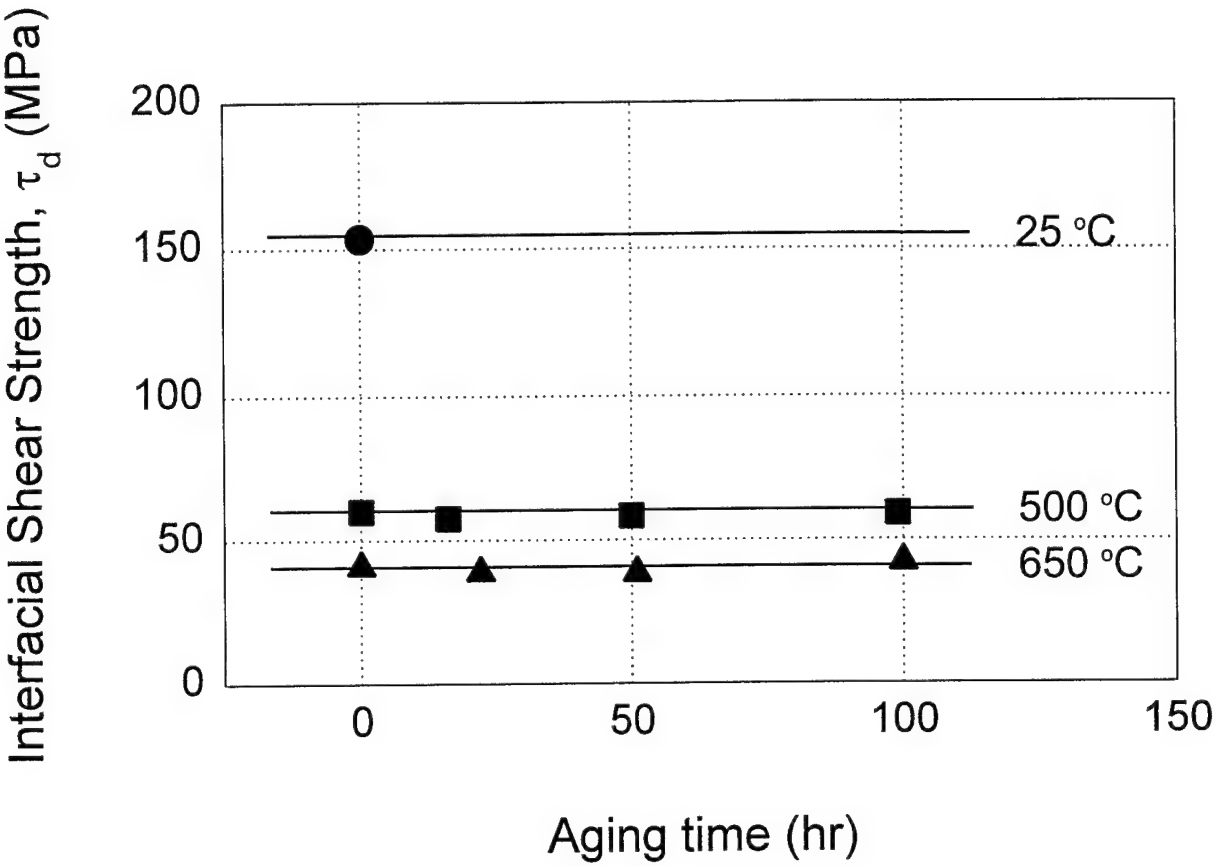

Fig. 3-2 Influence of aging time and temperature on the interphase shear strength of SCS-6/Timetal-21S at various temperatures

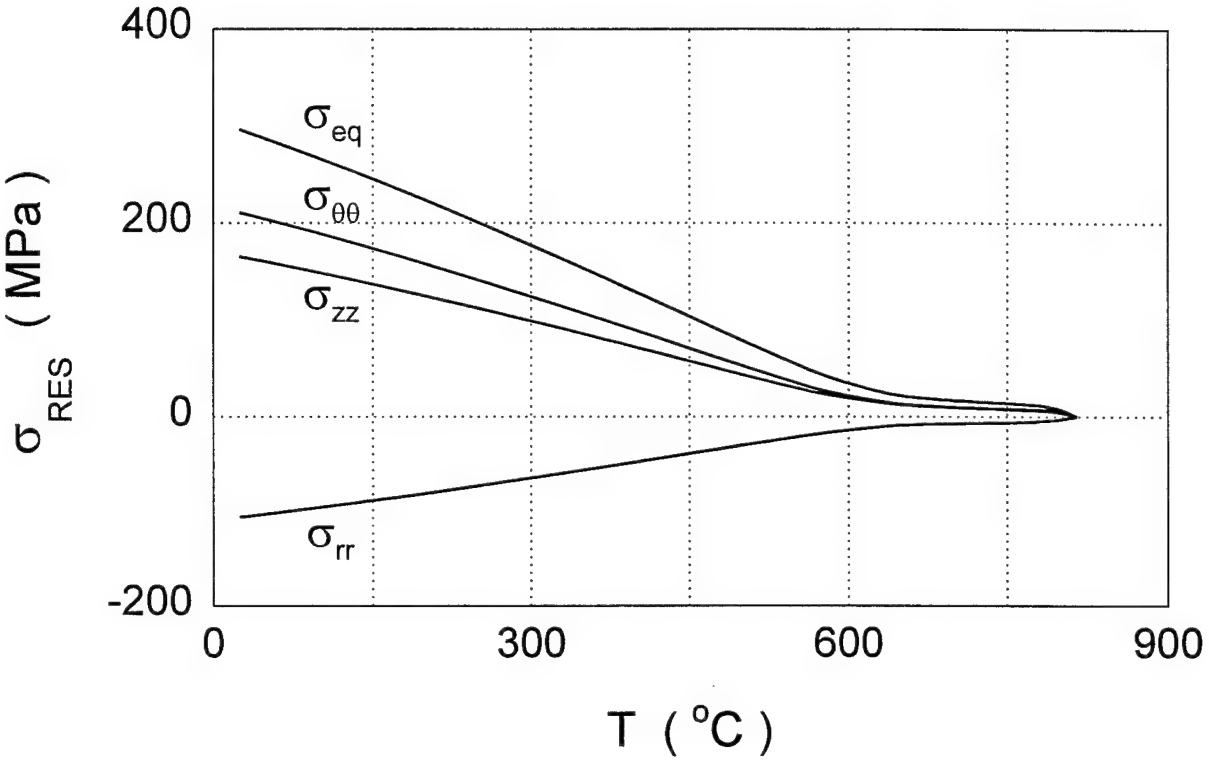

Fig. 3-3 Evolution of residual radial, axial, and hoop stress upon cooldown from 815 °C to room temperature in SCS-6/Timetal-21S

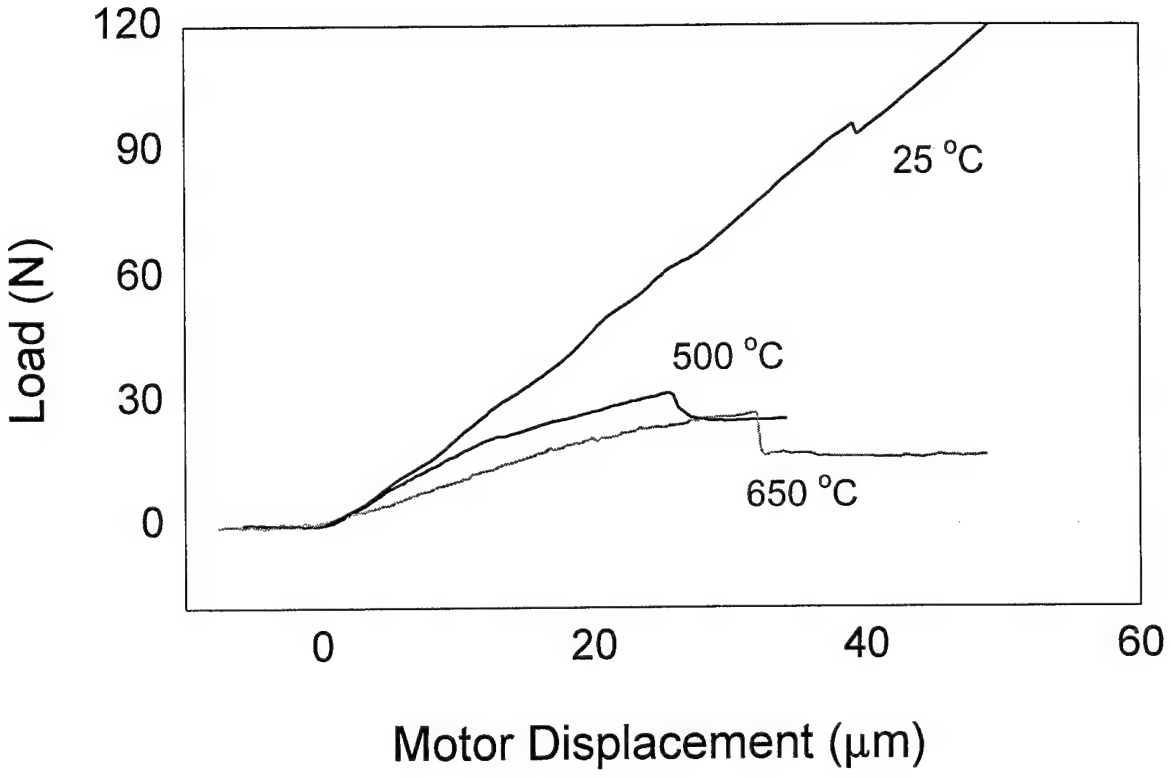

Fig. 3-4(a) Typical high temperature pushout curves for SCS-6/Timetal-21S at ambient and elevated temperatures

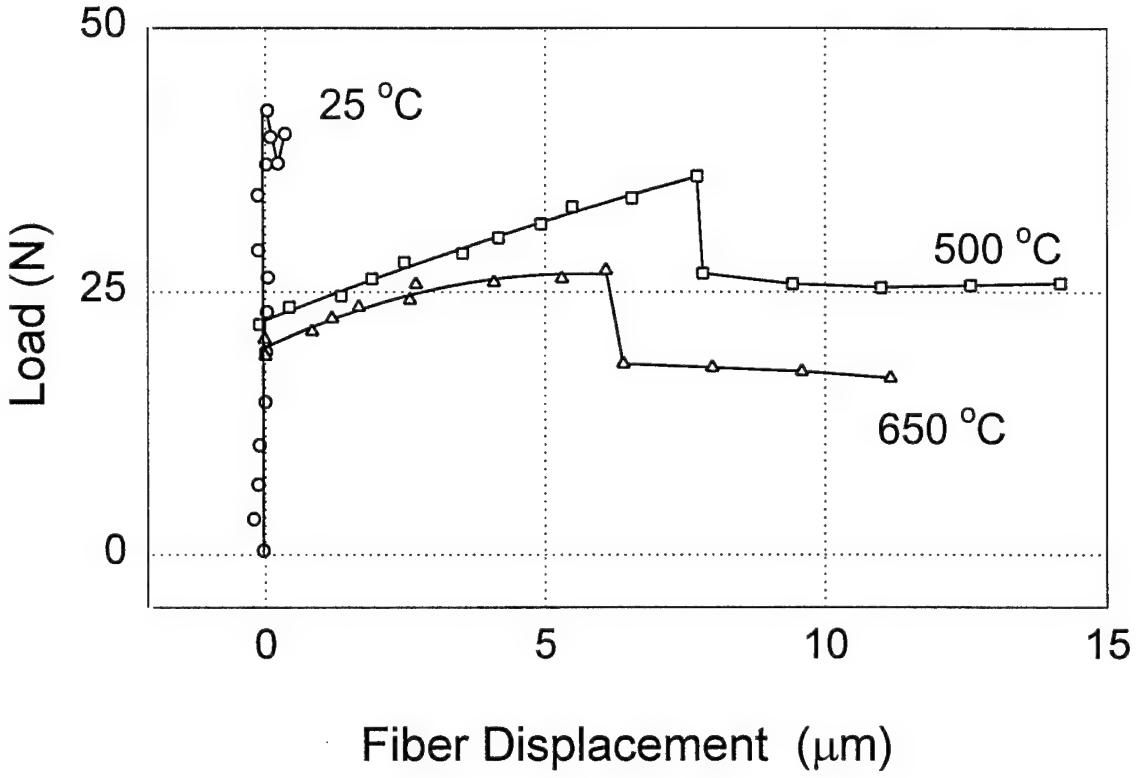

Fig. 3-4(b) Typical high temperature pushout curves (with compliance removed) for unaged SCS-6/Timetal-21S at ambient and elevated temperatures

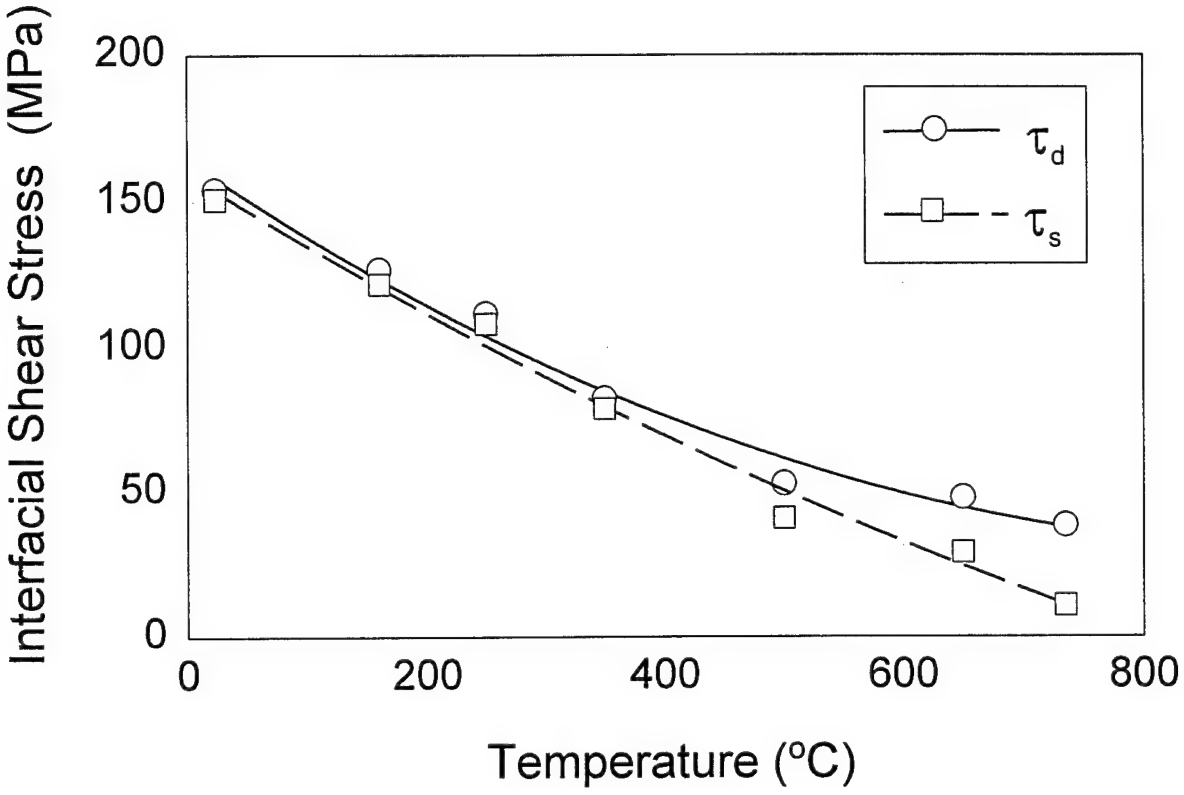

Fig. 3-5 Debond shear strength, τ_d, and frictional shear stress, τ_s, for SCS-6/Timetal-21S at various test temperatures

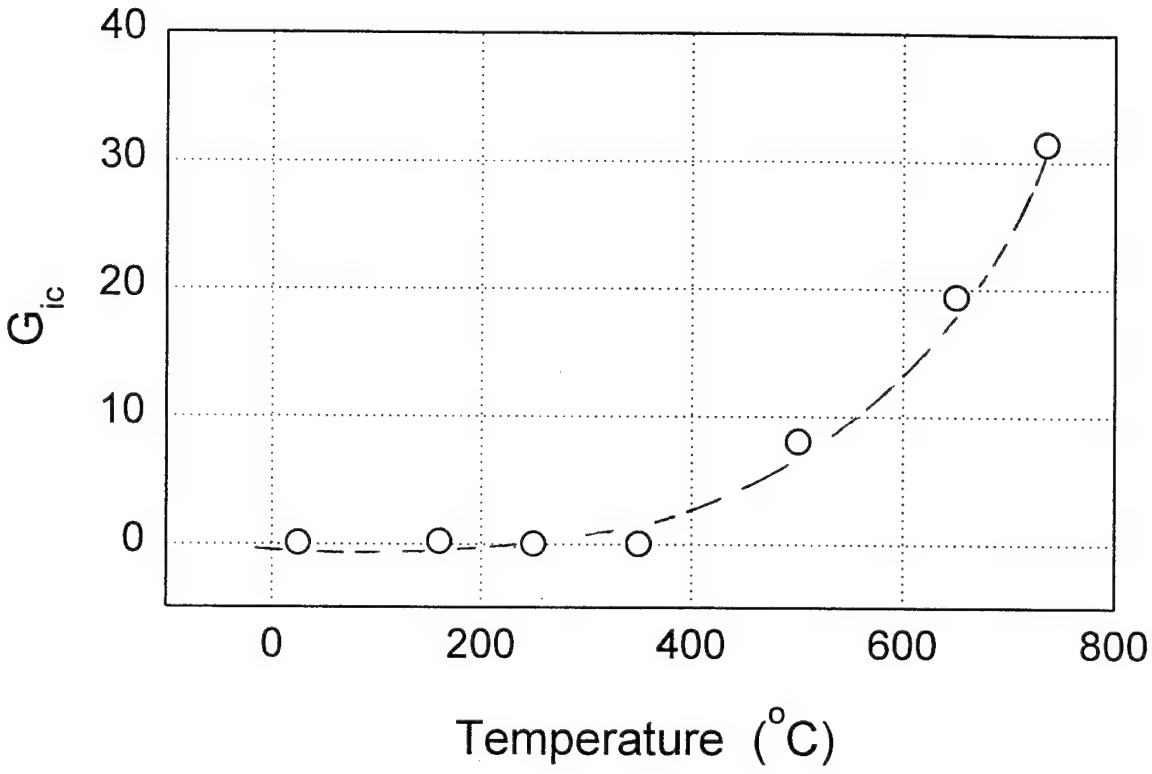

Fig. 3-6 SCS-6/Timetal-21S interface toughness as a function of temperature

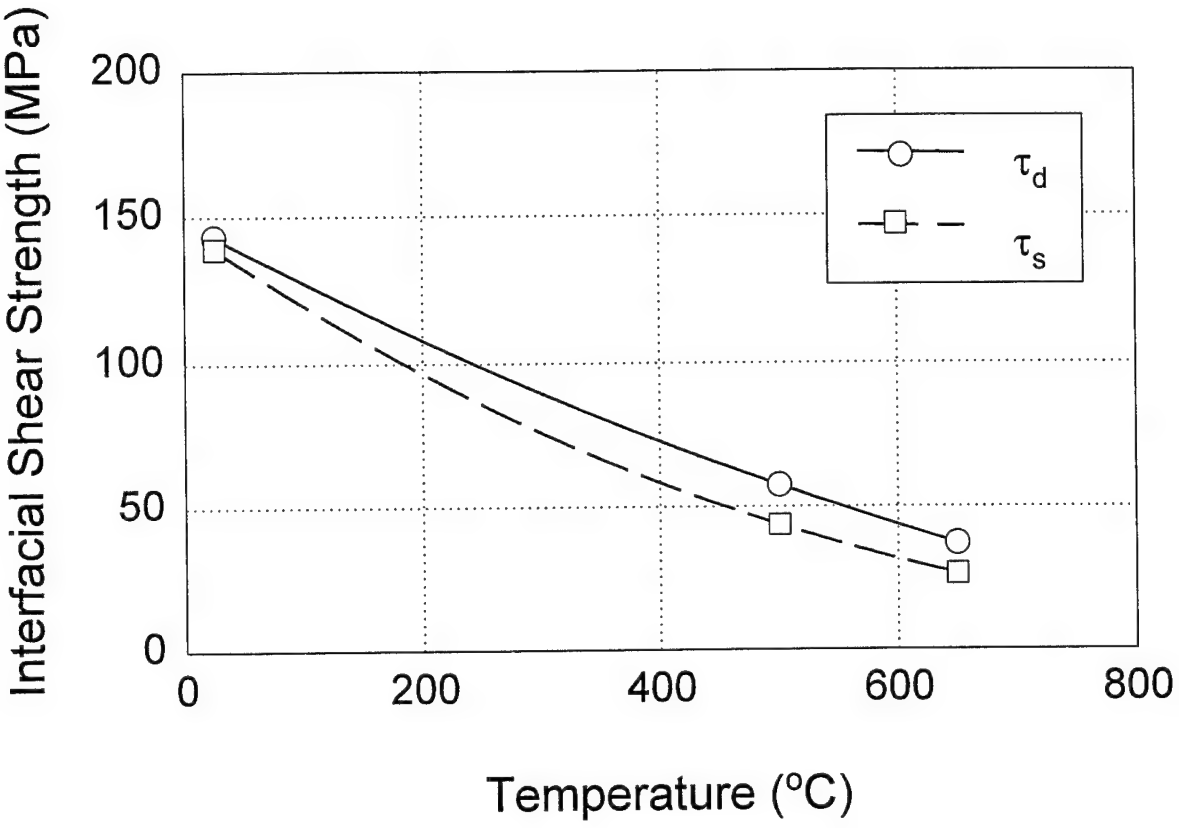

Fig. 3-7 Debond shear strength, τ_d, and frictional shear stress, τ_s, for SM1240/Timetal-21S at various test temperatures

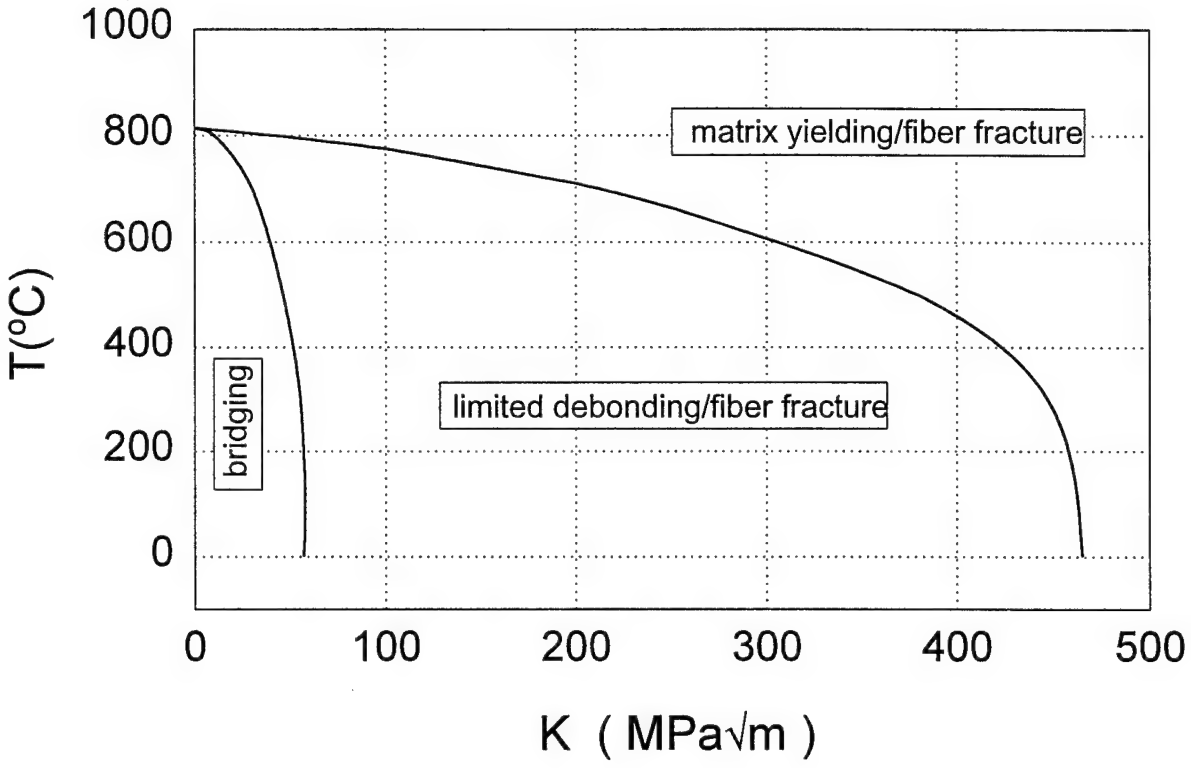

Fig. 3-8 Temperature dependent composite failure map for SCS-6/Timetal-21S

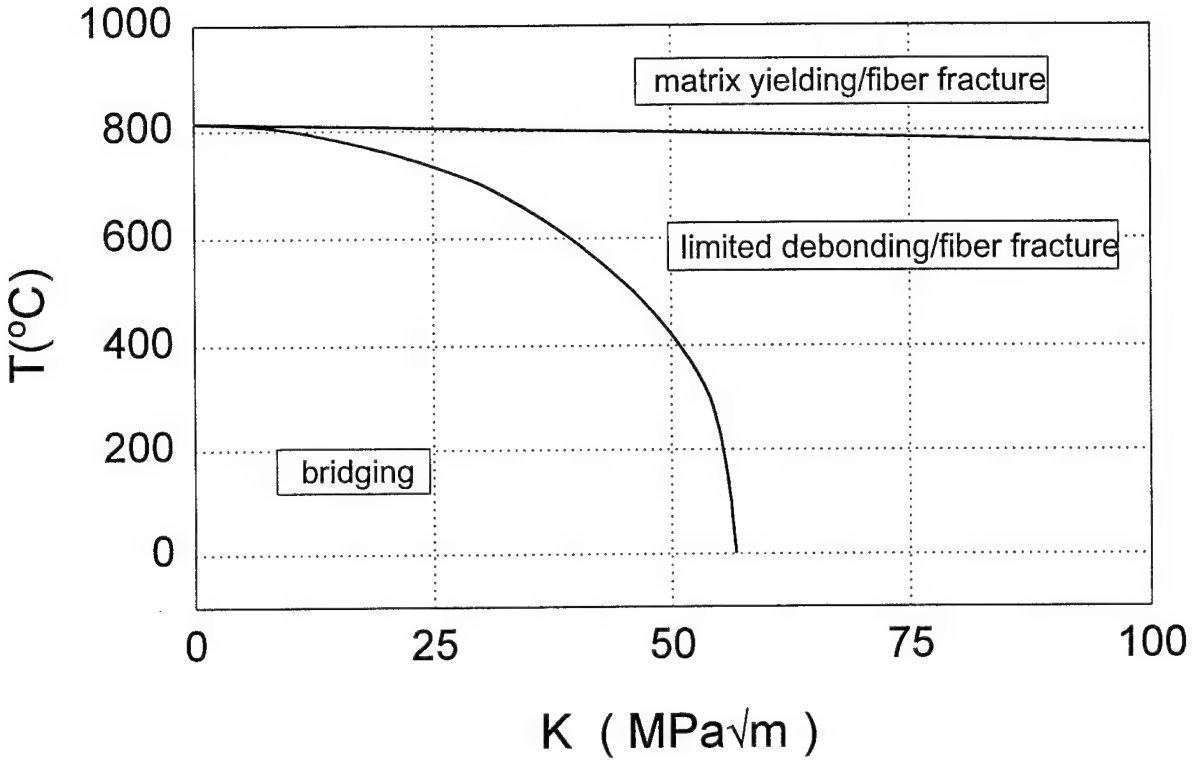

Fig. 3-9 Temperature dependent composite failure map for SCS-6/Timetal-21S showing region of practical application

3.6 APPENDIX A: OPTIMIZATION OF SAMPLE THICKNESS

In order to optimize the sample thickness with respect to the residual stress state and bending considerations, a "slice" of composite is modelled using the finite element method as follows. The internal stress state at each of the test temperatures is calculated using an axisymmetric model of a single fiber embedded in the matrix phase. For the Timetal21S/SCS-6, the interphase is taken to be a 2 μm thick carbon layer. The fiber distribution is idealized as a hexagonal array architecture with a fiber volume fraction of 35%. A longitudinal plane of the composite cylinder is discretized into finite elements as illustrated in Fig. 3-A1. A constraint is imposed on the radial displacement of the outer free surface of the cylinder to acknowlege the effect of the surrounding fibers on the fiber being modelled.

The process induced residual stress is established by a procedure involving initial cool-down of the composite from a stress-free temperature to room temperature and reheating back to the test temperatures of are 25, 500, and 650 °C at a rate of 0.1° C/s. During this process, an isostrain condition is imposed on one end of the cylinder to simulate the far-field axial condition. The cutting of this specimen is then simulated by releasing this constraint, creating a traction-free surface. This step is associated with redistribution of the stress and strain fields in the cylinder model. The free in Fig 3-A2. The octahedral stress state is considered to represent the characteristic stress state along the interface. The results indicate that the residual stress state in the composite sample is representative of that in the true composite for a minimum sample thickness of approximately 0.8 mm at room temperature. At reduced thicknesses, the stress state begins to show significant free surface edge effects which facilitates bending in the specimen.

This residual stress state in the composite "slice" is modified by the applied load on the fiber during the pushout process. The loading is simulated as follows: The composite "slice" is constrained axially along the bottom surface a fixed distance from the fiber, representative of the size of the groove over which the fiber is clamped during the pushout test. A distributed load is applied to the top surface of the fiber over an area corresponding to the diameter of the punch. This loading induces changes in the stress state at the interface which is most severe along the bottom face of the sample. The effect of bending is to generate a tensile radial stress which must be added to the residual compressive stress at this location. Thinner samples experience a greater reduction in the clamping force on the fiber due to the increased effects of bending. For a sufficiently thin sample, this bending effect could result in a Mode I debond crack along the interface at the bottom of the sample. These results are used to find an optimum sample thickness; thick enough to avoid large bending stresses in the specimen during push out, and ensure that fiber debond initiation occurrs at the top face of the sample, while not exceeding the load carrying capability of the punch used for push out testing.

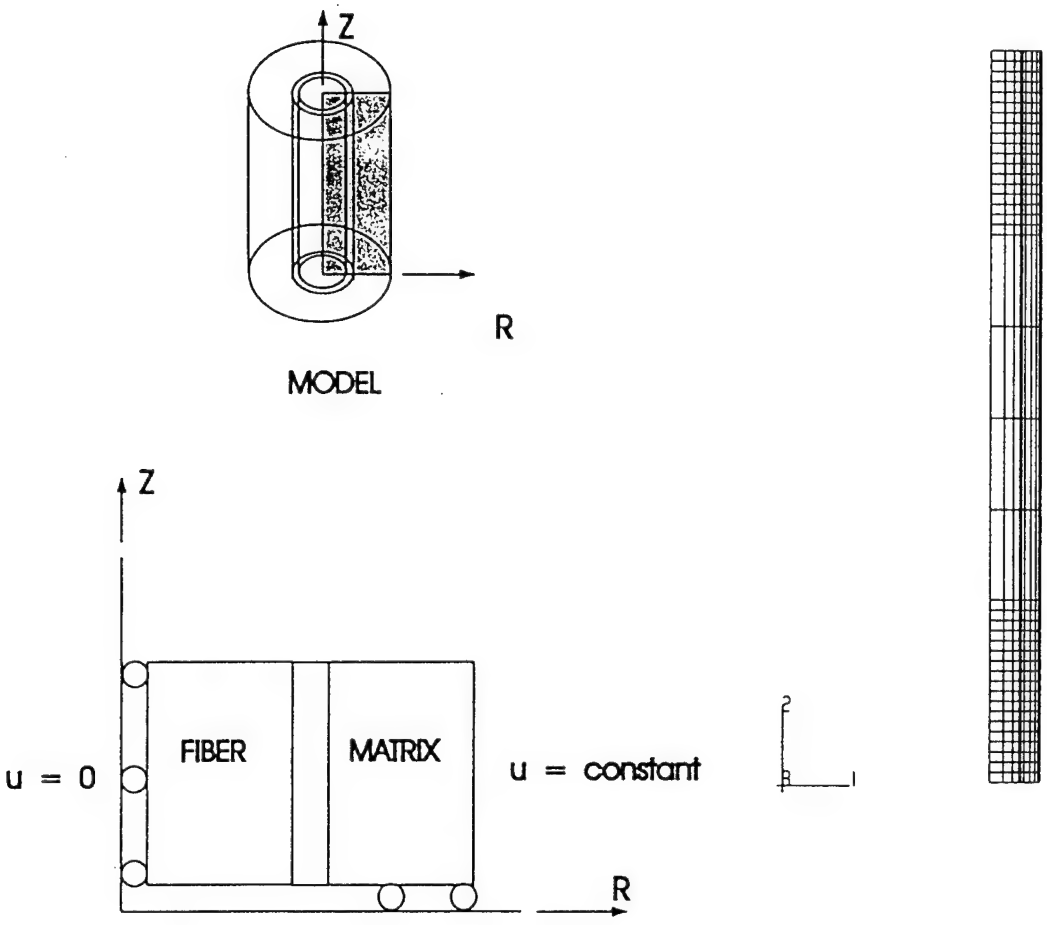

Fig. 3-A1 Model of composite cylinder showing constraints and the finite element discretization

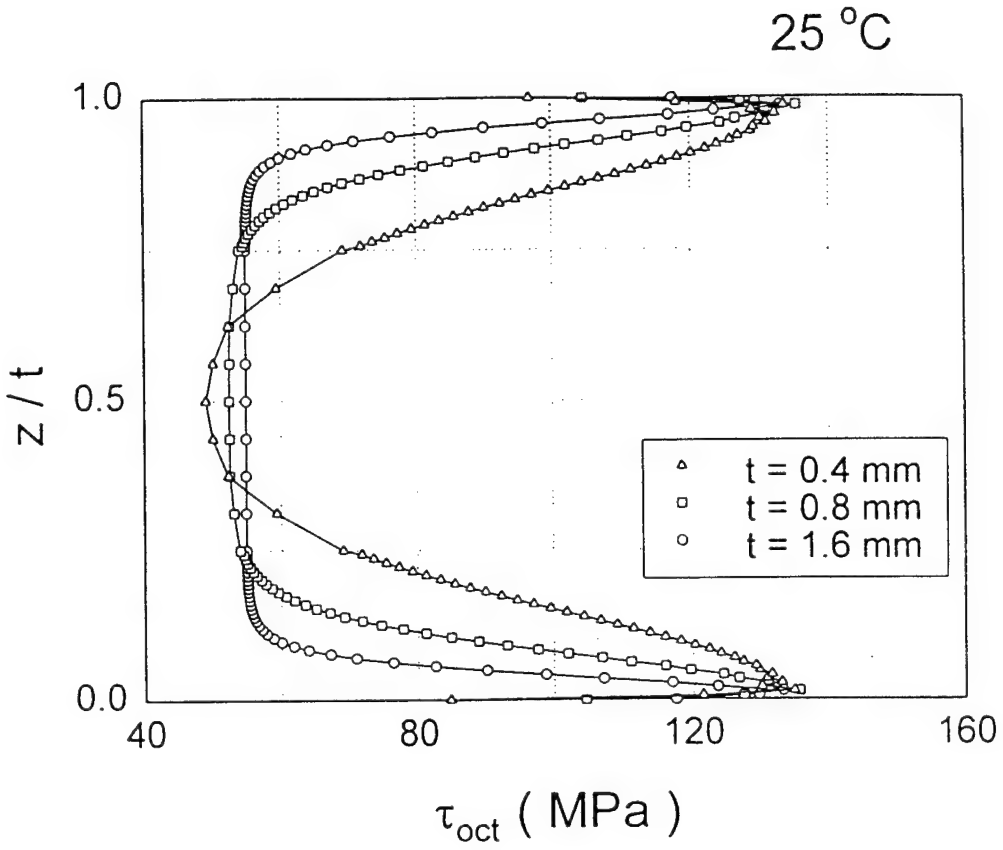

Fig 3-A2 Effect of traction-free surface on the residual stress state in the SCS-6 composite for several specimen thicknesses

3.7 APPENDIX B: CALCULATION OF DAMAGE MECHANISM BOUNDARIES

For the case of a crack approaching a bimaterial interface, comparisons of the energy release rate, G_d, to the energy release rate for interface penetration, G_p, have shown that the ratio G_p/G is independent of the crack length, a [24]. Deflection of the crack when it reaches the bimaterial interface will take place if this ratio is greater than the ratio of interface toughness, G_i to the Mode I toughness of the fiber, G_f, i.e,

$$\frac{G_i}{G_f} < \frac{G_d}{G_p}$$

since interface propagation will require a lower load than for penetration across the interface [24]. The interface toughness at complete debonding

$$G_i = \frac{B_2 R_f}{E_f}\left[\frac{(\tau_d - \tau_f) l}{R_f}\right]^2$$

where

$$B_2 = \frac{(1+\nu_f)(1-2\nu_f)E_m + (1+\nu_m)E_f}{(1-\nu_f)E_m + (1+\nu_m)E_f}$$

and

$$G_f = \frac{(1-\nu^2)\,\sigma_f^2\,\pi\,a_f}{E_f}$$

In these equations, ν_f, ν_m, E_f and E_m are the Poissons ratio and Young's modulus of the fiber and matrix respectivley, σ_f is the fracture strength of the fiber and a_f is the fiber crack length. The ratio of G_i/G_f is found to be propertional to $[(\tau_d - \tau_f)/\sigma_f]^2$ [25]. From this result, it was hypothesized that the critical ratio for describing the failure mechanisms in MMCs is τ_d/σ_f. Using this critical ratio, Chan established a failure diagram which considers bridging, limited and extensive interfacial debondiing, and matrix yield, based on room temperature material and interfacial properties.

Good agreement was obtained through a comparison of this criterion with experimental results, by plotting a delamination diagram and comparing the relative placement of the experimental data either below or above the delamination line. This analysis was restricted to interface delamination and penetration of a crack only. It has been established experimentally that when the ratio of G_i/G_f is high, fiber bridging accompanies the interface decohesion, while when this ratio is low, fiber fracture is the

accompanying mechanism [25]. Due to the proprtionality between G_i/G_f and τ_d/σ_f, it can be assumed that these observations hold for this critical ratio also.

Matrix Failure

Through the analysis of matrix yieilding by a concentrated slip model, Chan et al [30], have shown that matrix slip lowers the normal stress directly in front of the fiber crack tip for $x/L \leq 0.1$ only. Therefore, the stress in a fiber (with diameter D) located directly in front of the crack tip (y=0, x=D/2) can be written based on the K field of a semi-infinite mode I crack [31] as

$$\sigma_{yy} = \frac{K}{\sqrt{\pi D}}$$

At the onset of fiber fracture, $\sigma_{yy} = \sigma_f$ so that

$$\sigma_f = \frac{K}{\sqrt{\pi D}}$$

A criterion for matrix yielding, based on the critical ratio τ_d/σ_f, can be written as

$$\frac{\tau_d}{\sigma_f} > \frac{\tau_y}{\sigma_f}$$

That is, matrix yielding followed by fiber fracture will occur prior to interface debonding if the critical ratio τ_d/σ_f exceeds the ratio of yield strength of the matrix material in shear to the fracture stress of the fiber , σ_f,

$$\frac{\tau_d}{\sigma_f} > \frac{\sigma_y \sqrt{\pi D}}{\sqrt{3}\, K}$$

Recognizing that the debond strength of the interface, τ_d and matrix yield strength, $_y\sigma$ are temperature dependent, the equation for the boundary of the matrix yielding region can be rewritten as

$$K > \frac{\sigma_y}{\tau_d} \left[\sigma_f \frac{\sqrt{\pi D}}{\sqrt{3}} \right]$$

where the proprtionality factor between the stress intensity factor and the temperature dependent material parameters, τ_d and φ, is the constant function of temperature independent material parameters in the paranthesis.

Fiber Bridging

Similarly, for fiber bridging, the fiber stress in the bridging zone can be described [25] as

$$\sigma_{yy} = C\,\tau_s^{1/2}\left(\frac{K_{tip}}{D}\right)^{1/2} r^{1/4}$$

with

$$C = \frac{4}{(1-\nu_f)}\left[\frac{2(1-\nu^2)E_C}{\sqrt{2\pi}\,(b_2'+b_3')\,A\,E_m}\right]^{1/2}$$

$$E_c = \nu_f E_f + (1-\nu_f)\,E_m$$

where ν_f is the fiber volume fraction, A is the orthotropy factor described by Budiansky & Amazigo [32], E_m is the Young's modulus of the matrix, $\nu = \nu_f = \nu_m$ is the Poisson's ratio of the both the fiber and matrix, K_{tip} is the local stress intensity factor at the crack tip, and r is the distance behind the crack tip. The parameter's b_2' and b_3' are nondimensional coefficients which are functions of the elastic properties of the fiber, matrix and composite, which have been defined by Hutchinson and Jensen [33] as follows:

$$b_2' = \frac{(1+\nu)\,E_m\left\{(1-\nu)^2 E_f + (1-2\nu)\,[1-\nu+\rho(1+\nu)]\,(E_m-E_f)\right\}}{(1-\nu)\,E_f\,[(1+\nu)\,E^* + (1-\nu)\,E_m)]}$$

$$b_3' = \frac{\rho(1+\nu)\left\{(1-\rho)(1+\nu)(1-2\nu)(E_f-E_m) + 2(1-\nu)^2 E_m\right\}}{(1-\nu)(1-\rho)[(1+\nu)\,E^* + (1-\nu)\,E_m]}$$

with

$$E^* = \rho E_m + (1-\rho) E_f$$

where the area fiber fraction, $\rho = (R_f/R)^{1/2}$, R_f is the radius of the fiber and R is the radius of the cylindrical shell of composite used in the model. At the onset of fiber bridging, $K = K_{tip}$ and $r = D/2$ for a bridging zone the size of one fiber diameter behind the crack tip.

Noting that $\sigma_{yy} = \sigma_f$ in the bridging zone, the above equation can be expressed in terms of the critical ratio, τ_d / σ_f as

$$\frac{\tau_d}{\sigma_f} = \frac{\tau_d D^{1/2}}{C \tau_f^{1/2} K^{1/2} r^{1/4}}$$

Seperation of the temperature dependent components, τ_s and C (which is a function of the fiber Young's modulus) leads to a description of the boundary for fiber bridging at any temperature

$$K < \frac{1}{C^2 \tau_s} \left(1.416 \sigma_f^2 \sqrt{D} \right)$$

Interface debonding

Between the boundaries of matrix yielding and fiber bridging on the damage process map is the interface debonding region, where fiber fracture will follow debonding before significant bridging will occur.

SECTION 4

PROCESSING-RELATED INTERFACE PROPERTIES IN TITANIUM METAL MATRIX COMPOSITES

ABSTRACT

This section deals with the influence of processing-related residual stresses on the shear strength of the fiber/matrix interphase in a SiC/Ti MMC. For this purpose, three identical SCS-6/Timetal-21S composites were consolidated with different sets of processing variables and post-processing heat treatments. The evolution of residual stress fields in each composite throughout initial cool down from consolidation to room temperature is calculated using finite element method. In this analysis, the relaxation characteristics of the residual stresses at elevated temperature and their effects on the stress field at room temperature are identified. A series of fiber pushout tests on thin-slice samples of each composite were carried out to determine the load values at which partial and full debonding occurs. Finite element calculations of the stress field were employed to assess the interphase strength of the composite as function of temperature. In these calculations, the semi-infinite thickness and the traction-free surface effects of the pushout specimens on the corresponding stress field are considered. For each of these specimens, the distribution of shear stress along the fiber/matrix interface is determined in order to identify a region of stress localization which is taken in this study to be a measure of the interphase shear strength. This strength is then identified as the balance of forces at this localized field due to the traction-free surface of the composite section. Both contributions from process-induced residual stress and geometry-induced constraint of the traction-free surface to the strength are considered. The results of this study showed that the interphase shear strength decreases with an increase in temperature and processing-related residual stress contributes about 35 % to the interphase shear strength at room temperature. Furthermore, the interphase shear strength as calculated in this paper was found to be larger than that determined by considering uniformly distributed shear stress along a pushout fiber.

4.1 INTRODUCTION

The various types of damage modes observed in a unidirectional metal matrix composite, MMC, subjected to fatigue loading include matrix cracking, fiber/matrix interface debonding, delamination, and fiber fracture[1-3]. In an unnotched MMC specimen, matrix cracks are initiated from the interphase region causing stress localization and delamination along the fiber/matrix interface. In a transverse loading of the composite, this damage mode results in a decrease in the composite modulus and a consequent decrease in strength. In the presence of a dominant matrix crack propagating perpendicular to the fiber orientation, unbroken fibers in the crack wake bridge the crack surfaces. Crack bridging, which is an important toughening mechanism in a unidirectional MMC, is based on the ability of the fiber to carry the evolving stress caused by the relative displacement between the fiber and the matrix. In a MMC with strong fiber/matrix interface such as the B_4C-B/Ti-6Al-4V

composite, limited relative displacement results in an early fiber fracture [4]. On the contrary, the relatively weak fiber/matrix interface in a SiC/Ti MMC allows for interface debonding to occur with a corresponding increase in the crack opening displacement. The initiation of damage in this interphase layer is affected by the localization of stresses as the matrix crack tip approaches the interface.

Both delamination and interface debonding modes of fracture, have been shown to be influenced by the fiber/matrix interphase strength [5-7]. The strength of the interphase dictates the extent of interface failure which, in turn, determines the durability of a composite system. In a SiC/Ti-MMC, the chemical bonding has been shown to be insignificant or nonexistent [8,9]. The strength of fiber/matrix interphase region, therefore, is derived from mechanical clamping on the fiber due to the residual stress field. The residual stress states in each constituent of the composite are the results of fabrication method and post-processing heat treatment procedures. The interphase strength could then be viewed as a processing by-product parameter which can be tailored to optimize the resistance of the composite to fatigue failure. In addition, the strength is influenced by the growth kinetics and thermal aging characteristics of the interphase region. While direct measurement of the interphase strength is difficult to obtain, information leading to the determination of the strength values could be extracted from results of fiber pullout or pushout test of the composite samples. The influence of temperature and its consequent modification of the damage mechanism in a SiC/Ti MMC has not been studied. In the present work, the authors have examined the idea that the interphase strength is influenced by the composite processing approach where the nature of the interface region and the internal stress field both define this strength.

Effects of different processing variables and different post-processing heat treatments on the residual stress field in the interphase region of a SiC/Ti MMC are studied in this paper. Fiber pushout procedure and numerical calculations of the associated stress field in thin-slice specimens cut from these differently processed composites are utilized to assess the interphase shear strength of a SiC/Ti MMC as function of test temperatures. The contributions of process-induced residual stress and geometry-induced modification of the stress field on the shear strength are evaluated.

The first part of this section describes the material used in the study as well as experimental procedure and related results. This is followed by a description of a finite element cylinder model employed in calculations of residual stress field in the different composites and in finite thickness specimens used for fiber pushout experiments. The calculated stress field in the pushout specimen at the debond load is then presented and the interphase shear strength is defined. The last portion of this section discusses the implication of the calculated interphase shear strength on the damage modes encountered in metal matrix composites.

4.2 MATERIAL AND EXPERIMENTAL PROCEDURES

The material used in this study is a unidirectional SCS-6/Timetal-21S composite. The metastable β titanium matrix, Timetal-21S, is alloyed with (in wt. %) 0.1 Fe, 16.0 Mo, 3.06 Al, 2.9 Nb, 0.2 Si, 0.22 C, 0.12 O and 0.005 N. The SCS-6 reinforcing fibers are 140 μm-diameter, carbon cored SiC body, with a 2-μm dual carbon-rich coating.

Three identical composites, denoted as C1, C2 and C3, are consolidated with a Foil/Fiber/Foil lay-

up using a vacuum hot pressing technique. Each composite is fabricated with a different set of processing variables to generate different processing-related properties. The temperature and applied pressure histories employed during post-fabrication cool down are illustrated in Figs. 1(a) and (b), respectively. The first two temperature profiles include an 8-hour heat treatment in vacuum at 650 °C. The cross section of each composite samples exhibited a staggered array of fiber arrangement with full consolidation taking place around the fiber and at the foil/foil interfaces resulting in complete consolidation. The nominal fiber volume fraction in all cases is 0.35.

Sample thickness is governed by two requirements essential for a valid fiber pushout test. Minimum thicknesses must be sufficient to ensure that the residual stress in the composite is preserved. The minimum thickness to satisfy this requirement is determined for each test temperature using the finite element method, as will be discussed later. Maximum thickness is limited by the maximum pushout load that can be sustained by the punch. With this knowlege, the composites are sliced into thin-samples with thickness ranging from 0.5 to 1.4 mm. Each sample is then ground, polished and mounted in a pushout testing machine and heated to the test temperature levels in vacuum condition. The fiber pushout tests are performed at ambient temperature, 500 and 650 °C. At each test temperature, several fibers which were aligned with grooves in the bottom side of the specimen were pushed out in a displacement-control mode. A load-motor displacement curve is obtained for each fiber pushout. The pushout test matrix is shown in Table. 1.

Table 4.1 Test matrix for fiber pushout tests of SCS-6/Timetal-21S composites.

ID	T (°C)	H (mm)	P_i (N)	P_s (N)	$\tau_{d\text{-}ave}$ (MPa)
C1	25	0.50	38.0	32.0	172.8
C1	500	0.91	16.0	13.6	40.0
C2	25	0.50	40.3	35.0	183.3
C2	500	0.91	17.0	10.3	42.5
C3	25	0.50	46.0	37.5	191.0
C3	163	0.52	31.0	23.9	135.5
C3	250	0.91	50.0	40.0	124.9
C3	350	1.10	44.0	28.0	90.9
C3	500	1.40	23.0	25.5	34.1
C3	650	1.40	20.5	17.9	30.9
C3	735	0.95	12.0	2.5	28.7

An average load-displacement curve obtained from fiber pushout tests at 650 °C is shown in Fig. 2. The compliance of the load train has been subtracted from these results. The pushout load corresponding to a noticeable displacement marks the onset of interface debonding event (Point A), with a noticeable drop in load. Additional load is required to propagate the debond crack to a critical length before sliding occurs (Point B). The magnitude of the load drop is reflective of the toughness of the interphase while the load level corresponding to the end of the drop (Point C) is representative of the frictional shear characteristics of the debonded interface surfaces.

4.3 RESIDUAL STRESS ANALYSIS

In a SiC/Ti MMC, interface debonding has been observed to occur along the carbon-rich coating which is a thin layer in relation to the fiber or matrix dimension. The interface can therefore be represented by a mathematical plane with zero thickness. A concentric two-phase cylinder model of a fiber embedded in the matrix phase is utilized here to calculate the evolution of stress fields along the interface up to the initial debonding stage. The interface plane is assumed to accommodate radial and shear stress components. In an infinitely long composite where the free surface effect is negligible, and perfect bonding is assumed to exist, the shear stress component diminishes and the mechanical bonding is provided by the compressive radial stress only.

This cylinder model is applied to a SCS-6/Timetal-21S composite with an idealized hexagonal array architecture of fiber distribution. The mechanical and physical properties of the SiC SCS-6 fiber and the titanium alloy Timetal-21S are obtained from several publications [10-12]. The matrix inelastic strain response is described using a unified viscoplastic theory [13,14]. Due to the axisymmetric geometry of the model, only a longitudinal plane of the composite cylinder need to be analyzed. An isostrain condition is imposed on one end of the cylinder to represent the generalized plane strain condition or removed to simulate a traction-free surface. A constraint of constant radial displacement is imposed on the outer surface of the modeled cylinder to acknowledge the existence of surrounding fibers. A detailed description of the model can be found in Ref. [15].

The process-induced residual stress is established in each composite by a procedure involving cooling down from a stress-free temperature with the corresponding temperature history shown in Fig. 1(a). The applied fabrication pressure, however, has not been modeled in the simulation due to the selection of the representative volume element. The calculated evolution curves for the matrix phase, as shown in Fig. 3(a), indicate that while the elastic portion of the evolution curve is controlled by the coefficient of thermal expansion, its magnitude is set by the degree of inelastic flow permitted in the viscoplastic affected range, from consolidation to about 600 °C. However, the relaxation of the residual stress in this temperature range is limited due to its small magnitude as shown in Fig. 3(b). In addition, the evolution curves for all three composite samples considered in this study are practically identical, thus, the residual stress contribution to mechanical strength of the interphase is expected to be correspondingly similar.

The effect of traction-free surface on the residual stress field in a thin-slice sample is examined by relaxing the isostrain condition on both the top and bottom surface of the cylinder model. The tensile and compressive axial residual stresses in the matrix and fiber, respectively, are ramped to

zero on the traction-free surface of the sample causing strain mismatch across the interface. Consequently, continuum shear stress develops in the interphase region along the fiber with greatest magnitude which is located immediately below the traction-free surface and diminishes to zero at a distance of about three fiber radius beneath the surface. In addition, the displacement of the stress-free surface of the matrix produces a tensile radial stress component in the immediate region below the surface. These variation of both radial and shear components of residual stresses along the interface in the thin-slice specimen at room temperature is shown in Fig. 4.

The pushout configuration is simulated by constraining the axial displacement of the matrix on one side (bottom) and pushing the fiber from the other (top). The applied load is increased from zero to the value corresponding to initial debond level as obtained from fiber pushout curve (Point A in Fig. 2). The load at initial debonding, P_i, observed during fiber pushout tests at various test temperatures are listed in Table 1 along with the corresponding average shear stress, $\tau_{d\text{-}ave}$, acting along the cylindrical surface of the fiber. The calculated variation of shear stress along the interface due to this pushout load is shown in Fig. 5(a) for the test temperature of 25 °C. The shear stress magnitude at the interface due to pushout load is greatest just beneath the bottom surface of the thin-slice specimen. The variation of the residual shear stress component along the interface is also plotted in the same figure.

The superposition of both stress contributions from residual and pushout load resulted in an intense shear stress localization at the bottom side of the specimen. On the other hand, the residual and pushout load effects on the shear stress are canceled at the top surface, as illustrated in Fig. 6(a). The distribution of the resulting interphase shear stress at the onset of debonding is shown in Fig. 5(b) for the three temperatures considered; 25, 500 and 650 °C. The high shear stress magnitude at the bottom surface of the specimen, coupled with a tensile radial component of residual stress, suggests that interface debonding initiates from this location. At the onset of debonding, assuming that the debonding event is a shear stress controlled process, the stress magnitude reached the strength level of the interphase. The shear strength of the interphase, therefore, can be determined from this distribution.

4.4 INTERPHASE SHEAR STRENGTH

The interphase shear strength, τ_d, is viewed in the present work, as the shear stress level at the interface which needs to be overcome to initiate interface debonding. As discussed above, interface debonding is assumed to begin at the bottom or constrained side of the thin-slice specimen in a typical fiber pushout test. It is worth noting that the calculated shear stress, in its limit, is infinite at the surface due to the traction-free surface boundary condition. Since this is not a physically admissible value, an initial debond crack of finite length is expected to form due to cutting of the thin-slice specimen. In this work, an initial debonding length of one fiber radius is assumed to exist prior to fiber pushout. The strength of the interphase region, therefore, is determined by the resultant shear stress magnitude along the interface at a distance of one fiber radius from the bottom surface of the specimen.

The contribution from process-induced residual stress, $\tau_{d\text{-}res}$, and geometry-induced constraint,

$\tau_{d\text{-}Pi}$, of the traction-free surface to the interphase shear strength is listed in Table 2. The resultant variation of interphase shear strength with temperature is shown in Fig. 7 while the strength values at 25, 500 and 650 °C are listed in Table 2. It is noted that the residual stress contributes approximately 35 percent to the shear strength of the interphase at room temperature while at 500 and 650 °C, the contribution is less significant. The average shear strength, $\tau_{d\text{-}ave}$, determined using the shear-lag model with the applied load taken at the initial debond and the assumption of uniformly distributed shear stress, is also plotted in Fig. 7. The discrepancy between these two approaches indicates that this assumption of uniform shear along the interface greatly underestimate the shear strength of the interphase region.

Table 4.2 Process-related interphase properties of SCS6/Timetal-21S composites

T (°C)	τ_d (MPa)	$\tau_{d\text{-}res}$ (MPa)	$\tau_{d\text{-}Pi}$ (MPa)	τ_s (MPa)	G_i (Jm^{-2})
25	221.2	76	145.24	149.2	45.9
500	160.5	23	137.5	41.2	1039
650	138.6	8.75	130	20.6	1034

4.5 DISCUSSION

An interface debonding length is a consequence of debonding and sliding process taking place along a bridging fiber. Such a damage process relies on the stresses acting along the interface as well as the strength properties and toughness of the interphase region. The onset of debonding, in particular, is controlled by the amount of allowable relative displacement across the fiber/matrix interface and the debonding strength of the interphase region. In the present work, the debond crack initiation is assumed to be a stress-controlled event. The interphase strength, therefore, can be derived from the local stress field at the interface corresponding to the onset of debonding.

The interface debonding process begins as the matrix crack reaches a bridging fiber causing the longitudinal matrix stress to ramp to zero at the stress-free crack surface. The associated crack opening displacement, then, introduces additional constraints in clamping the fiber along some distance above the matrix crack plane. In addition, this geometry configuration introduces a distribution of the continuum shear stress along the fiber which is maximum at the matrix crack surface and diminishes at the far-field region in the composite. These local stress and strain fields which arise from geometrical constraints contribute to the interphase strength, in addition to the contribution from the process-induced residual stress.

The fiber pushout test on a thin-slice composite sample provides information on the onset of interface debonding and frictional sliding of the debonded interfaces. The applied pushout load level at initial debonding is obtained from the resulting load-displacement curve. The stress distribution

corresponding to this pushout load level in the interphase region of the thin-slice specimen along a fiber can be calculated using the finite element method. The location of interface debonding can be inferred by examining the localization of the stress field along the pushed out fiber, due to the traction-free surface effect of the specimen. Since this stress field is present in the thin-slice specimen at the onset of debonding, the shear stress magnitude at the debonding location should have reached the shear strength of the interphase. This objective was achieved here by combining experimental procedure of fiber pushout and numerical calculations of stress distribution in pushout specimens in order to accurately quantify the interphase shear strength, τ_d . The significance of the results of this work is apparent in the fact that τ_d defines the fracture toughness of the interphase, G_i. In the work of Liang and Hutchinson [16], the interphase toughness, G_i, is expressed to be proportional to the square of the difference between the debond strength and the frictional shear stress,τ_s, i.e., $(\tau_d - \tau_s)^2$. This frictional shear stress is determined, in this work, as the average stress corresponding to the load, P_s, at the end of the load drop (Point C in Fig 3) These load levels for all tests are listed in Table 1 and the corresponding τ_s is plotted in Fig. 6 as function of temperature. The different values of interphase shear strength determined from consideration of stress localization and using the assumption of a uniform stress distribution, therefore, yield different values of G_i. These calculated values of the interphase toughness are compared in Table 2 for temperatures of 25, 500 and 650 °C.

Since the interphase region is the key in defining the damage process in a MMC, the knowledge of interphase toughness, in relation to the applied stress, would determine the operating mode of fracture. The failure mode between interface delamination and fiber fracture can be predicted from the ratio of τ_d / σ_f, where σ_f is the fracture strength of the fiber [17,18]. In bridging fatigue crack growth, the crack tip shielding is defined in terms of crack opening displacement, COD, along bridging fibers, which in turn, is dependent on the debonding length of the fiber. This debonding length can be determined on the basis of the knowledge of stress field along the interface and toughness of the interphase region, G_i. Both the debonding length and the interphase toughness are governed by the interphase shear strength, τ_d.

The extension of the matrix crack at the fiber location, during crack bridging, creates similar geometrical constraints, both in the traction-free matrix surface and in inducing additional clamping on the fiber, as observed in a thin-slice pushout sample near the free surface. In view of these identical configurations existing at the initial debond location, the shear strength, determined in the present work, can be treated as the true interphase shear strength value in modeling fatigue crack bridging in Ti-MMCs. Since the
interphase shear strength governs the debonding length along a fiber, which in turn controls the extent of fiber/matrix interface debonding, it also controls the amount of crack tip shielding in the crack bridging process. An accurate determination of this interphase property is, therefore, essential in successfully modeling the bridging fatigue crack growth.

4.6 CONCLUSIONS

The interphase shear strength in a SCS-6/Timetal-21S composite have been determined utilizing results from fiber pushout tests on thin-slice composite samples combined with calculated distribution

of shear stress along the fiber/matrix interface. The results can be summarized as follows:

1. Significant variations in composite post-processing heat treatment produce limited variation in the residual stress field in the range of consolidation temperature to 600 °C.

2. The localized stress field along the fiber/matrix interface during a pushout test shows a higher interphase shear strength than the strength values calculated with the assumption of a uniform shear stress distribution.

3. The shear strength of the interphase consists of contributions from process-induced residual stress and geometry-induced constraint of traction-free matrix surface. The residual stress contributes approximately 35 % of the interphase strength at room temperature. The contribution at 650 °C is only about 7 %.

4. The interphase shear strength decreases with the increase in temperature while the toughness of the interphase region is proportional to temperature.

4.7 REFERENCES

[1] S. M Jeng, P. Allassoeur and J. M. Yang, Materials Science and Engineering, **A154**, 11(1992).

[2] P. Bowen, A. R. Ibbotson, and C. J. Beevers, Fatigue of Advanced Materials, R. O. Ritchie, R. H. Danskardt and B. N. Cox, eds., Materials and Component Engineering Publications Ltd., UK, 379 (1991).

[3] D. Zheng and H. Ghonem, Metallurgical and Materials Transactions A, **26A**, 2469(1995).

[4] D. L. Davidson, R. M. Arrowood, J. E. Hack, G. R. Leverant, and S. P. Clough,, in Mechanical Behavior of Metal Matrix Composites, J. E. Hack and M. F. Amateau, eds., TMS-AIME, Warrendale, PA, 117(1981).

[5] M. L. N. McCartney, Proceedings of The Royal Society London, **409A**, 329(1987).

[6] M. D. Sensmier, and P. K., Wright, Fundamental Relationships Between Microstructure and Mechanical Properties of Metal Matrix Composites, M. N. Gungor and P. K. Liaw, eds., The Mineral, Metal and Materials Society, Warrendale, PA, 441 (1990).

[7] R. M. McMeeking and A. G. Evans,Mechanics of Materials, **9**, 217 (1990).

[8] D. C. Phillips, Journal of Material Science, **9**, No. 11, 1847 (1974).

[9] K. M. Prewo and J. B. Brennan, Journal of Material Science, **15**, No. 2, 463 (1980).

[10] Y. Le Petitcorps, M. Lahaye, R. Pailler and R., Naslain, Composites Science and Technology, **32**, 31 (1988).

[11] P. L. Martin, W. H. Bingel and M. Mahoney, Workshop Proceedings for Titanium Matrix Components, P. R. Smith and W. C. Revelos, eds., Wright-Patterson AFB, Ohio, WL-TR-92-4035, 277(1992).

[12] H. Ghonem, Y. Wen, D. Zheng, M Thompson and G. Linsey,Materials Science and Engineering, **161**, 45(1993).

[13] S. R. Bodner and Y. Partom, Journal of Aplied Mechanics, **42**, 385 (1975).
[14] R. W. Neu and S. R. Bodner, Contributive Research and Development- **6**, Prepared for Wright-Patterson AFB, Ohio, Sept 1995.
[15] M. N. Tamin and H., Ghonem, Advance in Fatigue Lifetime Predictive Technique, 3rd Volume, ASTM STP 1292, M. R. Mitchell and R. W. Landgraf, eds., American Society for Testing and Materials, 24(1996).
[16] C. Liang, and J. W. Hutchinson, Mechanics of Materials, **14**, 207 (1993).
[17] M. Y. He, and J. W. Hutchinson, International Journal of Solids and Structure, **25**, 1053 (1989).
[18] K. S. Chan, Acta Metall. Mater., **41**, No. 3, 761 (1993).

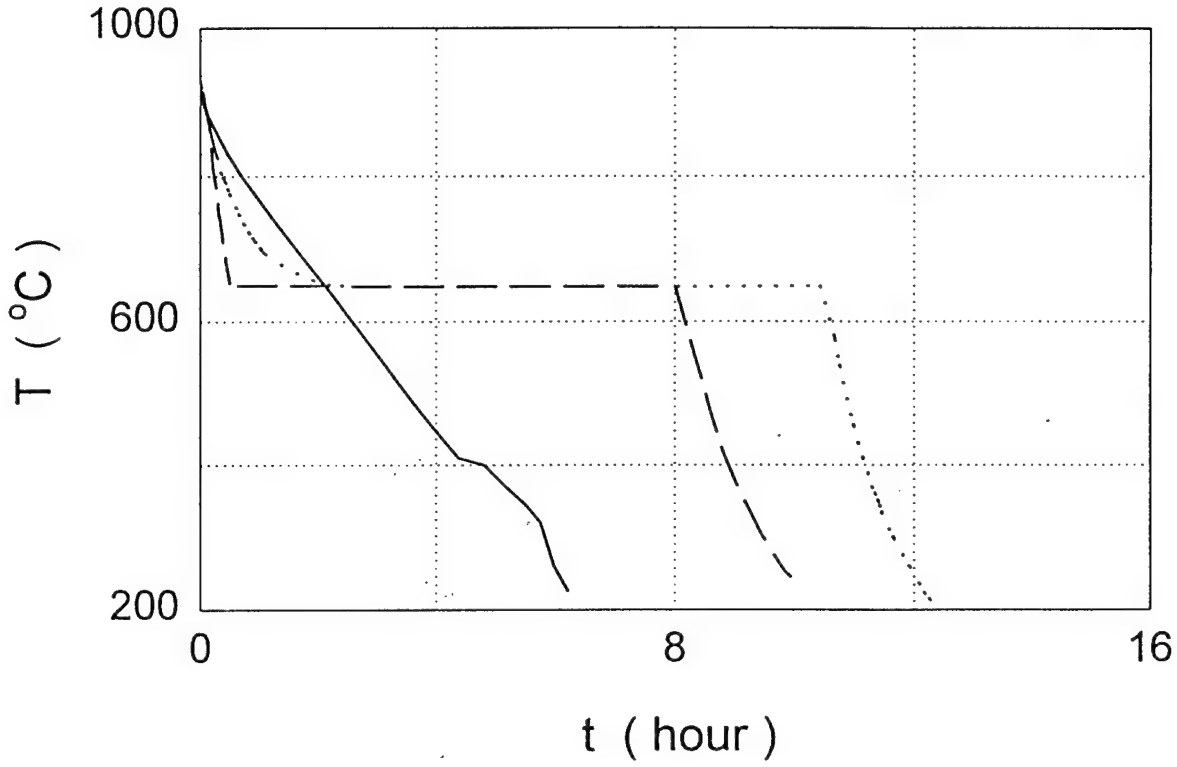

Fig. 4-1(a) Processing control variables employed during post-fabrication cool down of the composites - temperature profile

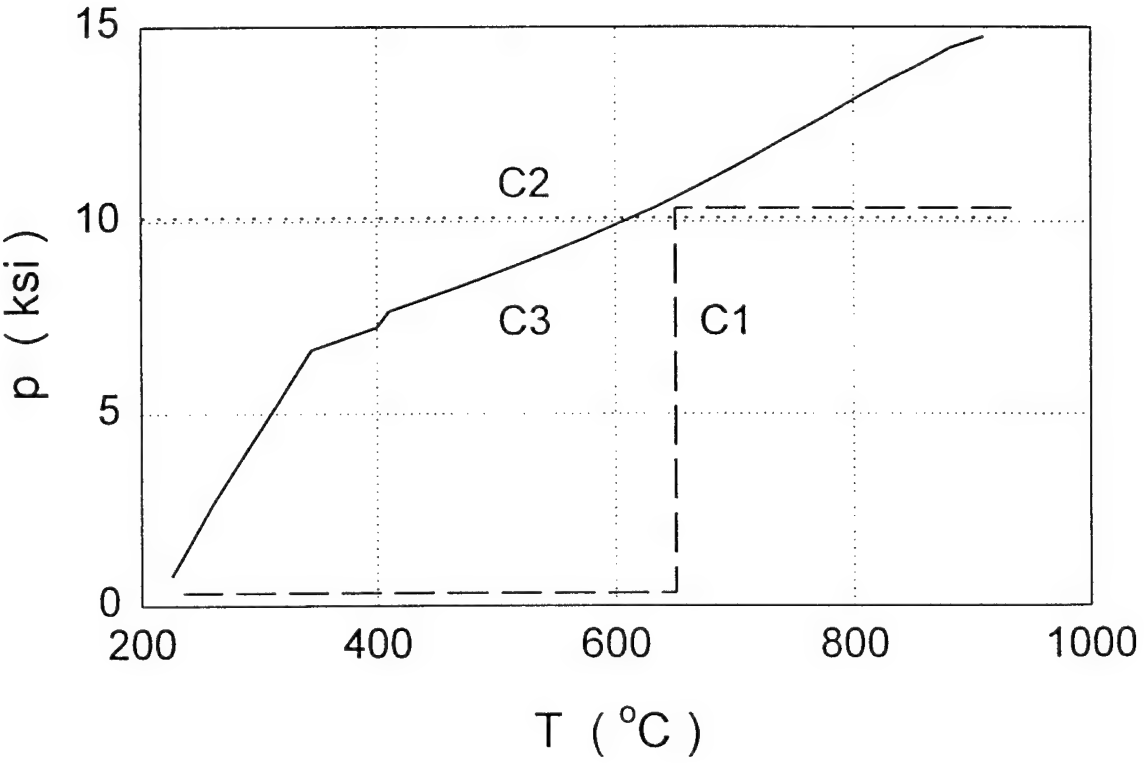

Fig. 4-1(b) Processing control variables employed during post-fabrication cool down of the composites - applied pressure history

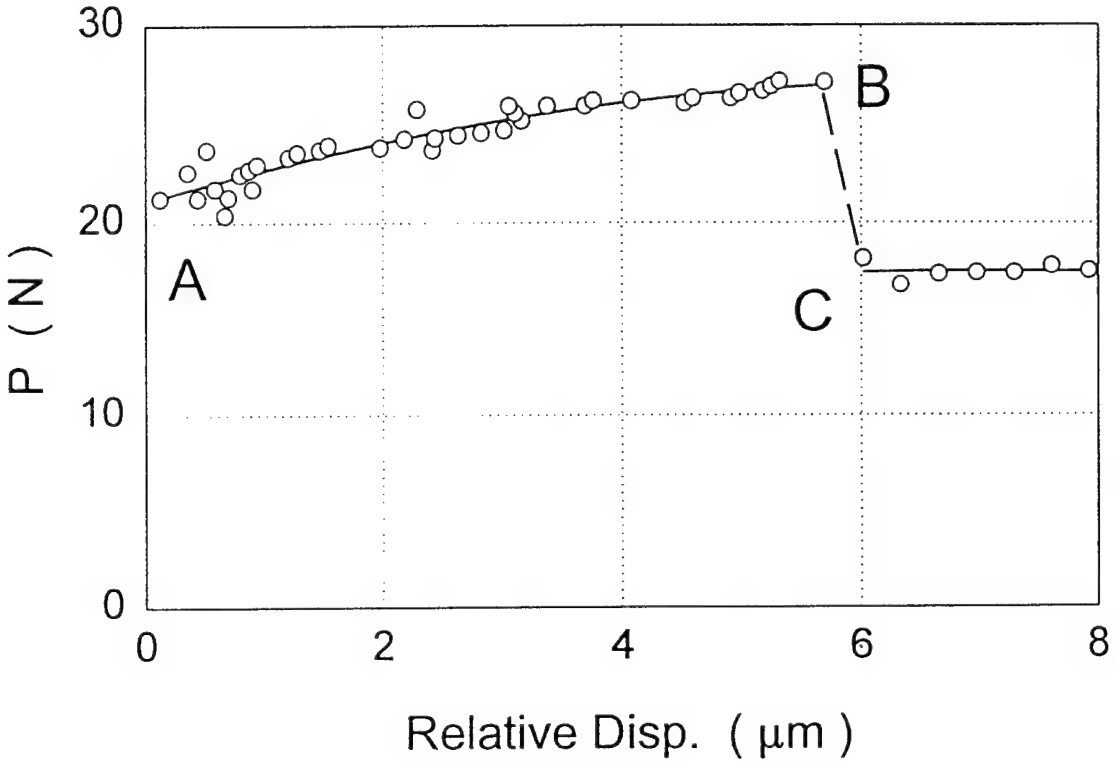

Fig. 4-2 Average pushout load-displacement curve of a SCS-6/Timetal-21S composite during fiber pushout tests at 650 °C. The sample thickness, H = 1.44 mm.

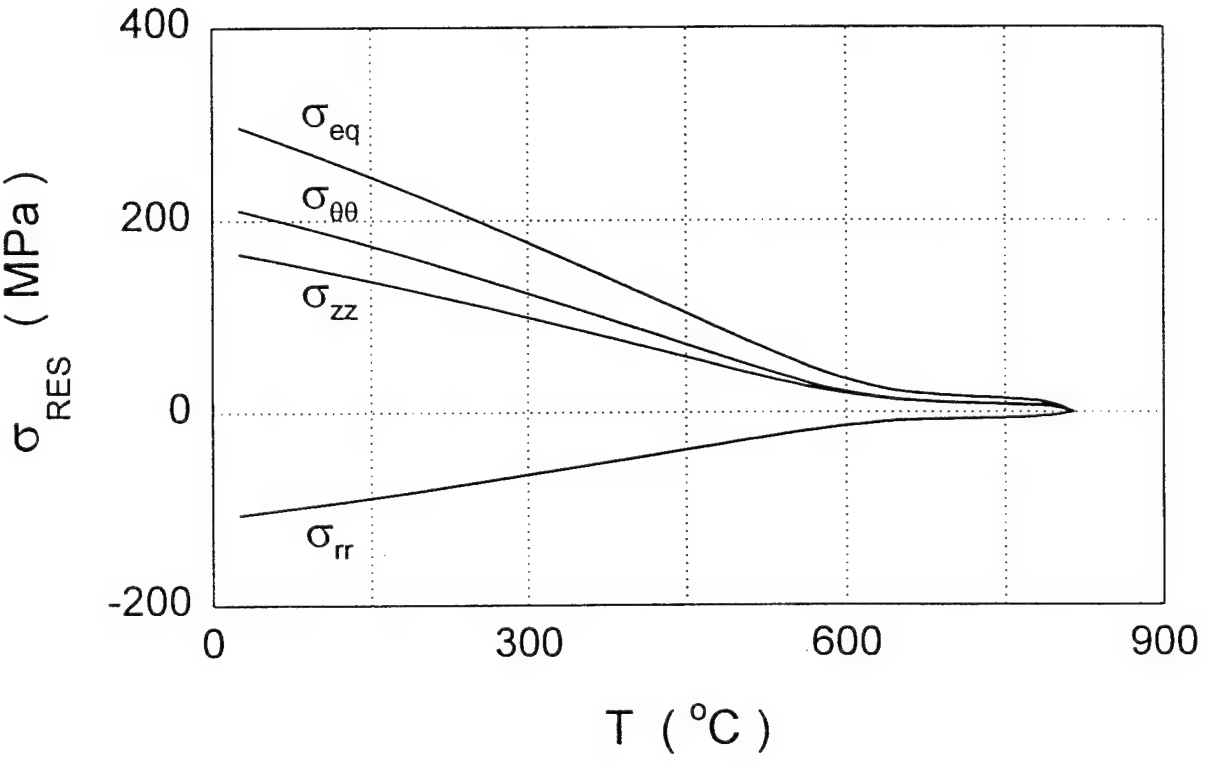

Fig. 4-3(a) Evolution of residual stresses in the matrix phase of SCS-6/Timetal-21S composite during initial cool down from stress-free to ambient temperature.

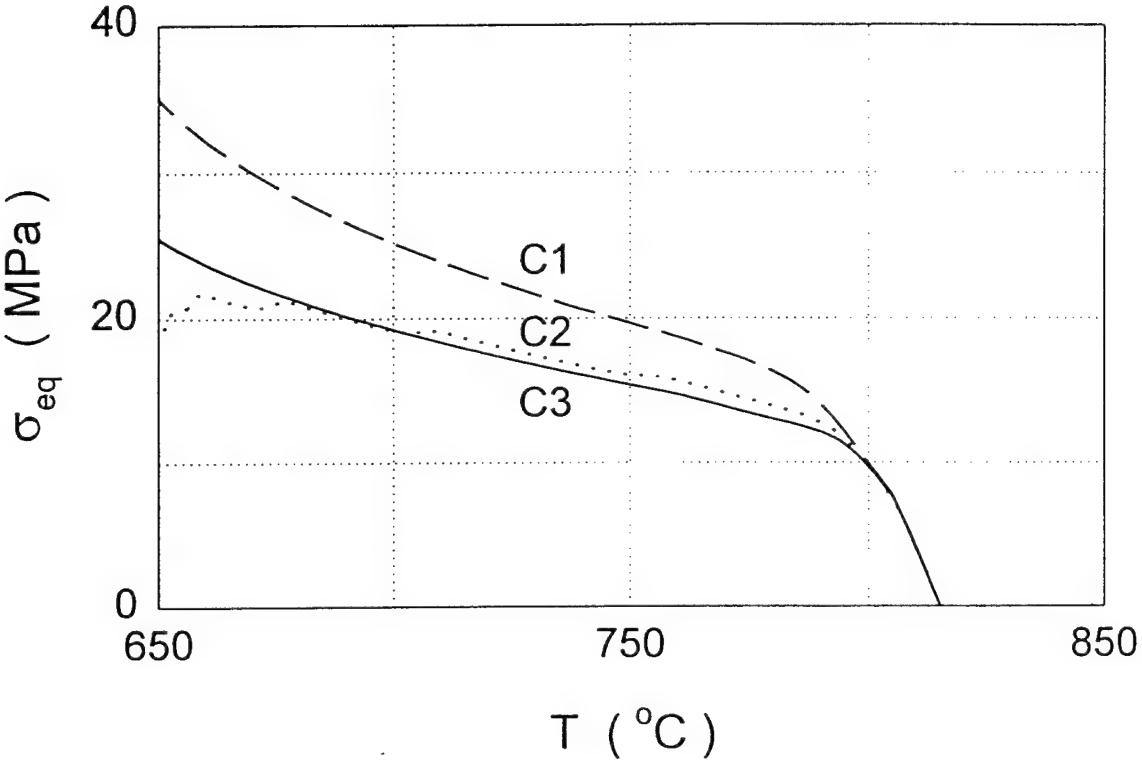

Fig. 4-3(b) The buildup of effective residual stress in the matrix phase of each composite during cool down to 650 °C.

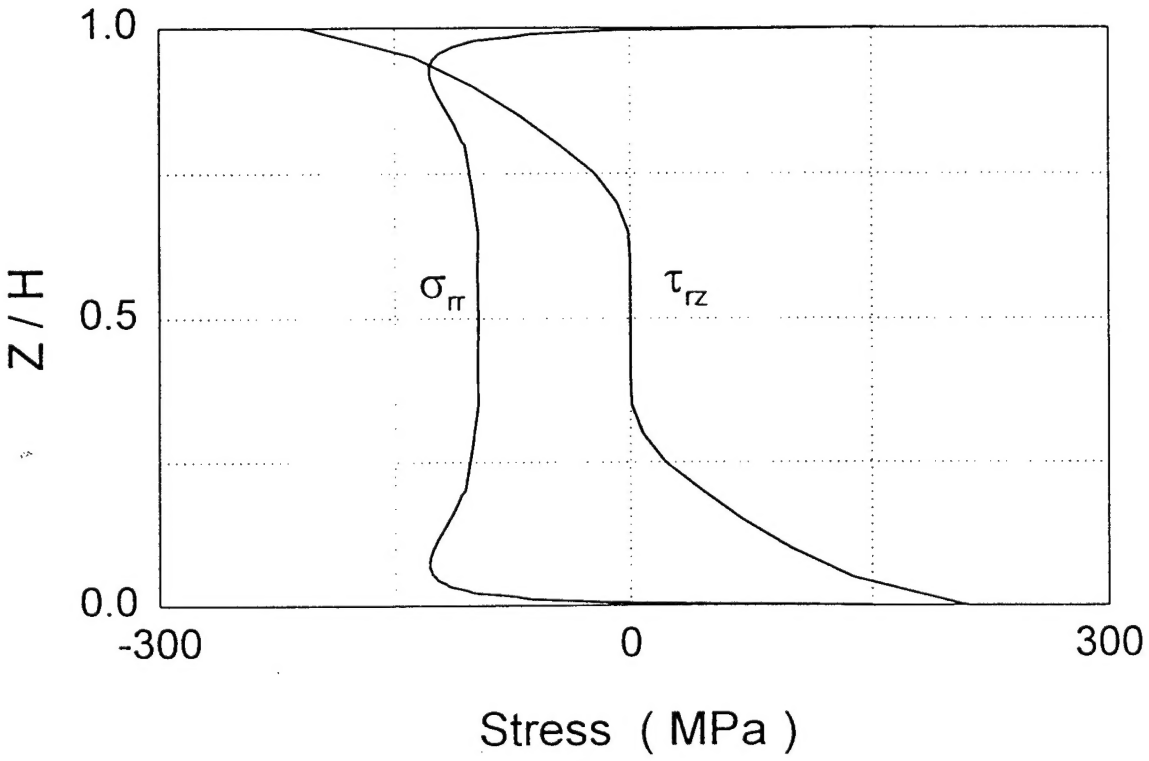

Fig. 4-4 Variation of residual radial and shear stress componenets along the fiber/matrix interface in a thin-slice composite sample at 25 °C. The sample thickness, H = 0.50 mm.

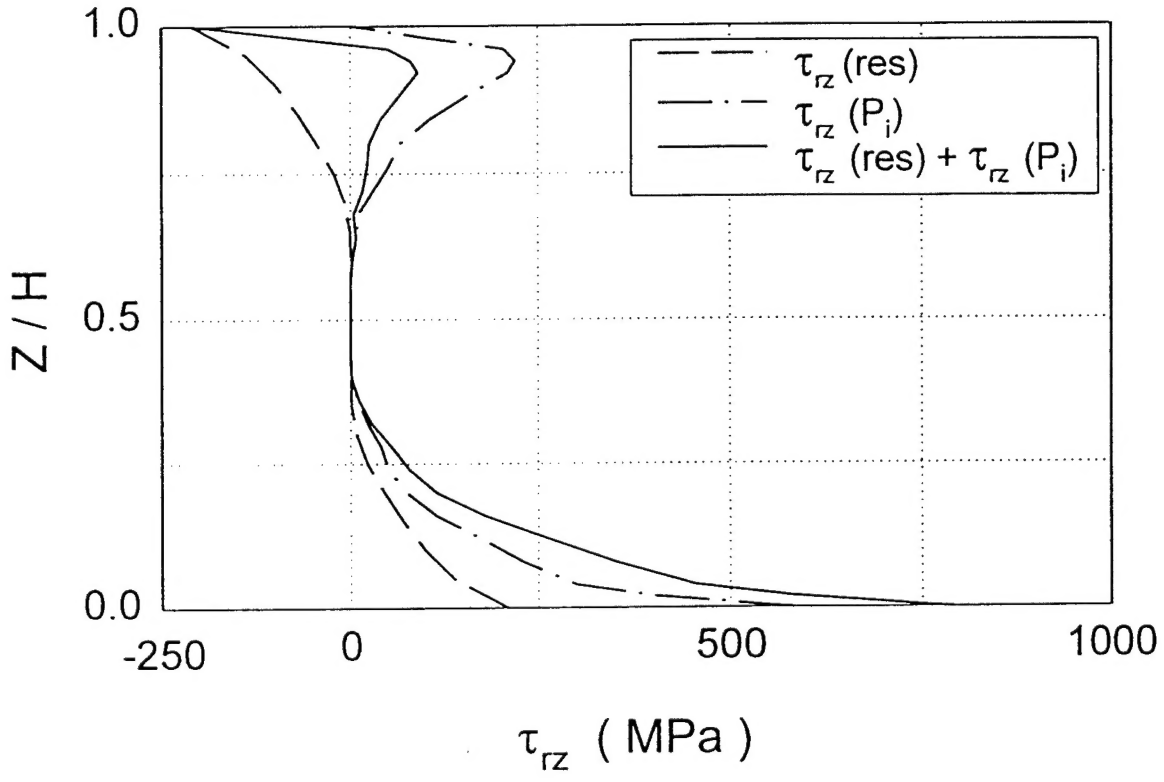

Fig 4-5(a) Shear stress distribution along the interface due to residual stress, $\tau_{d\text{-}res}$, and applied debond load, $\tau_{d\text{-}Pi}$, for pushout test performed at 25 °C.

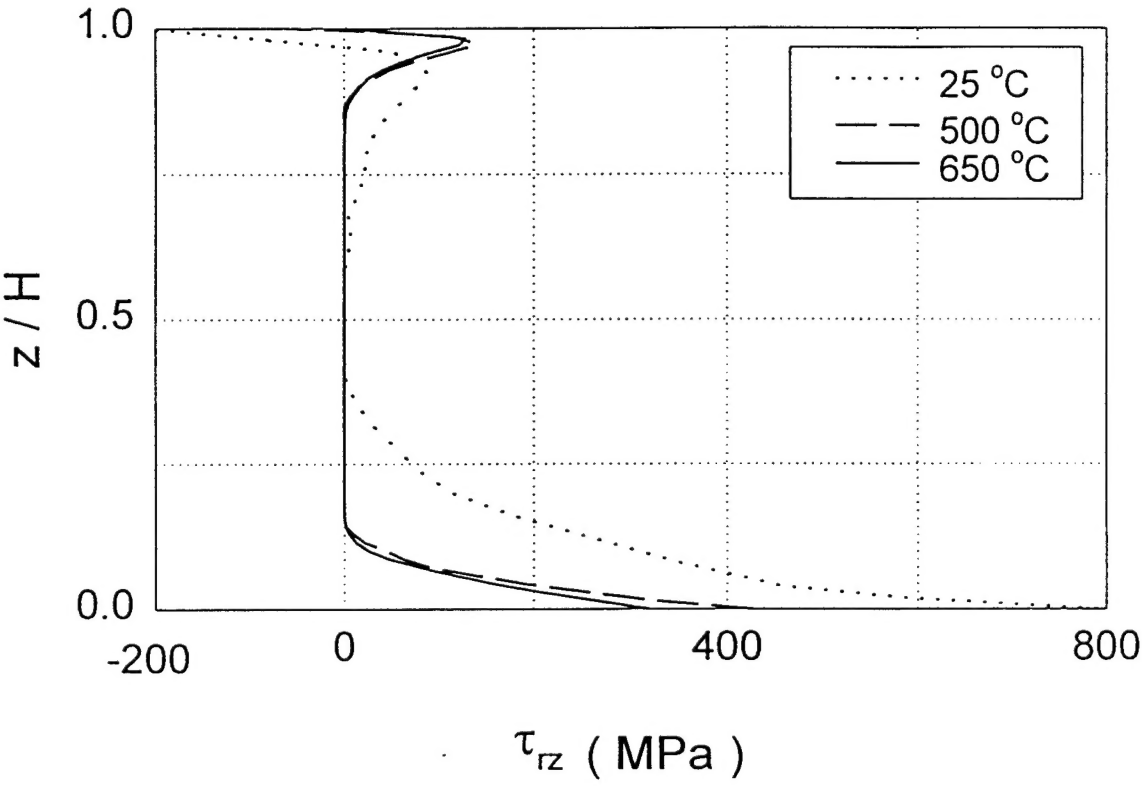

Fig 4-5(b) Resultant interface shear stress distribution. The specimen thickness, H = 0.50 mm, for 25 °C and H = 1.4 mm for 500 and 650 °C.

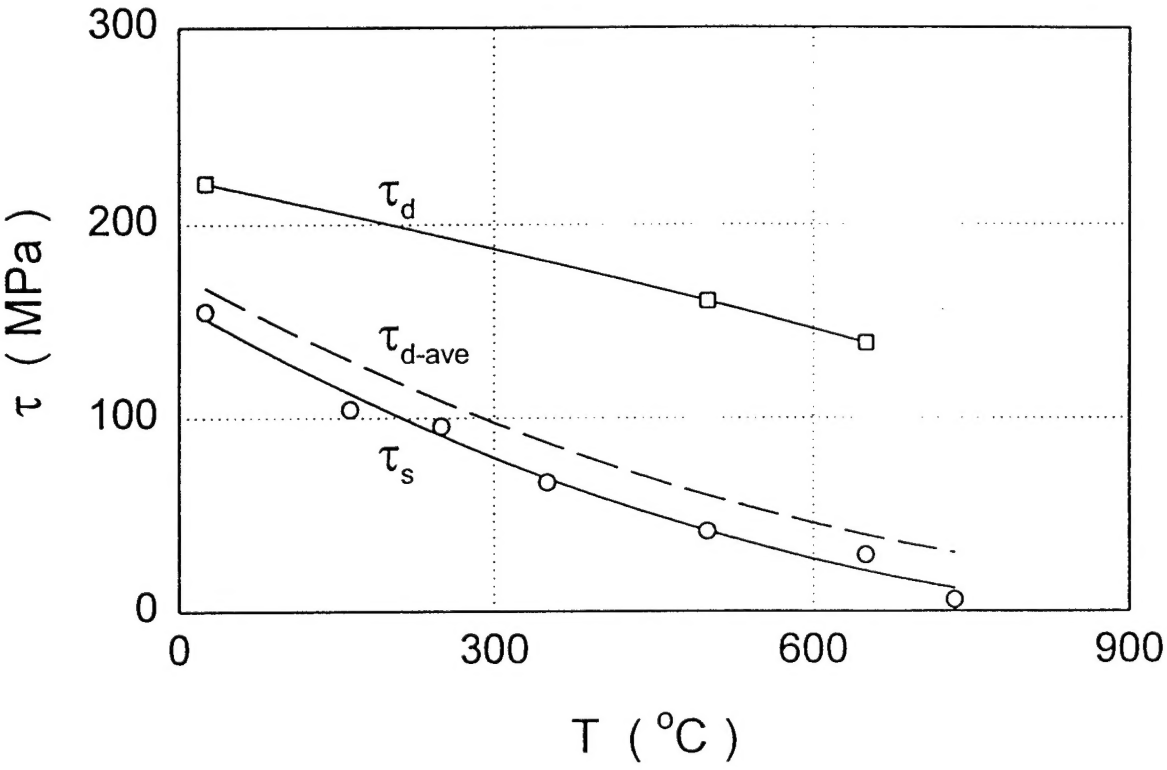

Fig. 4-6 Influence of temperature on interphase shear strength, τ_d, and frictional shear stress, τ_s. The dashed line represents the average shear strength values, $\tau_{d\text{-}ave}$, determined using the assumption of uniformly distributed shear shear force along the pushout fiber.